EPA-650/2-74-046-a

June 1974

Environmental Protection Technology Series

DEVELOPMENT OF A GAS LASER SYSTEM TO MEASURE TRACE GASES BY LONG PATH ABSORPTION TECHNIQUES:

VOLUME I - GAS LASER SYSTEM MODIFICATIONS FOR OZONE MONITORING

FINAL REPORT

Office of Research and Development
U.S. Environmental Protection Agency
Washington, DC 20460

EPA-650/2-74-046-a

DEVELOPMENT OF A GAS LASER SYSTEM TO MEASURE TRACE GASES BY LONG PATH ABSORPTION TECHNIQUES:

VOLUME I - GAS LASER SYSTEM MODIFICATIONS FOR OZONE MONITORING

FINAL REPORT

by

S. E. Craig, D. R. Morgan,
D. L. Roberts, and L. R. Snowman

General Electric
Electronic Systems Division
100 Plastics Avenue
Pittsfield, Massachusetts 01201

Contract No. 68-02-0757
ROAP No. 26ACX
Program Element No. 1AA010

EPA Project Officer: W. A. McClenny

Chemistry and Physics Laboratory
National Environmental Research Center
Research Triangle Park, North Carolina 27711

Prepared for

OFFICE OF RESEARCH AND DEVELOPMENT
U.S. ENVIRONMENTAL PROTECTION AGENCY
WASHINGTON, D.C. 20460

June 1974

This report has been reviewed by the Environmental Protection Agency and approved for publication. Approval does not signify that the contents necessarily reflect the views and policies of the Agency, nor does mention of trade names or commercial products constitute endorsement or recommendation for use.

TABLE OF CONTENTS

TABLE OF CONTENTS (Cont'd)

APPENDICES

LIST OF ILLUSTRATIONS

LIST OF ILLUSTRATIONS (Cont'd)

Page No.

APPENDICES

LIST OF TABLES

A. INTRODUCTION

The Final Report of EPA Contract 68-02-0757, Development of a Gas Laser System to Measure Trace Gases by Long Path Absorption Techniques consists of two (2) volumes:

I Gas Laser System Modifications for Ozone Monitoring

II Field Evaluation of Gas Laser System for Ozone Monitoring

The work reported here stems from development activity begun in 1966 at GE's Electronics Laboratory. Under this contract, a breadboard laser long path monitor called ILAMS (Infrared Laser Atmospheric Monitoring System) was modified to improve its sensitivity as indicated by previous field experience. System parameters were selected to optimize system performance for ozone monitoring. A field evaluation of the modified system was conducted.

In this volume of the Final Report, the work of ILAMS modification and the selection of system parameters, lasing wavelengths and linear weights, is reported. Significant system modifications included introduction of a spatial filter in the laser output beam. In addition, a digital signal processor was incorporated in the system, replacing an analog device. The problems associated with incorporating a sealed, isotopic fill CO_2 laser were studied and a laser design proposed. The selection of the four laser wavelengths were preceded by extensive spectral data collection to determine the infrared absorption characteristics of target gases and expected interferences. The selection process was facilitated by a previously developed computer program. Similarly, the calculation of linear weights was done on an existing computer program.

The change to digital processing was particularly important in the evolution of the ILAMS design. It greatly enhanced the flexibility of the system, offering significant advantages over the analog approach as discussed in the next section.

B. SIGNAL PROCESSOR

1. INTRODUCTION

The spectrally scanning CO_2 laser periodically steps through a number of lasing modes. In each mode, the laser generates a quantity of energy at a particular wavelength. Figure 1a. illustrates the energy output of the laser in time where $x_k(t)$ is the energy generated of wavelength, λ_k, and τ is the period of one scan.

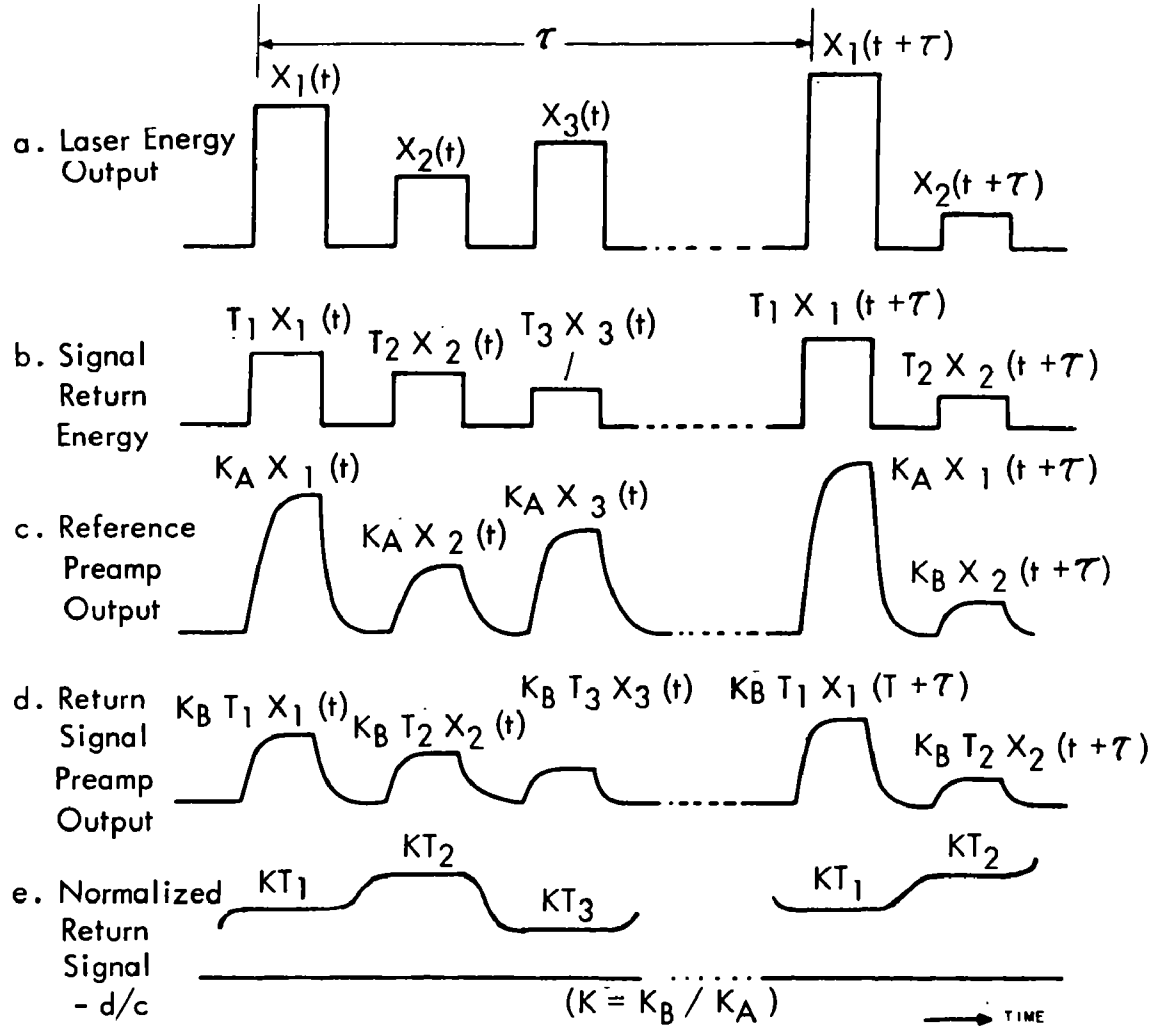

Figure 1. SIGNAL WAVEFORMS

This energy is transmitted over a path in which a spectral attenuation takes place that is dependent upon the nature of the medium. Figure 1b. illustrates the energy after passing through a medium where T_k is the transmission of the medium at wavelength, λ_k.

The desired information consists of the transmissions $T_1, T_2, T_3, \ldots$, which characterize the medium. As shown in Figure 1a., the laser output at each wavelength is generally not constant from wavelength to wavelength, or even from period to period. This problem necessitates the use of a reference that directly senses the output of Figure 1a. Conversion of the optical energy to an electrical signal is accomplished with a suitable IR detector followed by a preamplifier. If the return signal, Figure 1d. is divided by the reference signal, Figure 1c., the desired information is obtained, as in Figure 1e.

Information is extracted at each wavelength by synchrounous demodulation which is performed by filtering or integrating gated portions of the signal. Typical signal waveforms and gating signals are shown in Figure 2. A null gate is also provided in order to derive a zero energy reference for dc restoration since the signal is ac coupled through the preamp.

The normalization division process may take place before or after synchronous demodulation as long as the reference signal-to-noise-ratio is large enough. Division before synchronous demodulation requires a fast, stable divider and necessitates state-of-the-art hardware for precision measurements. On the other hand, division after synchronous demodulation requires a relatively slow separate divider for each wavelength and twice as many synchronous demodulators.

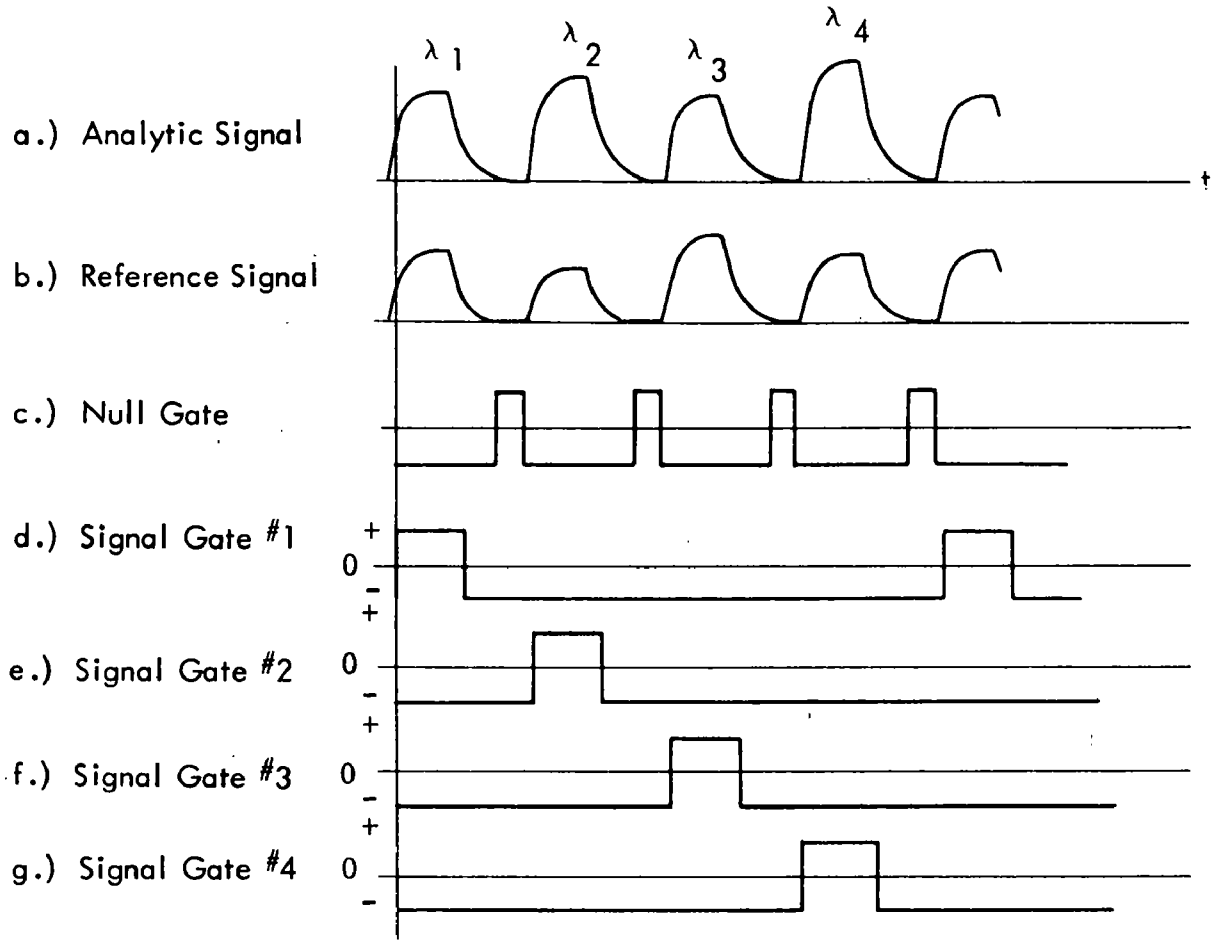

Figure 2. SIGNAL AND GATING WAVEFORMS

For large absorptions, logarithmic processing is desirable in order to linearize the exponential transmission-concentration characteristic exhibited by gases. Again, there is some choice as to where this transformation is applied. If the signal-to-noise-ratio (SNR) is very high, then log processing can be accomplished before synchronous detection without any degradation in performance. However, in general, it is preferable to do as much filtering as possible before the log conversion in order to maintain reliable performance.

Linear weighted sums of the filtered log transmission measurements are then derived in order to estimate the concentrations of particular atmospheric gases. This technique is discussed in detail in Appendix B.

2. MINI-COMPUTER PROCESSOR

The mini-computer signal processor includes a general purpose (stored program) mini-computer and appropriate interface electronics. The collection and reduction of data is entirely under computer, i.e., program control; results are displayed on simple displays incorporated in the equipment, and on an optional teletype, which need not be used (or even be connected) during field or test range exercise of the system.

The use of the stored program control and data reduction means:

- changes in system design, or variations in data reduction algorithms, may be accommodated without alteration of the data collection or reduction hardware; only changes in the control program will be required.
- modification of signal processor parameters such as number of wavelengths (up to 8), gate locations, system response time, weighting factors, etc., do not even require software changes, these parameters are expediently entered by the teletype input.
- the precision of data processing may be made as accurate as desired; similarly the impact of imprecise calculations may be assessed by direct simulation for purposes of evaluating future low cost special purpose instruments.

- additional data, e.g., environmental conditions, time, date, signal variability, laser parameters, etc., may be measured and recorded without modification of or addition to the existing system hardware.

- the performance of one or more data processing and display systems can be directly analyzed, e.g., data from several ozone monitors could be crosscorrelated and recorded.

The data collection and reduction system is sketched in Figure 3. A Digital Equipment Corporation PDP 11/05 is used for the central processor. The data collection and reduction equipment in Figure 3 consists of three major subsystems:

Interface Subsystem

The Interface Subsystem is composed of an 8 input analog signal multiplexer, which is followed by a sample-and-hold amplifier and an analog-to-digital converter at 10-bit precision. (The analysis path detector preamplifier output is connected to one multiplexer input, the reference path to a second multiplexer input, the remaining 6 are available for sensing other voltage levels of interest). Additional subsystem elements include an AGC attenuator, a wheel position counter and demultiplexer/storage capability for analog data displays like the meters shown in Figure 3.

Central Processor Subsystem

The central processor and its own control panel form this subsystem. Power supplies for this equipment are contained within the CPU cabinet proper. The central processor control panel ordinarily is disabled during operation.

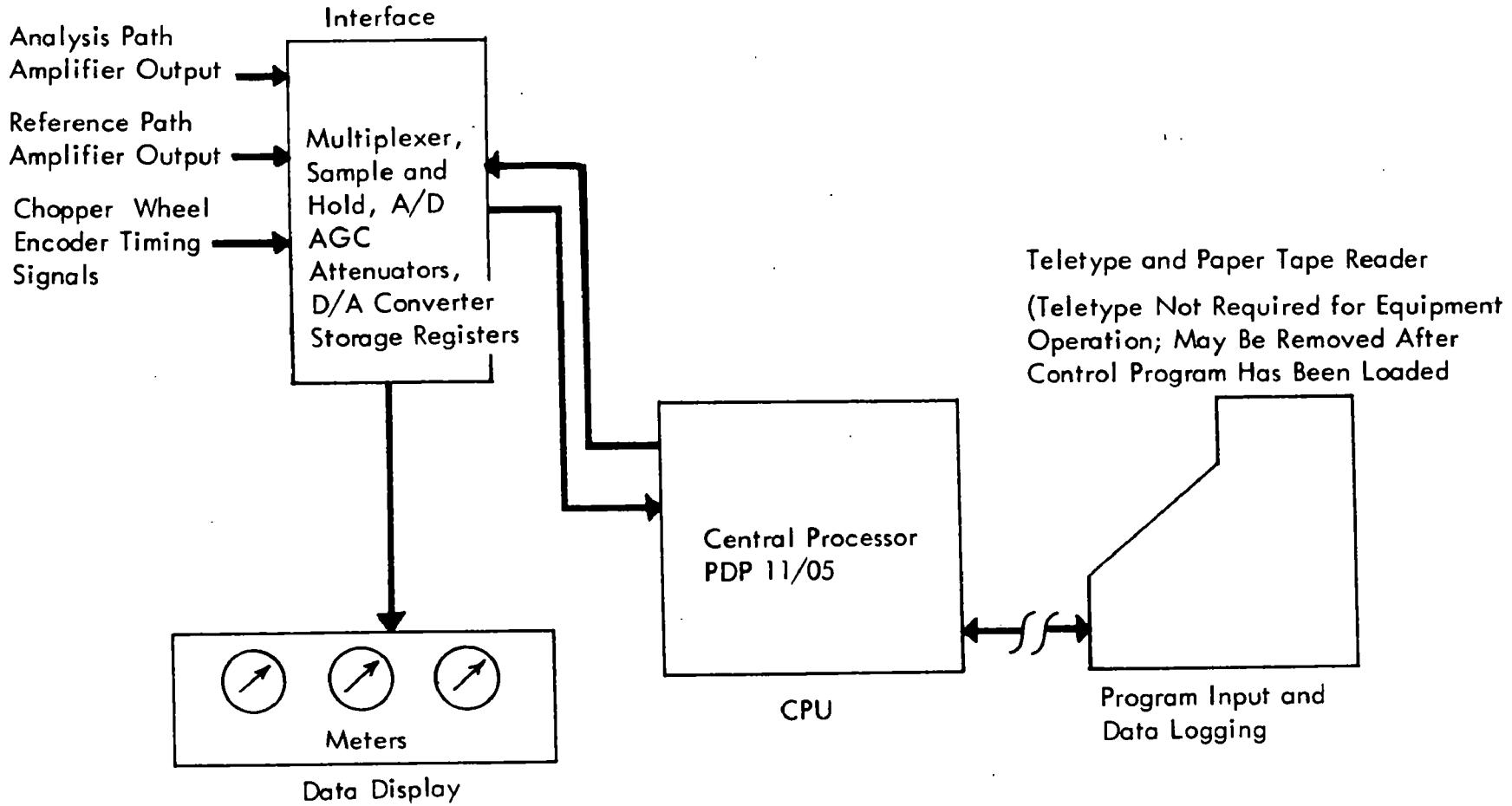

Figure 3. DATA COLLECTION AND REDUCTION SYSTEM

Program Input and Data Logging Subsystem

A Teletype Corporation ASR-33 teletype with appropriate interface circuits constitutes this subsystem. As indicated, it plays two roles. First, it permits entry (ordinarily via paper tape) of the control program. Second, it permits detailed reporting of directly measured quantities, or derviced (computed) quantities.

The central processor is designed so that programs stored in its core memory may be caused to remain intact during periods of no primary power. This option is exercised, so that once a control program has been entered in the CPU, it need not be reentered until there is a need to change it, regardless of whether the CPU remains energized or not. The control program is designed so that it will run properly regardless of whether the teletype is connected or not. Thus the teletype unit is an optional data display device, not an essential component of the system once the control program has been entered.

Details of the mini-computer signal processor are described in the following sections.

3. LOGIC BLOCK DIAGRAM

A logic block diagram of the complete system is shown in Figure 4. The analysis path or analytic detector is followed by a preamplifier which generates a 10 mV - 10 V signal level depending upon path attenuation. In this diagram a wide-band analytic detector is shown. However for the modified ILAMS system, a thermistor bolometer detector with equalization will be alternatively used.

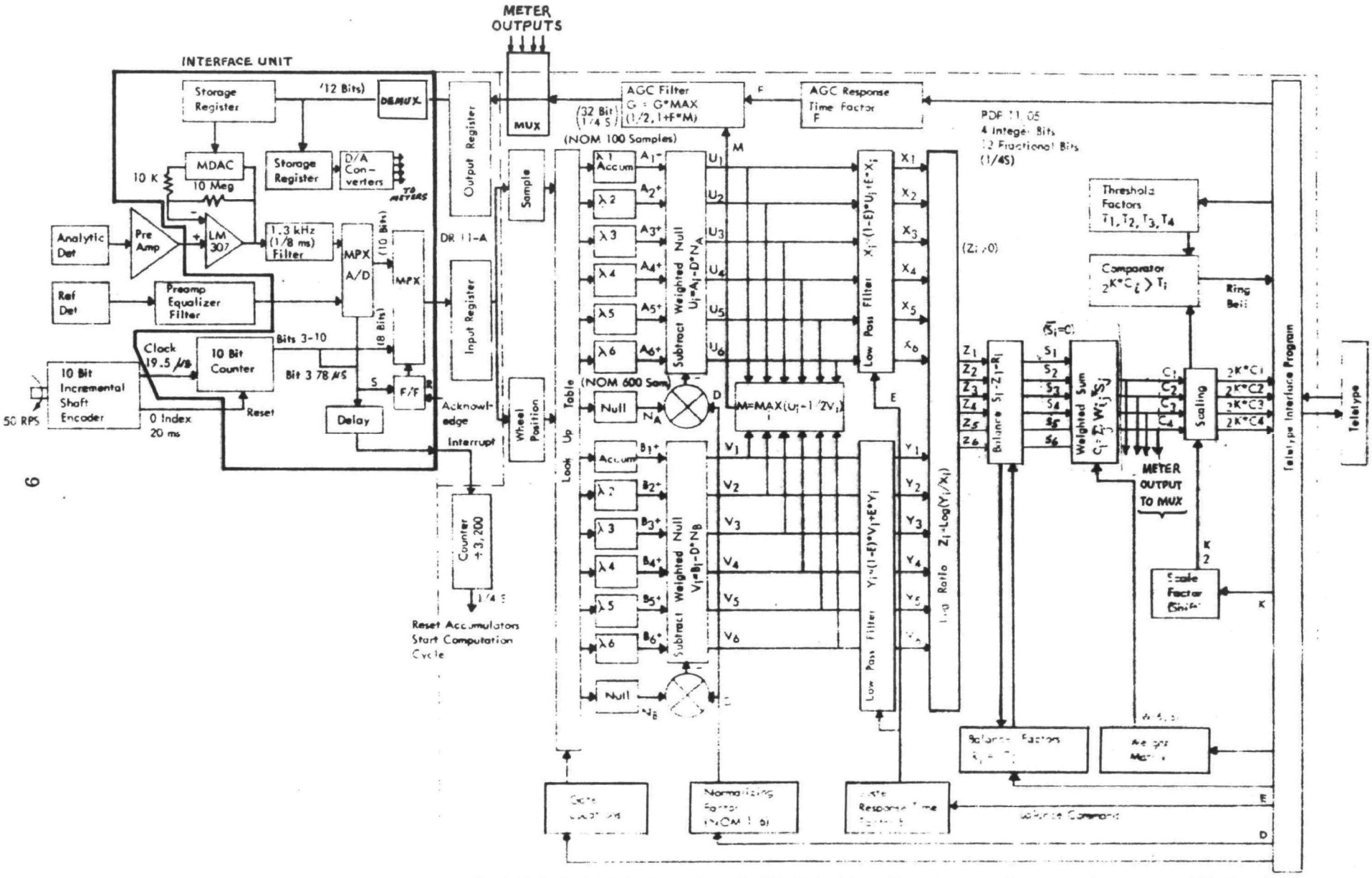

Figure 4. LOGIC BLOCK DIAGRAM

A digitally-controlled amplifier, using a multiplying D/A converter (MDAC), automatically controls this signal level to about 10 V in order to limit the dynamic range requirements of the A/D converter. The mini-computer generates a feedback signal to control the gain of this circuit and also performs the required filtering necessary to realize a given loop response time which is usually set to about 1 second.

A single pole low-pass filter preceeds the A/D converter in order to limit the bandwidth and thereby establish the required sampling rate. The cutoff frequency is chosen large enough in order to limit the interpulse interference to an acceptable level. An analysis of bandwidth, sampling time, and interpulse interference as well as other effects appears in Reference 1.

For the ILAMS system, the reference detector is followed by a similar pre-amplifier, equalizer, and filter. However, no gain control is necessary for this channel.

An A/D converter and multiplexer alternately samples the analytic and reference channels at a rate compatible with the signal bandwidth.

A digital shaft encoder which is attached to the laser wavelength selector wheel is used with a counter in order to provide the synchronous gating information shown in Figure 2. This arrangement provides an 8-bit number which determines the wheel position at any instant in time. The lowest order bit is also used to control the A/D converter and multiplexer so that the samples are synchronized with the waveforms.

Each data collection cycle consists of serially reading a signal and wheel position sample into the DR11-A interface unit. The samples for each analytic and reference wavelength and nulls are accumulated in separate registers according to wheel position. This performs the synchronous demodulation of the signals.

Digital filtering of the data is done in two steps. In the first step, samples are accumulated for 1/4s at each analytic and reference wavelength. A null is also accumulated for analytic and reference. Both accumulated nulls are appropriately weighted and subtracted from the corresponding accumulated wavelength samples. The null weight for each wavelength is determined so as to account for the different number of samples accumulated in the wavelength and null accumulators over one scan; i.e.

$$\text{null weight} = \frac{\text{nbr of samples in wavelength accumulator in one scan}}{\text{nbr of null samples in one scan}}$$

The second step consists of low pass filtering the 1/4s sequences to obtain the desired system response time. This approach allows a quasi-continuous readout of all monitoring signals. In addition, the 1/4s signal sequences can also be filtered for AGC feedback with arbitrary response time.

The factor E shown in Figure 5 controls the system response time

$$\tau = (1 - \ln E)/4 \text{ seconds}$$

where E is a positive number less than one.

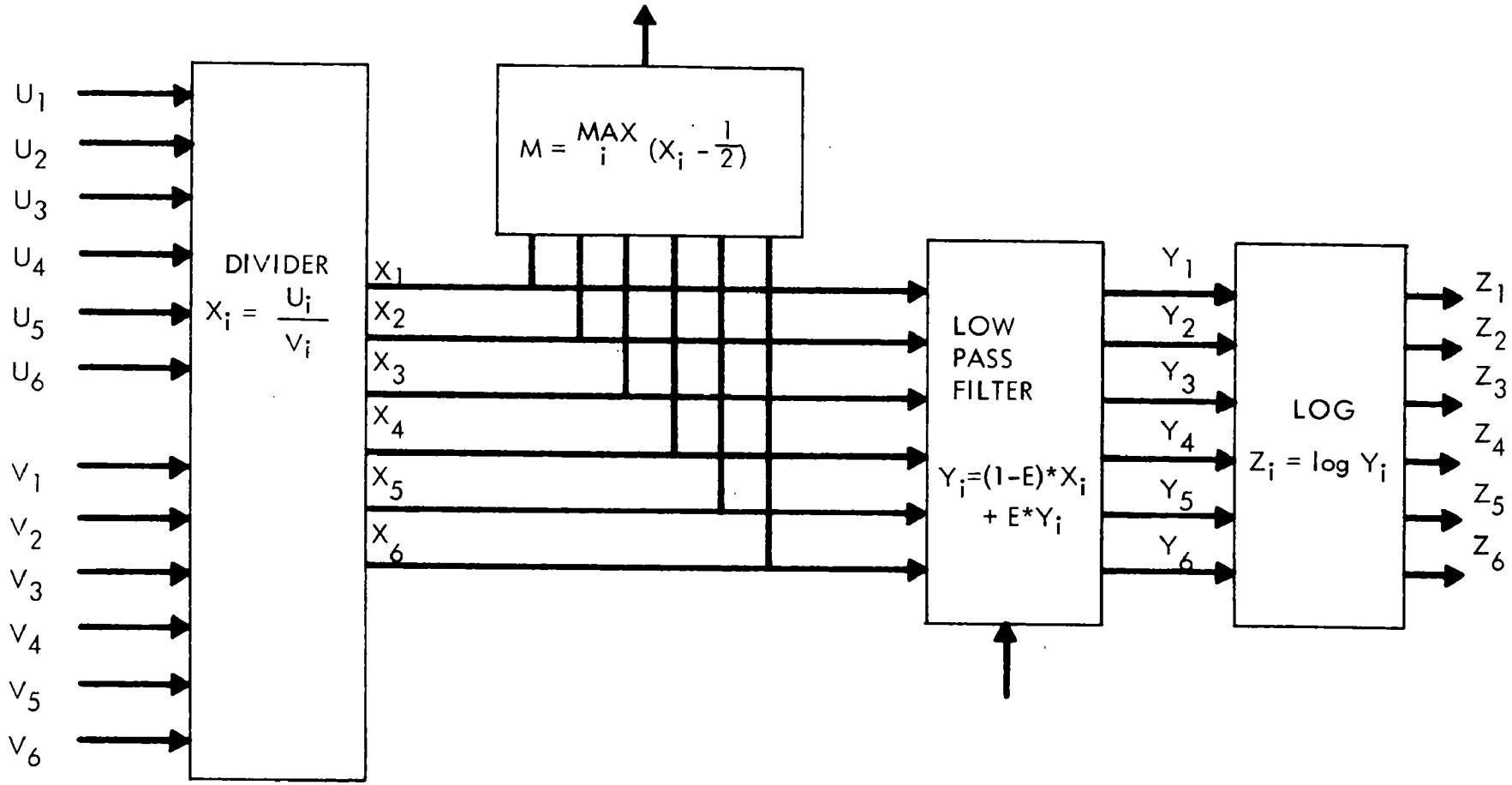

Figure 5. PROGRAM MODIFICATION

A "geometric" integrator is used for AGC feedback filtering. The error signal is derived in such a manner as to maintain each analytic level at less than or equal to half of its respective reference level, on the average. For this arrangement, the response time of the AGC loop is dependent upon the reference level. However, an improved design which eliminates this dependency as well as simplifies the computations is shown in Figure 5. This version will probably be adopted in any future generation software.

After the final low-pass filtering, the log ratios of the 1/4 second analytic and reference samples are computed. A balance register is provided at this point in order to initially calibrate the instrument for a zero output in the absence (hopefully) of any absorbing gas.

The normalized log ratios are then weighted, scaled and outputed to the teletype unit as the final concentration estimates. A later modification also provided meter readouts. A threshold feature is also included in order to signal exceptionally large concentration levels.

An existing analog signal simulator (Reference 2) is being used to generate arbitrary absorption patterns and thereby checkout the entire signal processor in the laboratory.

4. SOFTWARE

Operational Modes

The system normally operates in either one of two modes: collection, and data reduction and display.

Collection Mode

In this mode repeated measurements of the analysis path signal and reference path signals are made and recorded. Additional measurements on the behavior of other system elements also may be made before, during or immediately after the repeated transmission measurements.

The output of the analysis path detector amplifier is connected to one of the multiplexer inputs indicated in Figure 3; the output of the reference path amplifier is connected to a second multiplexer input.

The chopping wheel, which both modulates the laser beam output and controls the laser wavelength, is driven by a motor which is monitored by a digital shaft encoder. The net effect of this apparatus is to generate a binary number which reports the position of the wheel and thus laser wavelength and modulation. The wheel position is reported to 1 part in 256, i.e., to about 1.4^{o} precision. One can think of a 256 tooth gear or index on the chopper wheel. The wheel rotates about 3000 rpm, or 50 revolutions/second, so that the wheel advances one "tooth" every 78 microseconds. (In reality, the binary counter advances 1 count each 78 microseconds.) At each new count, the CPU is interrupted and the present reading of the counter and one A/D converter reading are transmitted to the computer. The counter reading is interpreted to determine the nature and proper disposition of the A/D converter reading; that disposition is made and the processor then waits for another interrupt. (Typical data dispositions are the addition of a current reading to the previously

accumulated sum for that wavelength and that path, or ignoring the reading because it is the transition interval between "on" and "off".)

At preset intervals, e.g., once every N cycles of transmissivity data collection, the normal data collection sequence may be altered to measure any other parameter of the system which is connected to one of the multiplexer ports. Each of these measurements may be recorded separately if the total number is small (e.g., 100), or averaged. Each measurement would require 50 to 100 μs to complete. Upon completion of the measurement, data collection would continue as before, picking up again at the next full revolution of the chopper wheel.

At the conclusion of a preset number (e.g., M) of transmission observations, operation in the data collection mode is terminated.

The parameters M and N are stored in the processor at some previous time, either by teletype, or by use of the numeric input controls of the operator control subsystem.

Data Reduction and Display Mode

The second mode of operation is data reduction and display.

At the conclusion of a data collection sequence, signal measurements have been accumulated on each of typically 4 wavelengths, at both the reference and analysis paths. The transmission measurements consist of both "peak"

measurements at each wavelength and "valley" measurements made during the off period between open shutter intervals. In all, for 4 wavelengths, 10 quantities will be available, (4 reference paths, 4 analysis paths, reference amplifier null and analysis amplifier null).

The data reduction program now operates on this data, reporting, for example, relative transmission at each wavelength or estimated concentration of each of one or more gases.

The first two results might best be reported via the teletype; the latter results might be reported both via the teletype and via the simpler displays included in the operator control subsystem. (As indicated earlier, the teletype system and software are configured so that the absence of the instrument does not prevent successful computation and presentation of the results intended for display on the operator control subsystem.)

It may be noted that the only hardware that would have to be changed to accommodate the use of any reasonable number (say up to 10) different wavelengths of laser radiation would be the chopper wheel. The "data disposition" table stored in the processor would have to be changed, but this is merely a matter of reading a paper tape. A few additional memory locations would be needed for the accumulation of transmission measurements, but the 22 accumulators required for 10 wavelengths are readily available.

Program Structure

Software of the ILAMS system is composed of one real time analysis program and two non-real time support programs that modify tables used in the analysis

program. The functions of each program are:

- Real-time Analysis Program - a) collect real time laser outputs and compute a series of measurements for printing on the teletype, b) monitor and feedback of AGC.

- Parameter Entry Program - supplies and modifies, via the teletype keyboard, various weighting factors, integration constants, time constants, scaling factor, etc.

- Channel Assignment Program - builds tables of values which are used to assign individual data samples to specific input channels.

Instructions for Operating Real-time Analysis Program

These instructions apply when the analysis program and required support programs are already loaded into memory. For instructions on the loading of programs, see Chapters 2 and 6 of the "PDP-11 Paper Tape Software Programming Handbook". Steps required to start program are:

1. Turn console power key to ON.
2. Turn teletype console switch to LINE position.
3. Depress ENABLE/HALT switch.
4. Enter start location 12400_8 in the Switch register.
5. Depress LOAD ADRS switch.
6. Lift ENABLE/HALT switch.
7. Depress START switch.

The above starting point will cause the AGC value to be initialized to the minimum gain setting. An alternate restart location of 12414_8 will leave the AGC at its last computed value.

The program may be stopped at any time by depressing the ENABLE/HALT switch.

Program Output

a) A set of eight measures are printed on the teletype for approximately every 16th set of data gathered.

b) A new AGC value is computed and transmitted for every set of data gathered.

c) Eight meter outputs are transmitted for every set of data gathered.

Program Input - Keyboard

The depression of selected keys on the teletype allows the user to alter the flow of the analysis program.

Key	Reaction
"B"	Program performs the balancing function and then continues with normal processing.
"U"	Program performs an unbalancing function and then continues with normal processing.
"T"	Control is transferred to the channel assignment program which prints a "K" when ready to receive data. Restart at 12414_8 is necessary to return to analysis program.
"P"	Control is transferred to the parameter entry program which prints a "$" when ready to receive data. Restart at 12414_8 is necessary to return to analysis program.

Parameter Entry Program

Various parameters used by the program are stored in an 12 x 8 array which may be altered by the parameter entry program. The array structure and contents are as follows:

Array Location	Parameter	Range	Maximum Input Units	Input Units
1,1 → 1,4	Measure 1 weight	-1.0 → 1.0	± 250	± 1/250
2,1 → 2,4	Measure 2 weights	-1.0 → 1.0	± 250	± 1/250
3,1 → 3,4	Measure 3 weights	-1.0 → 1.0	± 250	± 1/250
4,1 → 4,4	Measure 4 weights	-1.0 → 1.0	± 250	± 1/250
5,1 → 5,4	Measure 5 weights	-1.0 → 1.0	± 250	± 1/250
6,1 → 6,4	Measure 6 weights	-1.0 → 1.0	± 250	± 1/250
7,1 → 7,4	Measure 7 weights	-1.0 → 1.0	± 250	± 1/250
8,1 → 8,4	Measure 8 weights	-1.0 → 1.0	± 250	± 1/250
9,1	E	0 → < 1	32767	1/32768
9,2	1-E	0 → < 1	32767	1/32768
10,1	F	0 → < 1	32767	1/32768
10,2	AGC value	$0 \rightarrow 7777_8$	4095	1/4095
11,1 → 11,8	Scaling constants (Multiply results by 2^n where n = 1→15)	1-15	15	1
12,1 → 12,8	Meter offsets	0 → 63	64	1/64

The parameter entry program may be started by depressing the "P" key while the analysis program is running - or - starting at 14000_8. The program will print a "$" when ready to accept data.

Input format:

x,xbnnnnn(CR) (CR) is a return

where

b - blank
x,x - signifies the array coordinates
nnnnn - any value up to 5 digits - may be preceded by a minus sign to signify a negative value

Examples:

1,1b125(CR) - Value of 1/2 entered for set 1 weight 1
3,7b-10(CR) - Value of -1/2 5 entered for set 3 weight 3
5,1b32767(CR) - Value of $1-2^{-15}$ entered for E

Channel Assignment Program

This program is used to assign data samples (as designated by wheel position count) to specific input channels. Channels are numbered:

01	Analytic	09	Reference
02		10	
03		11	
04		12	
07	Analytic nulls	15	Reference nulls

The channel assignment program may be started by depressing the "T" key while the analysis program is running - or - starting at 7000_8. The program will print a "K" when ready to accept data.

Input format:

	Examples
xxbnn,nnn,...,n(CR)	03b17,19,123,7(CR) 04b124(CR) etc.

where

b - blank

xx - is a two digit channel number

n or nn or nnn - is the wheel position count

Notes: 1. 00 - as a channel entry will clear the channel assignment table.

2. Wheel position counts are separated by commas with the last one followed by a return.

3. Any positive octal value placed in location 7446_8 will be added to the wheel positions as they are entered. Truncation at 256 is performed by the program (256 = 0, 257 = 1, etc.).

5. INTERFACE UNIT

The Interface Unit conditions the analog signals from the reference and analytic detectors and the signal from the shaft position encoder, converts them to digital form, and makes them available in the proper sequence as inputs to the computer. The capability for automatic gain control (AGC) is provided for the analytic signal channel. In addition the Interface Unit includes storage elements and digital-to-analog converters for output indicators such as meters or chart recorders. Up to eight values can be indicated or recorded simultaneously, and the eight quantities to be displayed can be selected by the computer program.

The Interface Unit is assembled in an aluminum enclosure measuring approximately 28 X 18.7 X 18.7 cm. It consists of a socket panel which holds most of the analog and digital circuitry, a Data Acquisition System, and power supplies. The power supplies allow the unit to operate directly from the 117 V AC line. They also furnish power for the shaft position encoder and the preamplifier for the analytic detector.

The Data Acquisition System is a modular unit made by Datel Systems, Inc. (Model DAS-16-L10B). It has a 10-bit analog-to-digital converter, a sample-and-hold circuit, and an analog multiplexer, connected to allow either random or sequential digitizing of up to 8 analog voltages. The Interface Unit uses only two of the eight inputs - one for the analytic signal and one for the reference signal. These two inputs are sampled and digitized alternately.

The functional elements of the Interface Unit are shown at the left side of the signal processor block diagram, Figure 4. The detectors and their pre-amplifiers, and the shaft position encoder, are not physically a part of the Interface Unit.

The AGC circuit makes use of a multiplying D/A converter (MDAC) in the feedback path of an operational amplifier. The closed-loop gain of this amplifier is inversely proportional to the value of a 12-bit binary number that is applied to the MDAC, except that the gain cannot exceed 39. Since the AGC control comes from the mini-computer, the algorithm used and its response time are the choice of the programmer.

The shaft position encoder is of the incremental type with a zero index. It produces 1024 pulses per revolution on one output, and one pulse per revolution on the other. The 1024 pulse output clocks a 10-bit binary counter, which undergoes a complete cycle once per revolution. The index resets the counter to insure that it always starts from exactly the same shaft position. In this way, the 10-bit number furnished by the counter indicates the position of the chopper wheel with an accuracy of about 0.1%.

Figure 6 shows the sequence of events and their relative timing during a conversion cycle. A time equivalent to 1/256 of a wheel revolution, or 78 μsec. at 3000 rpm, is allowed for this cycle. The first four lines in Figure 6 show the logic states of the four least significant bits of the wheel position counter. The 128-count line is used to switch the analog multiplexer in the Data Acquisition System, so that

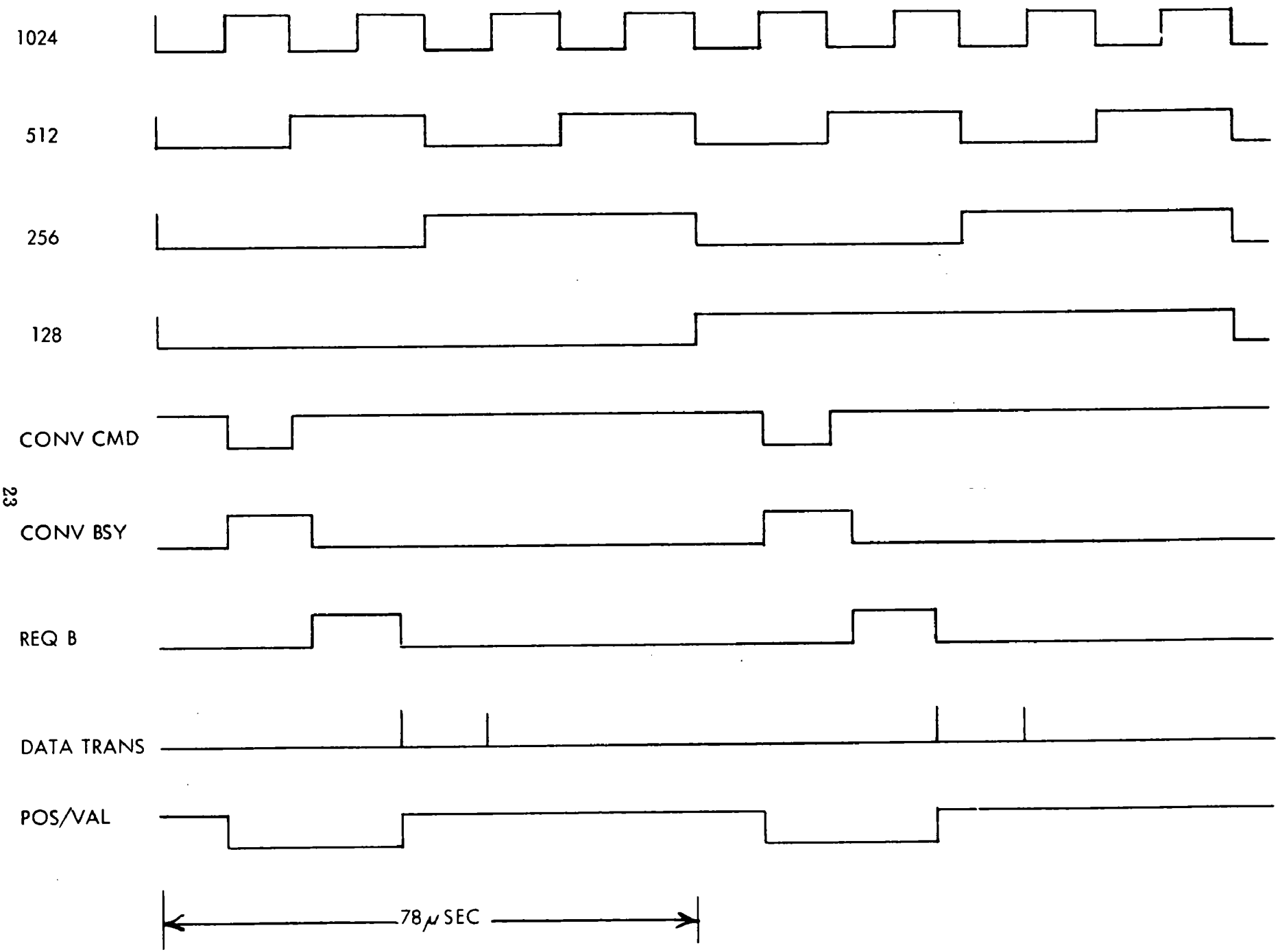

Figure 6. SEQUENCE OF EVENTS

the analytic channel and the reference channel are sampled and digitized in alternate cycles. After this multiplexer switches, a period of about 9.8 μsec. is allowed for settling before an A/D conversion is initiated by the negative transition of the "Convert Command" line. The A/D converter's "busy" line stays high while the conversion is taking place, and then goes low. At that point the "Request B" line goes high to indicate to the computer that data is ready for input. This data passes through a digital multiplexer which selects between the wheel position counter and the A/D converter. Initially, this multiplexer, controlled by the "Position/Value" line, is switched toward the counter.

When the computer has read in the wheel position, it sends a "Data Transmitted" pulse to the Interface Unit. This pulse terminates the "Request B" and changes the digital multiplexer to the A/D converter. The computer then reads the digitized input value and returns another "Data Transmitted" pulse. (The Interface Unit does not use this second pulse.)

Since the A/D conversion requires only about 13 μsec., the time available for the computer to read both the shaft position and signal values is about 65 μsec. Only the eight most significant bits of the wheel position counter are furnished to the computer, since that is sufficient to give each conversion cycle a unique wheel position value.

C. SPECTRAL STUDIES

1. INTRODUCTION

ILAMS measures directly the transmission (T_1, T_2, T_3, T_4) of the sample region between the transmitter and the retroreflector at four wavelengths. Assuming that the line width of the resonance absorption is broad compared to the transmitted laser line width, and assuming also that there is no saturation in the absorbing media, then, for a uniform concentration of the absorber over the path, the transmission at each discrete wavelength is of the form, $T_m = \exp(-A_m C_A L)$; where A_m is the absorption coefficient of absorber A at wavelength m, C_A is the concentration of absorber A over the total optical path, and L is the total optical path through the sample region. If the concentration is non-uniform over the path, as is the more usual case, then $C_A L$ can be replaced by the integrated concentration over the path or, more simply, let C_A represent the average concentration over the path.

Typically, C has units of grams/liter or atmospheres of partial pressure, and L is in centimeters. A_m is in units to make $A_m C_A L$ dimensionless.

If a second absorber B with absorption coefficients B_m is introduced into the region, the net transmission will be the product of the transmission due to each absorber.

$$T_m = e^{-A_m C_A L + B_m C_B L} \tag{1}$$

If the natural log of the transmission at each wavelength is taken electronically, then

$$S_m \overset{\Delta}{=} \ln T_m = -(A_m C_A L + B_m C_B L) \tag{2}$$

and the resulting signals have two convenient properties:

1) System response to any absorber is a linear function of the quantity (concentration x path) present

2) System response to several absorbers is the sum of the responses to the individual absorbers.

Therefore, it the system can be designed to give a zero response to spectrally interfering absorbers, the system will respond only to the pollutant to be measured, and the response will be proportional to the quantity present.

Speaking more generally, the above properties define a linear 4-dimensional vector space. Each gas is represented by a vector in this space whose length is proportional to the concentration. This formalization permits the application of known mathematical and statistical techniques.

Using decision theory and multivariate statistical analysis, it can be shown that the optimum signal processing involves the use of single or multiple linear weights. Application of a single linear weight, W, means taking a linear sum of the signals $S_1, S_2, \ldots S_n$ to give a new signal, $S = W_1S_1 + W_2S_2 + \ldots W_nS_n$. The quantity of absorbers present can be accurately determined by examining the magnitude of such linear sums.

Techniques may also be applied for choosing linear weights to accurately measure the quantity of a given pollutant in the presence of known interfering spectral absorbers, random spectral absorbers, scintillation, and other "noises". A definitive study on spectral absorption pattern detection and estimation techniques using linear weights appears in Reference 3. A summary of the applicable results are given in Appendix A and B.

For the CO_2 laser, there is a large number of lines from which the 4 wavelengths can be selected. On the basis of both analytical and experimental work, several basic conclusions about wavelength selection can be drawn. These are:

1) The relative success of a group of wavelengths depends directly on the measurement problem. The pollutants to be measured, pollutants and absorbers to be ignored, expected quantities of absorbers and the system noise levels, all affect the choice of wavelengths.

2) For a given problem, there will be an optimum set of wavelengths. Increasing the number of pollutants to be estimated or ignored will tend to increase the optimum number of wavelengths to be used; i.e., the more complex the environment, the more wavelengths are necessary.

3) The finer the spectral structure of an absorber, the fewer number of wavelengths areneeded to best measure the quantities of it present. The laser system is not limited to detecting pollutants with fine structure such as ammonia and ethylene. In fact, it does remarkably well in detecting or rejecting absorbers with rather smooth spectral characteristics.

4) On the basis of past experience, four wavelengths have done an excellent job in handling spectral recognition problems in environments representative of the real world.

The primary target gas considered in this program was ozone. Secondary targets, which are also, to some extent, interferences for the primary target as well as between themselves, were ethylene (C_2H_4) and ammonia (NG_3). The general topics of Interferences and Optimum Linear Weights are discussed, respectively, in Appendices A and B. A systematical approach to the wavelength selection problem using mathematical and computer techniques is presented in Appendix C.

2. SPECTRAL DATA

Introduction and Summary

In this section, absorption coefficient spectral data from a variety of sources is presented. This data was subsequently used for wavelength selection and linear weight computation as described in the following sections of the report.

Much difficulty was experienced in reconciling laser measurements with high resolution spectrometer measurements. In general, the adage of using only laser absorption measurements for designing a laser system has been reaffirmed.

The molecular species considered for this contract were ozone (O_3), carbon dioxide (CO_2), water vapor (H_2O), ethylene (C_2H_4), and ammonia (NH_3). Reliable data was obtained for all of these gases except for water vapor. This absorber is especially difficult to characterize because of the predominant self-broadening that occurs.

Tables I and II give a tabulation of the summarized absorption coefficient data.* A composite spectral plot that illustrates the data in the 9.4 micron CO_2 band is shown in Figure 7. Two considerations must be taken into account when attempting to interpret this plot. First, only the deviation from a horizontal line is significant since neutral attenuation is rejected. The second consideration is that only deviations from the mean concentration are significant because the instrument is initially balanced. For example, if the CO_2 concentration only varies 32 ppm from the nominal 320 ppm shown in the plot, then the actual interference level would be reduced by an order of magnitude from the nominal curve shown.

---

*Blank spaces between data are linearly interpolated; blank spaces outside of the data range are set to zero.

J Value	Wavelength Microns	Wave Number CM^{-1}	Absorption Coefficient - ATM^{-1} CM^{-1}				
			O_3	CO_2	H_2O*	C_2H_4	NH_3
P40	9.733474	1027.382		7.426E-04			
P38	9.713998	1029.442		9.415E-04			
P36	9.684831	1031.478	6.670E 00	1.190E-03	1.430E-04		
P34	9.675971	1033.488	2.990E 00	1.452E-03		2.400E 00	
P32	9.657416	1035.474	5.980E 00	1.769E-03		7.900E-01	3.400E-01
P30	9.639166	1037.434	6.440E 00	2.089E-03		1.400E 00	9.000E-02
P28	9.621219	1039.369	9.440E 00	2.418E-03		2.600E-01	6.000E-02
P26	9.603573	1041.279	5.980E 00	2.773E-03		2.500E-01	1.000E-01
P24	9.586227	1043.163	6.900E-01	3.082E-03		4.600E-01	4.700E-01
P22	9.569179	1045.022	1.840E 00	3.446E-03		9.000E-01	3.800E-01
P20	9.552428	1046.854	5.290E 00	3.586E-03		4.400E-01	2.580E 00
P18	9.535972	1048.661	6.450E 00	3.686E-03		8.700E-01	2.600E-01
P16	9.519808	1050.441	8.980E 00	3.765E-03		2.200E-01	2.200E-01
P14	9.503937	1052.196	1.266E 01	3.662E-03		1.500E-01	3.400E-01
P12	9.488354	1053.924	1.220E 01	3.518E-03		1.800E-01	1.030E 00
P10	9.473060	1055.625	5.980E 00	3.268E-03		4.600E-01	3.900E-01
P8	9.458052	1057.300	1.266E 01	2.706E-03			
P6	9.443325	1058.949		2.137E-03			
P4	9.428886	1060.571		1.467E-03			
R4	9.367339	1067.539		1.896E-03	1.390E-04		
R6	9.354414	1069.014		2.500E-03			
R8	9.341758	1070.462		3.071E-03			
R10	9.329370	1071.884	0.	32502E-03			
R12	9.317246	1073.278		3.839E-03		3.600E-01	2.600E-01
R14	9.305386	1074.646		4.053E-03		9.000E-02	3.700E-01
R16	9.293786	1075.988	0.	4.118E-03		8.000E-02	7.200E-01
R18	9.282444	1077.302	1.000E-01	4.077E-03		3.100E-01	**1.050E 01
R20	9.271358	1078.591	0.	3.890E-03		6.700E-01	1.400E-01
R22	9.260526	1079.852		3.685E-03		1.900E-01	3.000E-02
R24	9.249946	1081.087		3.480E-03		1.100E-01	7.800E-02
R26	9.239615	1082.296		3.031E-03		2.000E-01	7.000E-02
R28	9.229530	1083.479		2.677E-03		1.200E-01	1.200E-01
R30	9.219690	1084.635		2.334E-03		5.000E-02	4.200E-01
R32	9.210092	1085.765		2.000E-03		2.400E-01	
R34	9.200733	1086.870		1.602E-03			
R36	9.191612	1087.948		1.313E-03	1.360E-04		
R38	9.182725	1089.001		1.079E-03			
R40	9.174070	1090.029		9.293E-04			

* The H_2O absorption coefficient is proportional to H_2O partial pressure (see text). The values listed in the table are for 100% relative humidity at 23 degrees C (73 degrees F) which is equivalent to 19.8 torr.

** See text.

Table I Absorption Coefficients for $00^{0}1$ - $02^{0}0$ (9.4 micron) CO_2 Band

J Value	Wavelength Microns	Wave Number CM-1	Absorption Coefficient - ATM^{-1} CM^{-1} O_3	CO_2	H_2O*	C_2H_4	NH_3
P40	10.811105	924.975		5.3981-04			
P38	10.787380	927.009		7.037E-04			
P36	10.764052	929.018		8.651E-04			
P34	10.741113	931.002		1.099E-03			
P32	10.718560	932.961		1.303E-03	1.800E-04		8.000E 00
P30	10.686386	934.895		1.539E-03			
P28	10.674586	936.804		1.834E-03			
P26	10.653156	938.689		2.052E-03			
P24	10.632090	940.549		2.278E-03		2.400E 00	
P22	10.611385	942.384		2.500E-03		1.200E 00	
P20	10.591035	944.195		2.731E-03		1.800E-00	
P18	10.571037	945.981		2.756E-03		3.600E 00	
P16	10.551387	947.743		2.786E-03		5.000E 00	
P14	10.532080	949.480		2.736E-03		3.200E 01	0.
P12	10.513114	951.193		2.595E-03			
P10	10.494484	952.882		2.335E-03			
P8	10.476187	954.546		1.984E-03			
P6	10.458220	956.186		1.580E-03			
P4	10.440579	957.801		1.091E-03			
R4	10.365168	964.770		2.725E-03			
R6	10.349277	966.251		1.870E-03			
R8	10.333696	967.708		2.301E-03			
R10	10.318424	969.140		2.608E-03			
R12	10.303458	970.548		2.867E-03			
R14	10.288797	971.931		2.978E-03			
R16	10.274438	973.289		3.050E-03			
R18	10.260381	974.623		3.019E-03			
R20	10.246625	975.931		2.870E-03			
R22	10.233167	977.215		2.708E-03			
R24	10.220006	978.473		2.449E-03			
R26	10.207142	979.706		2.211E-03			
R28	10.194574	980.914		1.955E-03			
R30	10.182301	982.096		1.667E-03			
R32	10.170323	983.253		1.412E-03			
R34	10.158637	984.384		1.157E-03			
R36	10.147246	985.489		9.449E-04			
R38	10.136146	986.568		7.581E-04			
R40	10.125340	987.621		5.879E-04			

* The H_2O absorption coefficient is proportional to H_2O partial pressure (see text). The values listed in the table are for 100% relative humidity at 23 degrees C (73 degrees F) which is equivalent to 19.8 torr.

Table II Absorption Coefficients for $00^{\circ}1$ - $10^{\circ}0$ (10.4 micron) CO_2 Band

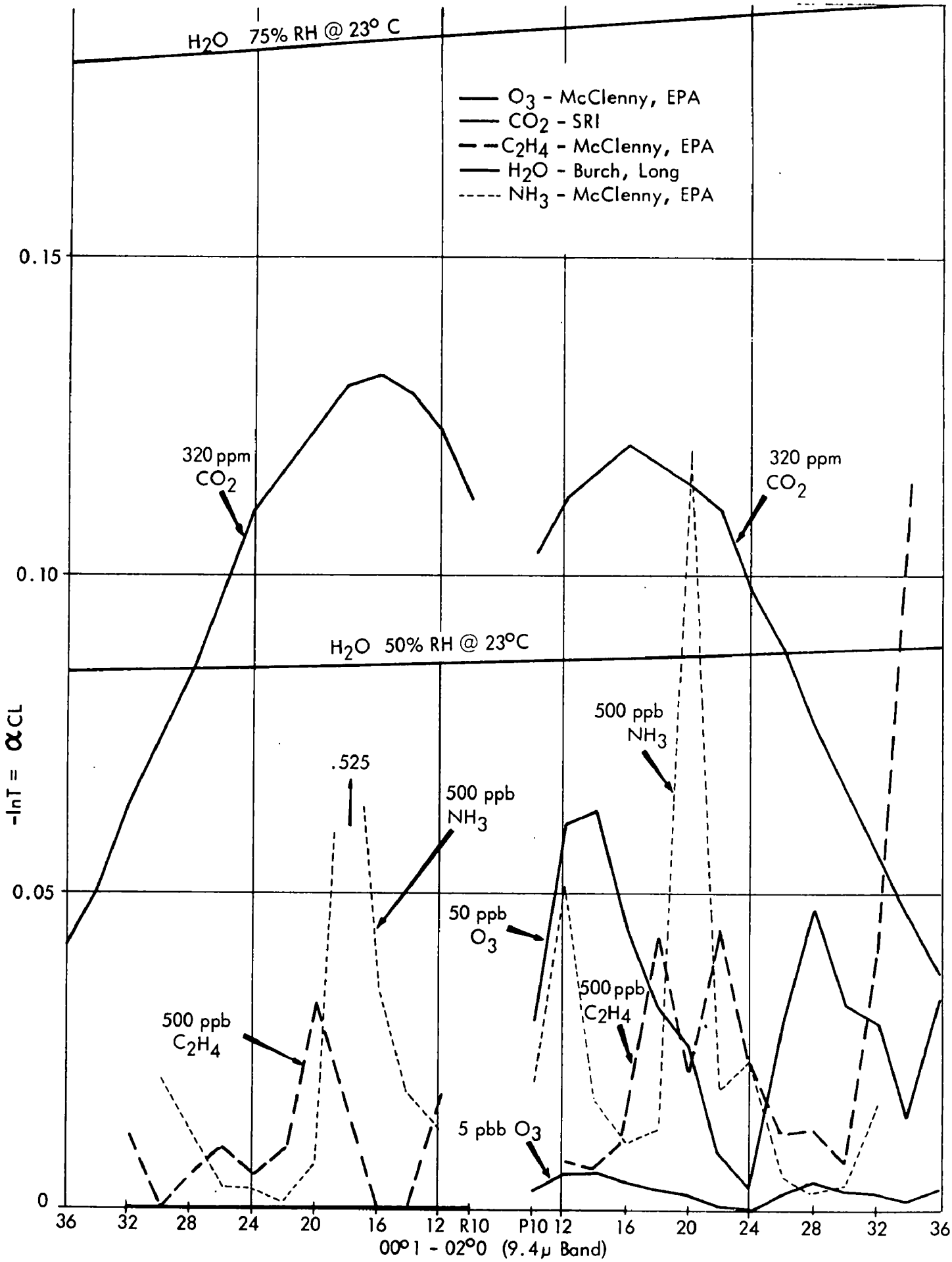

Figure 7. Composite Spectral Absorption in 9.4μ CO_2 Band

A more refined plot showing only the deviation about the mean for water vapor and carbon dioxide in the P branch is shown in Figure 8. As can be seen, water vapor is a serious interferent and its characterization is critical in detecting trace concentrations of ozone.

Observed stability of the monitoring system that uses linear weights derived from this spectral data has been poor under some conditions which are suspected to be attributable to relative humidity variations. Other sources of data noted in the following discussion of water vapor absorption coefficients also suggest significant departure from the assumed linear continuum as well as a bizarre interrelationship with aerosols. In Section C.5 a factor analysis of the system noise also points the finger of suspicion in this direction.

In particular, it is now believed that the R14 line that was used is sitting almost on top of a water vapor absorption line. At the writing of this report the number 1 system wavelength has been moved from the R14 line to the R16 line and operation under this modification is being evaluated.

For all of the above reasons, a water vapor laser measurements program is recommended for future air pollution monitoring systems that utilize laser absorption measurements in this spectral region. A research facility such as the 980 m cell at Ohio State University Electroscience Lab now operated by Dr. R.K. Long and associates would be ideal for this purpose. This particular facility is the one which was used in the past for obtaining the only reliable water vapor absorption laser measurements known to exist (Reference 4).

Some spectral instability can be attributable to variation in the CO_2 absorption coefficient with temperature. For the lines and linear weights that were used with the present system, a 40 degree F change in temperature causes an apparent change in ozone level of about 2.3 ppb. This level of unstability is not a limiting factor for the present system.

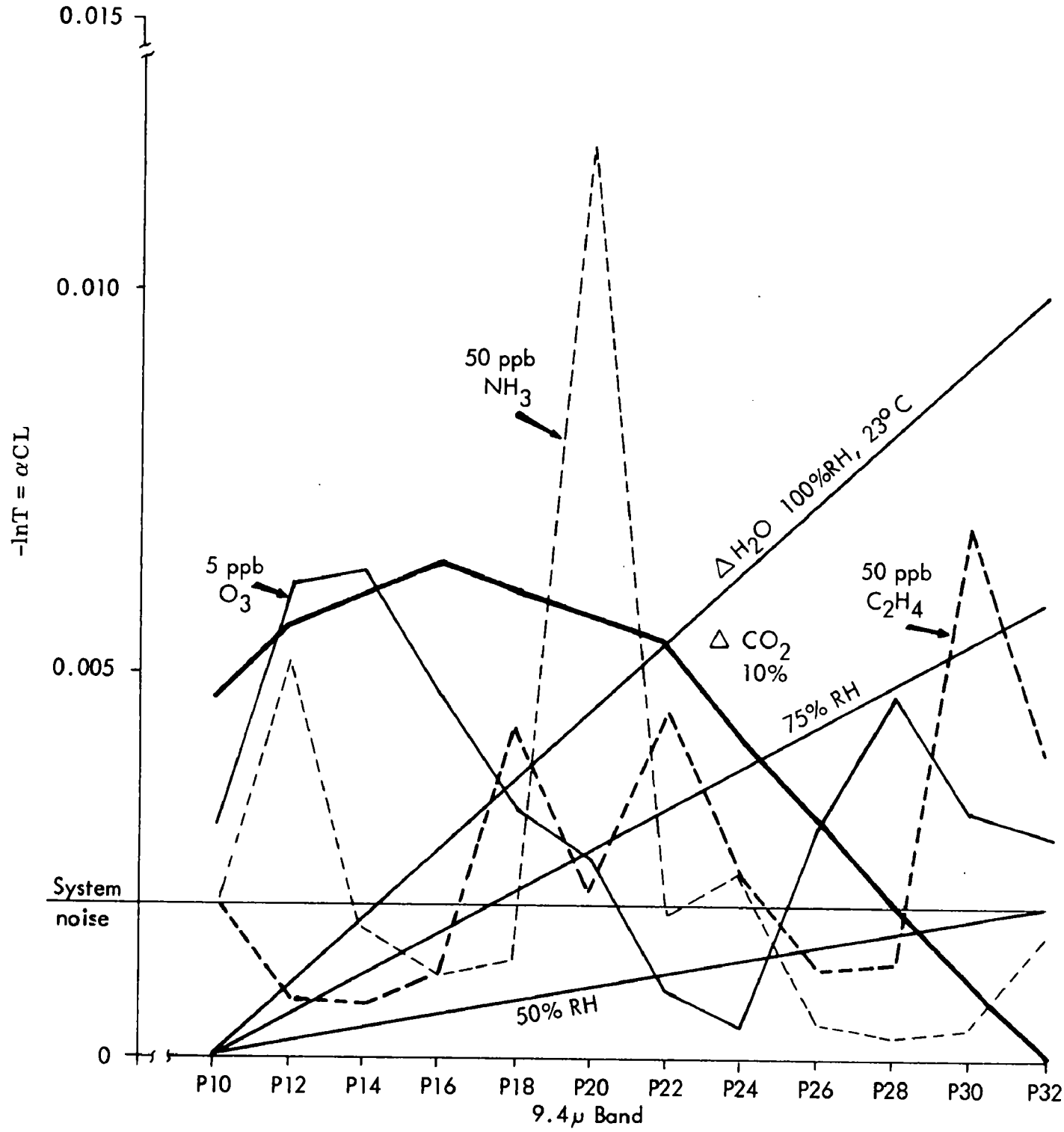

Figure 8. Composite Differential Spectral Absorption in P-Branch of 9.4μ CO_2 Band

However, if desired, this variation could be eliminated by changing linear weights as a function of ambient temperature or by considering the first order temperature variation as an additional interferent to be discriminated against.

A large absorption coefficient for ammonia was discovered in the 9.4 micron CO_2 band by direct laser absorption measurements performed by W.A. McClenny. This behavior has been previously unnoticed with spectrometer measurements which have obscured the true peaks because of resolution limits. In fact, this absorption coefficient is larger than the one in the 10.5 micron band which was heretofore thought to be the largest available.

Ozone (O_3)

Ozone absorption coefficient data was obtained from direct laser measurements (References 5 and 6) high resolution spectrometer (Reference 7) and theoretical computations (Reference 8) using line strength data (Reference 9). Figure 9 illustrates a comparison of the data which demonstrates very good consistency. In all cases, the measurements were made at standard temperature and pressure.* Because of the inherent accuracy of the laser measurements and good repeatability, McClenny's measurements were used as a basis for the ozone data and were transcribed onto our computer spectral library tape as listed in Tables I and II.

*It was subsequently determined that all of McClenny's measurements (References 5 and 12) were converted to 0 degrees C reference temperature by using the $T^{-1/2}$ proportionality law for the line half-width. It is noted that this scaling law is only appropriate at a line center. Moreover, the temperature dependence of the line intensity must also be taken into account (Ref. 9 (eq. 3) and (Ref. 11 (eq. 77)). In anv case, the difference is probably small compared to the spread of the other data. In addition, all of the wavelength selection and linear weight algorithms are more dependent on the relative ratios of absorption coefficients between wavelengths rather than the absolute magnitude.

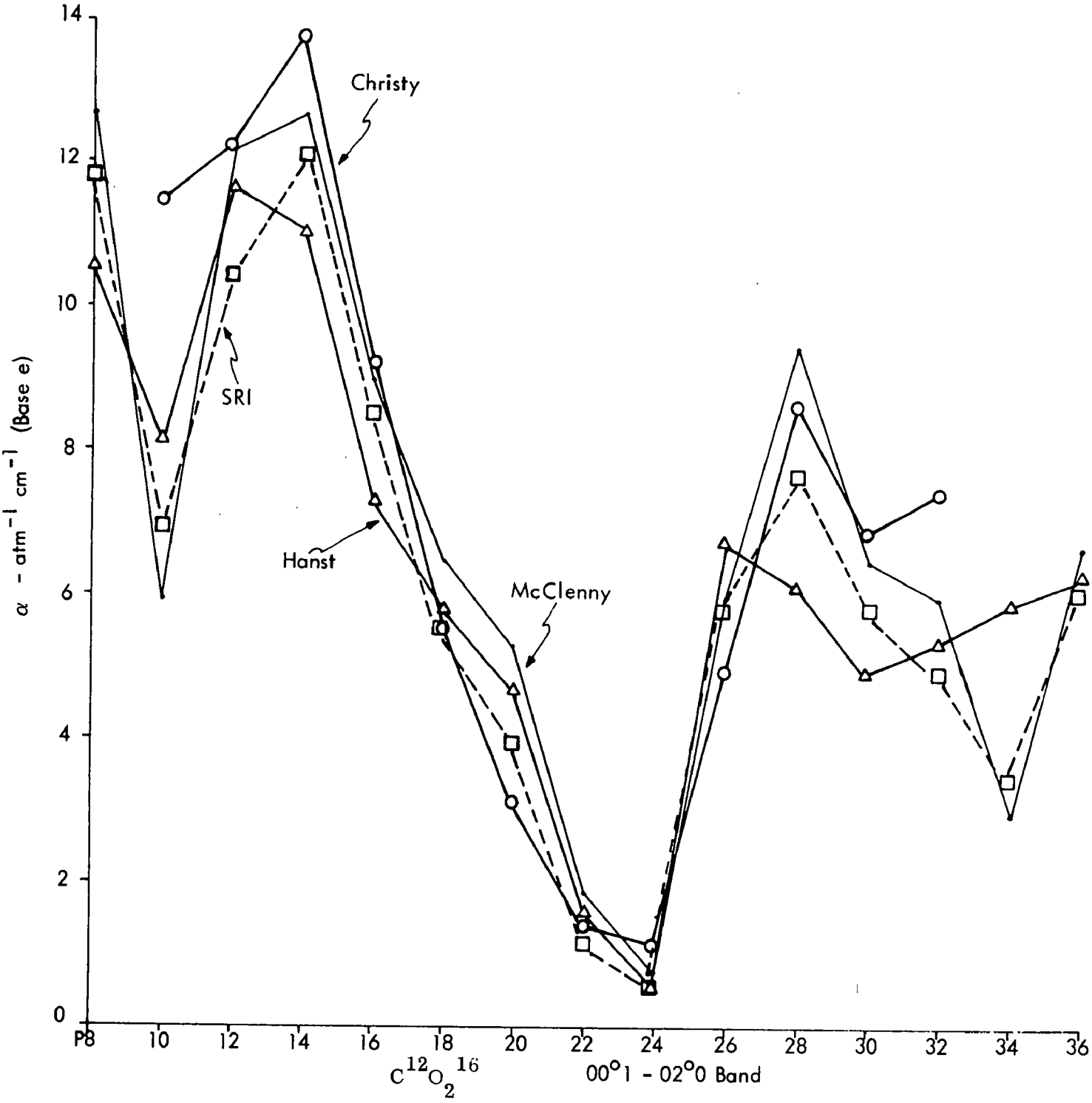

Figure 9. Ozone Absorption Coefficient Data Comparison in 9.4μ CO_2 Band

Carbon Dioxide (CO_2)

The CO_2 absorption coefficient data listed in Tables I and II was obtained from the SRI computer study (Reference 8) and is used exclusively as the basis for data on this species. These computed values are believed to be quite accurate as they are based on the most recent line strength and halfwidth data available (Reference 9). In addition, independent measurements of the P20 (10.591 micron) line absorption by Long (Reference 10) have determined the extinction coefficient to be about 0.08 km^{-1} at 320 ppm which corresponds to an absorption coefficient of 2.5×10^{-3}. This experimental value compares favorably with the computed value of 2.75×10^{-3} listed in Table II for the P20 line. Another report (Reference 11) that was obtained at a later date gives another theoretical set of data which agrees closely with the SRI data. Subsequent data from laser measurements (Reference 12) (see footnote in last section) was received and is compared with the SRI data in Figure 10. A close agreement is noted between the data.

The SRI computer printout included several sets of data for different temperature and pressures. A table of relative absorption coefficient variations for several lines is shown in Table III. As can be seen, the relative absorption coefficient is not very dependent upon pressure, however, it is somewhat affected by temperature for some lines. A relative variation between the P14 and P24 line of about 6% is noted for the temperature range of 50-90 degrees F. On the other hand, very little relative variation is evident between the R14 and P14 lines.

For the present system the R14, P14, and P24 (9.4 micron band) were weighted approximately as -0.5, + 1.0 and -0.5 respectively for the measurement of ozone. Refering to Figure 7, the 6% CO_2 absorption variation between the P14 and P24 lines for a 40 degree F temperature change can then be converted to an equivalent ozone variation of about 2.3 ppb. This level of unstability is not a limiting factor for the present system. However, if desired, this variation could be eliminated by changing linear weights as a function of temperature or by considering the first order temperature variation as an additional interferent to be discriminated against.

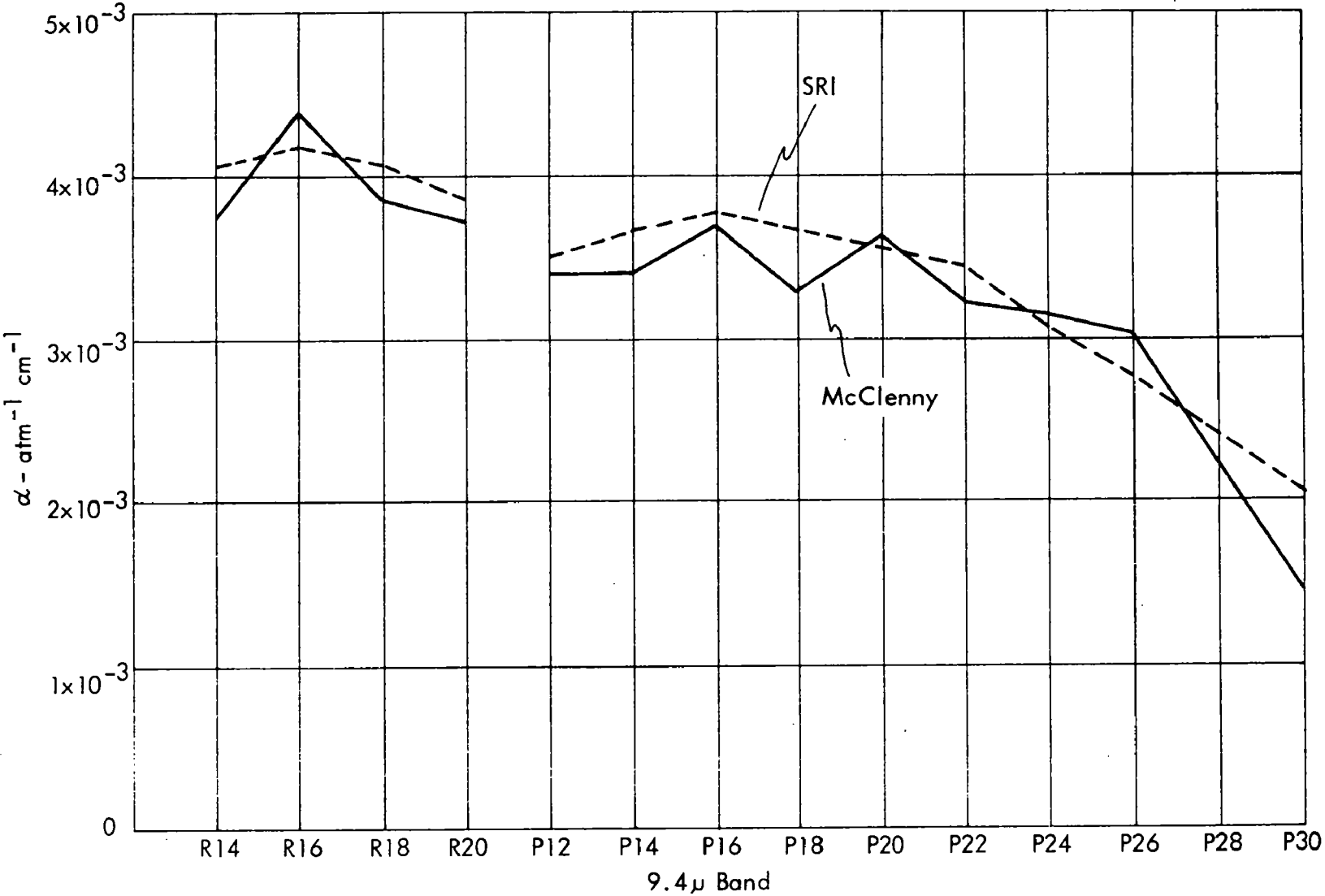

Figure 10. CO_2 Absorption Coefficient Data Comparison

Temperature	Pressure	Relative Absorption Coefficient Wavelength - microns					
Degrees F	Bars	9.305386 (R14)	9.503937 (P14)	9.586227 (P24)	10.532080 (P14)	10.674586 (P28)	10.718560 (P32)
70	1.0031(-1%)	1.106 621	1.000 000	0.841 477	0.747 132	0.500 629	0.355 691
70	1.0132(nom)	1.106 650	1.000 000	0.841 471	0.747 138	0.500 720	0.355 710
70	1.0233(+1%)	1.106 678	1.000 000	0.841 464	0.747 143	0.500 809	0.355 729
50	1.0132	1.106 080	1.000 000	0.816 962	0.731 860	0.468 236	0.327 494
70	1.0132	1.106 650	1.000 000	0.841 471	0.747 138	0.500 720	0.355 710
90	1.0132	1.107 239	1.000 000	0.864 891	0.761 726	0.532 764	0.384 019

Table III. Relative CO_2 Absorption Coefficient Variation with Pressure and Temperature

Water Vapor (H_2O)

In the 8-14 micron water vapor window, the absorption is a relatively smooth function of wavelength. This continuum is believed to be mostly due to the extreme wings of strong collison-broadened absorption lines centered more than 10-20 cm^{-1} away (Reference 13). However, the effects of pressure induced absorption resulting from forbidden transitions of unperturbed molecules and the possible existence of the water dimmer (H_2O:H_2O) have also been suggested (References 9 and 14).

The absorption coefficient due to the continuum can be written as (References 9 and 13).

$$k = C_s p + C_b p_b \qquad (3)$$

where C_s is the self-broadening coefficient, C_b is the foreign gas broadening coefficient, p is the partial pressure of the species, and p_b is the foreign gas partial pressure. As can be seen from (3), for small p, the absorption coefficient is nearly constant which is usually the case for most atmospheric gases. On the other hand, for large p, the first term dominates and the absorption coefficient is proportional to p. In this case, the log transmission is proportional to $-p^2$. It has been experimentally demonstrated that the latter situation occurs for atmospheric water vapor absorption under normal relative humidity conditions (Reference 4).

In the SRI computer study, (Reference 8) the water vapor absorption due to the superposition of many lines was computed. However, the effects of self-broadening, which is predominant for water vapor, were neglected and so these results were not useful.

Figure 11 shows the spectral dependence of C_s for water vapor continuum absorption for three temperatures that has been experimentally determined by Burch (Reference 14). The ratio of the coefficients at the 9.552 micron and 10.591 micron CO_2 P20 lines is seen to be about 0.8 which is in good agreement with McCoy, (Reference 4). After a suitable conversion of units (2.69×10^{19} mol/cm^3 1 atm = 760 torr), the absolute value of the 10.591 micron coefficient indicated in Figure 11 is about 11.6×10^{-4} torr^{-2} km^{-1} at 23 degrees C which is at variance with the value of 8.39×10^{-4} torr^{-2} km^{-1} reported by McCoy. In a recent report by Trusty, (Reference 11) spectrophone measurements of water vapor absorption at this same line were noted to be about 50% higher than McCoy's measurements, thus giving more credibility to Burch's measurements.

The C_b value for nitrogen has been measured to be $C_b \approx 0.005\ C_s$ at room temperature by McCoy (Reference 4) and Burch (Reference 9) considers this to be a reliable measurement.

The data in Figure 11 was used as a basis for the water vapor absorption coefficients. The values listed in Tables I and II were computed from (3) and Figure 11 for a relative humidity of 100% and at a temperature of 23 degrees C (73 degrees F), i.e., for a 19.8 torr partial pressure of water vapor. For other partial pressures, the absolute value of the coefficients will be scaled accordingly, however, the relative absorption coefficient pattern will be invariant.

The wavelength selection and linear weight computations described in Sections C.3 and C.4 were based upon the continuum values derived from Figure 11 (originally obtained from Reference 9) due to the unavailability of any other data at that time. Since then, additional data concerning the line structure has been uncovered.

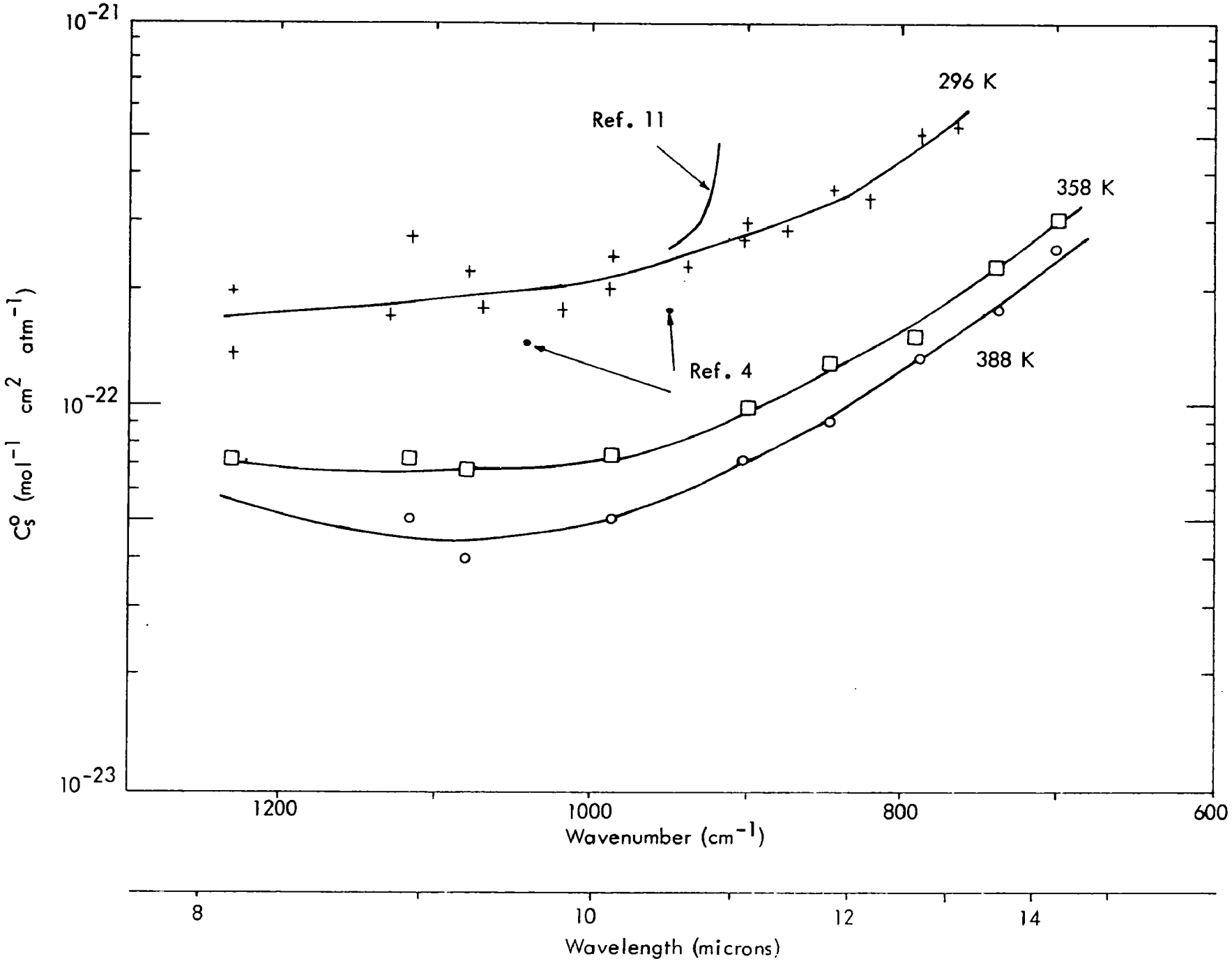

Figure 11. Comparison of the continuum absorption coefficient at three temperatures. (From Ref. 14)

Table IV lists some of the more significant water vapor line data that were used in the SRI study (Reference 8). This data was obtained from a magnetic tape described in Reference 9. Figures 12 and 13 show measured water vapor absorption spectra, from Burch (Reference 13) and Hanst (Reference 7) respectively, which are in remarkable agreement with Table IV. It is especially noted that the R14 (1074.65 cm^{-1}) CO_2 laser line that was used in the present monitoring system is sitting almost directly on top of the 1074.430 cm^{-1} water vapor line. This could explain some of the unstability that was noted.

In Reference 11, CO_2 laser measurements with a spectrophone have demonstrated a 2:1 variation in the water vapor absorption coefficient from P8 (954.54 cm^{-1}) to P36 (929.02 cm^{-1}). These measurements are plotted in Figure 11 and show a significant deviation from Burch's continuum.

Another source of anomoly has been suggested by Carlon (Reference 15) which attributes additional broadening to inelastic collisions involving water aerosols. This effect has been experimentally verified and has been used to reconcile apparent inequalities of absorptance and emittance in atmospheric field measurements.

In view of all of the uncertainties mentioned above, a water vapor laser measurements program would be highly desirable for future work in this area in order to pin down the true behavior of water vapor.

Ethylene (C_2H_4)

The absorption coefficients for ethylene listed in Tables I and II were obtained by direct laser absorption measurements (Reference 12) and represent the most reliable information to date. The maximum absorption coefficient of 32 at the P14 (10.532 micron) line agrees favorably with the value of 36 measured by Hanst (Reference.7).

Wavenumber cm^{-1}	Linestrength	Halfwidth cm^{-1}
922.142	1.690E-23	0.048
924.988	9.730E-24	0.050
948.260	1.980E-23	0.038
976.012	7.700E-24	0.040
1066.200	3.730E-23	0.047
1074.430	1.350E-23	0.050
1091.240	2.040E-23	0.056

Table IV. Partial Tabulation of H_2O Vapor Line Data (From Ref. 8).

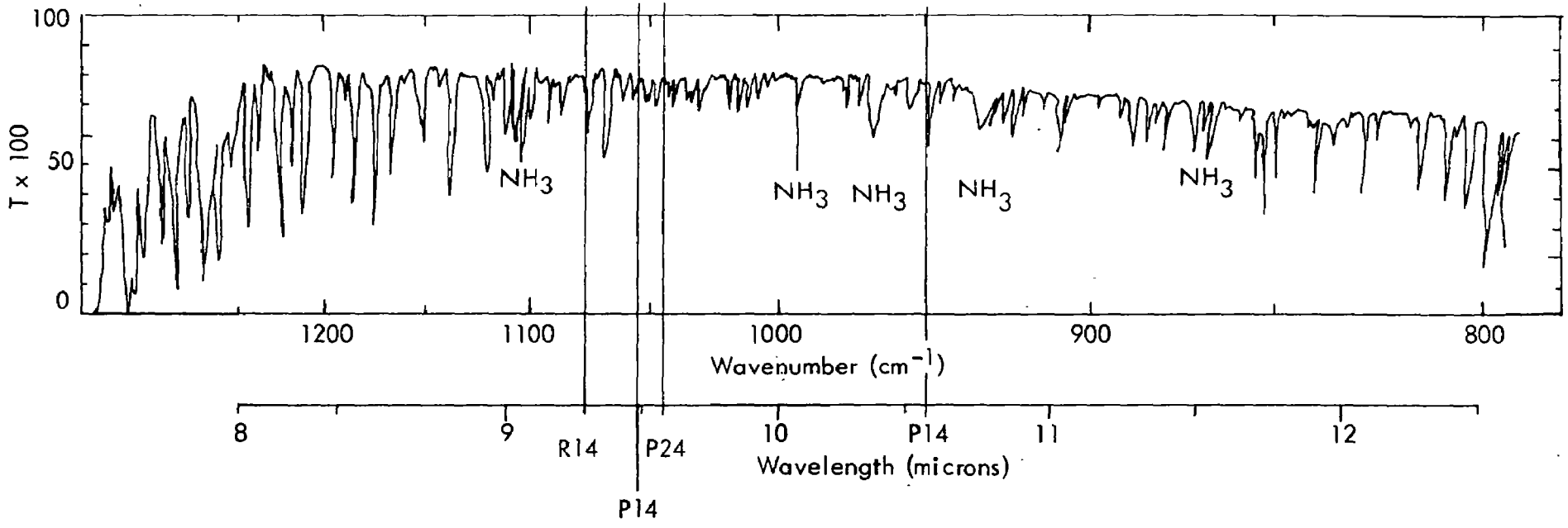

Figure 12. Representative spectrum of H_2O between 800 and 1250 cm^{-1}. The sample is pure H_2O at 14.2 torr; path length is 1185 meters; $u = 5.48 \times 10^{22}$ molecules/cm^2; temperature is 296K. The spectrum contains a few lines due to a trace of ammonia in the sample; some of the stronger lines are indicated. The ammonia lines can be accounted for by comparing the spectrum with one of pure ammonia. (From Reference 13).

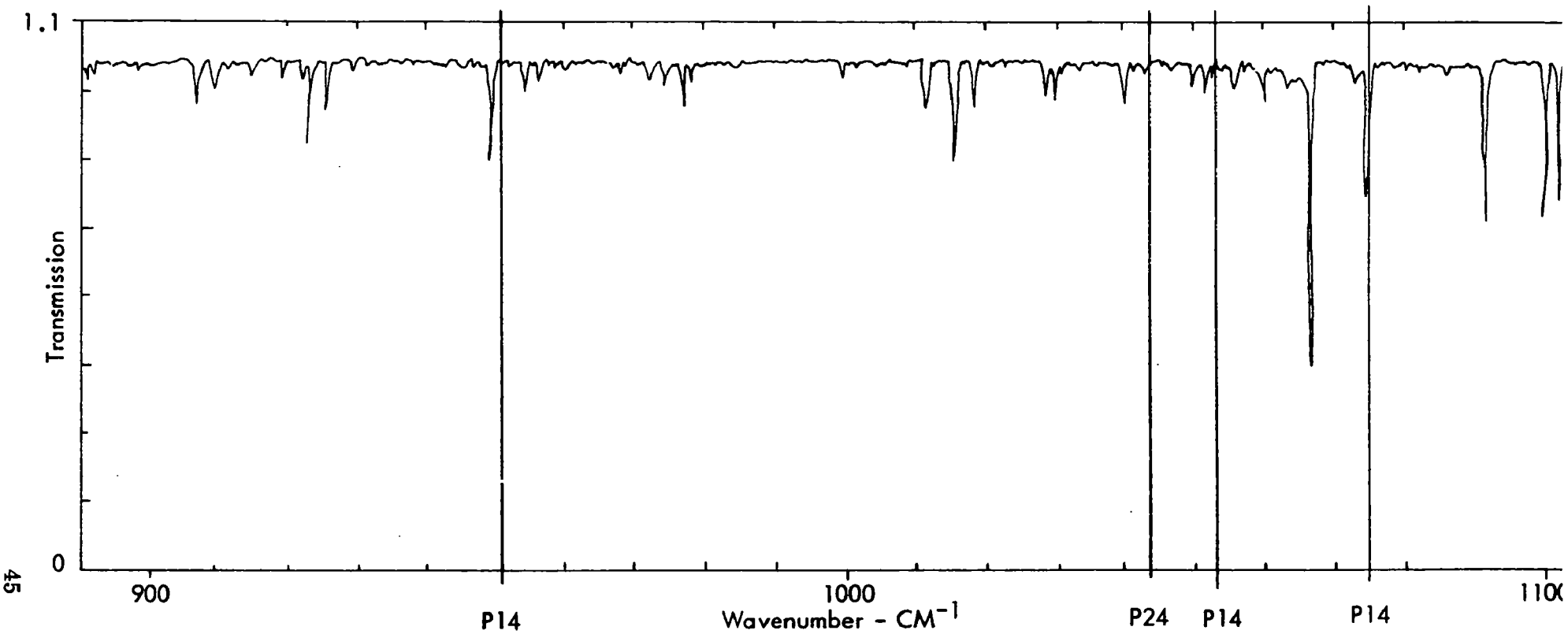

Figure 13. Spectrum of 383 meters of room air at 750 torr on a rainy day (March. 31, 1972) in Research Triangle Park, N. C. Recorded on the digital FTS system at 0.5 cm^{-1} resolution using a Hg-Cd-Tel detector. (From Hanst, Ref. 7).

Ammonia (NH_3)

The absorption coefficients listed in Tables I and II were also obtained by direct laser absorption measurements (Reference 12). The P32 (10.7186 micron) absorption coefficient of 8.0 is lower than the value of 32 previously measured by Hanst (Reference 16). However, at that time, the wavelength of the P32 line was not accurately known and the absorption coefficient was measured at 10.717 microns. In addition, the resolution of the spectrometer used by Hanst was not fine enough to adequately measure the fine line structure of ammonia.

The surprising feature of the data is the large absorption coefficient (2.58) in the 9.4 micron band at the P20 (9.5524 micron) line. A narrow peak has been previously noted with high resolution spectrometers at that wavelength, however, the magnitude of the fine structure was not evident.

It was recently determined that the ammonia coefficients shown in the R-branch of Table I are displaced one J value too high, e.g., the R12 value listed is really the R10 value. In addition, remeasurement of the true R16 coefficient has given a value of 14.0 rather than the value of 10.5 indicated by the table. However, for consistency, the values listed in Table I are shown as they were used in the subsequent wavelength selection and linear weight computations.

3. WAVELENGTH SELECTION

In Appendix C, the philosophy and methodology of wavelength selection is delineated as a two step process. First a preliminary wavelength selection is used to reduce the number of potential lines (74) to a manageable number (say 10) by using a computer program called LWSP. This program eliminates wavelengths of low information by an iteration process of adjusting the power allocation. The second step

in the selection process involves a combinatorial evaluation of the reduced set by which all combinations are ranked in accordance with their performance in measuring ozone. An existing program (MFIL) was modified to perform this operation and is called CMFIL.

A 25 iteration LWSP run resulted in the line selection illustrated in Figure 14. The solid lines in this figure represent the linear weights applied to each wavelength and their length is indicative of the relative importance of each line. The X's designate normalized ozone absorption coefficients and the +'s designate the average interferent noise level.

The top 9 wavelengths from the LWSP output were combined with the P14 (10.5321 micron) ethylene line to form the basis set for CMFIL. Combinations of this set were then evaluated and ranked using CMFIL and the output listing is shown in Figure 15. As expected, the P12 and P14 (5 and 6) lines, which correspond to the peak ozone absorption, appear in all of the highest rankings. The R16, R14, and P24 (3, 4, 8) lines also predominately appear in all of the highest rankings and are therefore indicated as good reference lines.

The combination 4, 6, 8, 10 (R14, P14, P24, P14) was selected as the combination that gave the highest signal-to-noise-ratio (SNR) while retaining the ethylene line. In retrospect, this may have been a bad initial choice since the R14 line has been shown in Section C 2 (water vapor) to fall right on top of a water vapor absorption line. Using the R16 line instead of the R14 line would result in the 3, 6, 8, 10 combination which, as can be seen from Figure 15, is only slightly inferior to the 4, 6, 8, 10 combination.

The effect of the number of lines used to detect ozone has also been determined and is illustrated in Figure 16. As can be seen, a 3 wavelength system (which we essentially have at the present due to the retention of the 10.5321 micron ethylene line) provides near optimum performance with a minimum of complexity. A two-wavelength ozone system results in about 1/2 the sensitivity.

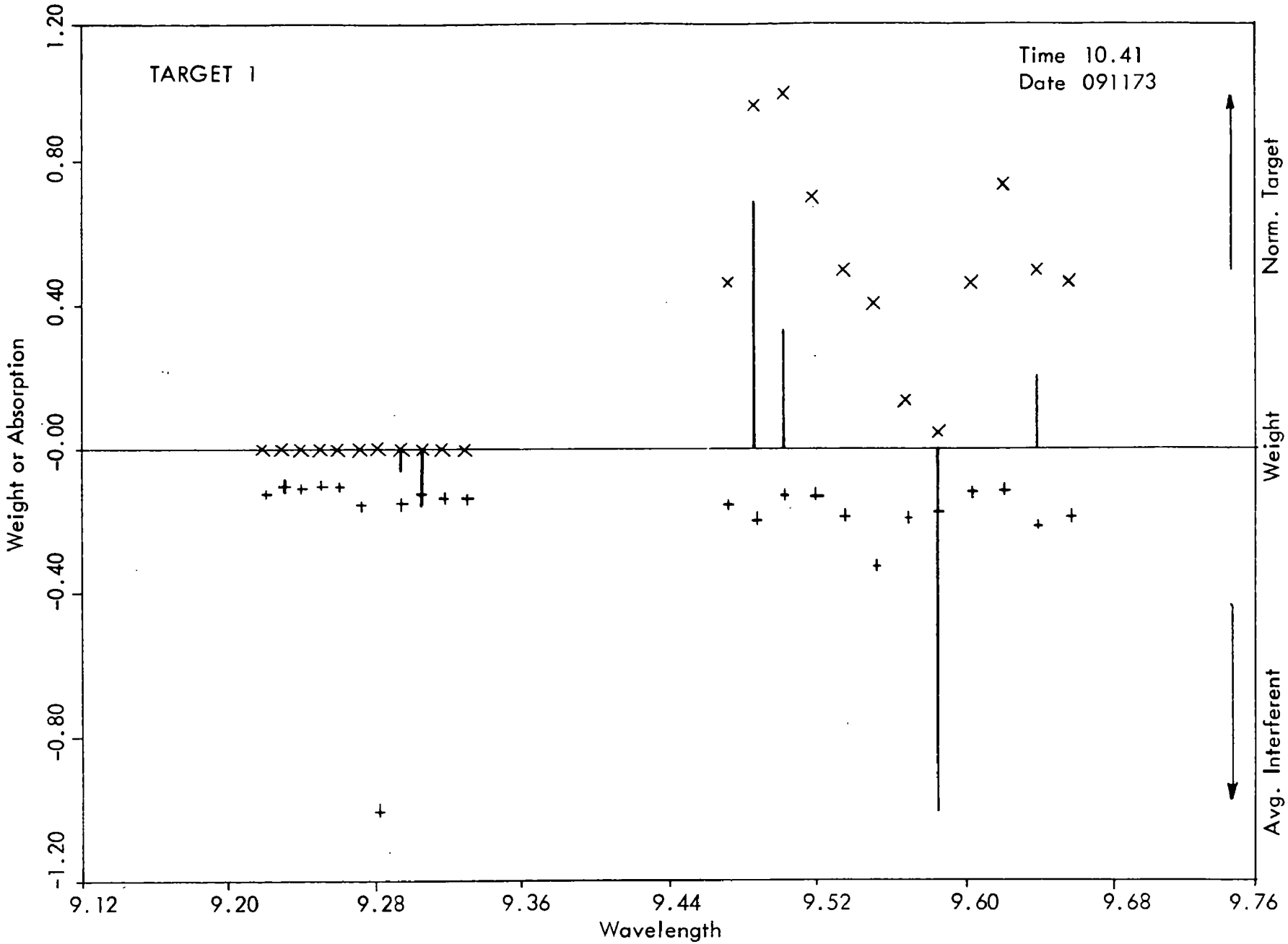

Figure 14. Resultant Line Selection From a 25 Iteration LWSP Run

COMBINATIONS OF 10 WAVELENGTHS, 4 AT A TIME, USING 1 THROUGH 10

1(R30)	2(R18)	3(R16)	4(R14)	5(P12)	6(P14)	7(P20)	8(P24)	9(P30)	10(P14)
9.219690	9.282444	9.293785	9.303396	9.488384	9.503937	9.552428	9.586227	9.639166	10.532080
1094.635179	1077.302490	1075.987762	1074.565454	1053.923584	1052.195926	1046.854263	1043.163269	1037.434158	949.480057

SNR	WAVELENGTHS			
342.76551	3	5	6	8
349.97922	4	5	6	8
312.19564	3	4	6	8
308.85627	4	6	8	9
306.03849	4	6	7	8
305.93972	1	4	6	8
305.91113	4	6	8	10
305.13256	2	4	6	8
304.51427	3	6	7	9
303.22335	2	4	5	8
303.15428	2	3	6	8
301.36205	2	3	8	9
297.51736	1	3	6	8
294.79319	3	6	8	9
293.85301	3	6	8	10
296.24268	3	5	7	8
279.90512	4	5	7	8
276.71186	3	4	5	6
275.89353	1	6	8	9
274.65038	4	5	6	7
274.63558	5	6	8	9
274.20047	3	5	6	9
273.74134	1	5	6	8
272.53618	3	5	8	9
269.06572	5	6	8	10
267.67399	1	2	5	8
267.29064	1	3	5	6
265.41749	3	4	6	9
264.66051	4	5	6	9
263.90549	2	5	6	8
263.39037	5	6	7	8
262.15083	3	4	5	8
261.71070	3	5	8	10
261.69417	1	3	5	8
261.33820	1	3	4	6
260.53625	1	4	5	6
256.36244	1	6	8	10
255.97542	4	5	8	9
255.81315	2	4	5	6
255.19032	3	4	6	10
254.97141	1	4	5	7
254.87717	2	5	8	9
253.81233	1	4	6	9
253.73939	1	4	6	10
253.57040	1	3	5	7
253.29642	2	3	4	6
252.58559	1	4	6	7
252.54690	3	4	5	7
252.36794	2	5	8	10
252.09652	1	2	6	8
251.93693	4	5	6	10
251.87298	3	5	6	7
251.85802	1	6	7	8
251.27319	1	5	7	8
250.61897	5	7	8	9
250.21135	3	4	6	7
250.19777	3	5	6	10
249.58182	2	6	8	9
249.22482	1	2	4	6
248.84101	1	2	4	5
248.78335	4	6	7	9
248.77027	5	7	8	9
248.29075	4	6	9	10
247.97900	5	8	9	10
247.93598	2	4	6	9
247.77067	1	3	6	9
247.45409	1	3	6	10
245.94080	2	4	6	7
245.82719	2	4	5	9
244.40575	2	3	4	5
243.89147	2	3	5	6
243.71170	5	7	8	10
243.60587	1	2	3	5
243.35941	1	2	3	6
242.83404	4	5	7	9
242.31198	2	6	8	10
242.21866	5	7	8	10
241.97637	2	3	6	9
241.61773	3	5	7	9
241.36281	1	3	6	7
240.94113	2	5	7	8
240.30483	2	3	5	9
240.02936	1	5	8	9
239.93545	4	6	7	10
239.43621	4	5	7	10
239.30415	2	4	5	7
239.06207	2	3	6	7
238.81597	2	4	6	10
238.67391	4	5	8	10
239.03473	3	6	7	9
237.79903	1	4	5	8
237.11015	3	6	9	10
233.40496	2	4	5	10
232.92765	3	5	7	10
232.72962	2	3	5	7
230.29138	2	3	6	10
230.07530	2	6	7	9
229.37146	5	8	9	10
225.27651	2	3	5	10
224.25596	3	4	5	10
223.71757	3	4	5	9
222.75214	3	6	7	10
221.91657	1	3	4	5
221.79184	1	5	6	7
221.72933	1	3	5	10
219.13799	1	3	5	9
217.17555	3	5	9	10
210.61611	1	5	8	10
207.95295	1	5	7	9
207.26697	1	5	7	10
207.69003	1	2	5	7
199.02153	1	4	5	10
196.10733	1	4	5	9
194.74768	4	5	9	10
194.55730	1	2	6	7
190.88354	1	2	5	6
189.43723	1	2	5	10
187.72115	1	6	7	10
187.11071	1	2	5	9
186.21151	1	6	7	9
178.41654	1	2	6	10
175.61229	1	2	6	9
170.94914	1	6	9	10
170.50025	1	5	6	10
167.66537	1	5	6	9
148.87980	1	5	9	10
133.66503	5	7	9	10
128.31329	1	8	9	10
126.12063	2	7	8	9
125.25156	2	5	6	7
121.69051	2	4	7	8
121.13097	2	3	7	8
120.92291	2	5	7	10
120.54597	7	8	9	10
120.22767	2	5	7	9
114.37204	2	6	7	10
113.42289	1	2	7	8
112.15117	2	6	7	9
111.14874	2	7	8	10
110.51521	5	6	7	9
109.34220	1	4	9	10
108.90607	6	7	9	10
108.72393	1	3	9	10
106.33460	1	2	9	10
106.23508	2	8	9	10
105.35591	1	7	9	10
105.16549	2	5	9	10
102.74894	4	8	9	10
101.46705	3	8	9	10
100.53568	2	4	7	10
97.74854	2	3	7	10
96.75291	1	7	8	9
96.41665	3	7	8	9
95.93617	4	7	8	9
95.44906	1	2	4	7
95.41243	2	3	4	7
94.81743	2	6	9	10
93.66670	1	2	3	7
92.95010	2	4	7	9
89.32134	2	3	7	9
89.11746	3	7	9	10
87.39312	4	7	9	10
86.63700	5	6	9	10
85.68824	5	6	7	10
83.73742	1	2	7	10
83.09687	1	3	8	9
81.86382	1	4	8	9
81.43993	2	5	6	9
81.24553	1	2	8	9
80.72606	2	4	9	10
80.66571	3	4	9	10
79.86368	1	2	7	9
79.75653	2	3	8	9
79.63809	2	4	8	9
78.25382	2	3	9	10
77.84106	3	4	8	9
72.77689	1	3	7	9
71.07554	1	4	7	9
70.41138	3	4	7	9
66.04934	1	3	4	9
66.03707	1	2	4	9
65.63147	1	2	3	9
59.21455	2	3	4	9
56.67115	1	3	7	8
53.56933	1	3	7	10
52.73161	3	4	7	10
52.03757	3	7	8	10
51.93213	1	3	4	7
51.89094	3	4	7	8
47.31789	1	4	7	8
46.38994	4	7	8	10
46.23492	1	4	7	10
45.73034	1	7	8	10
27.79319	2	5	6	10
13.52432	2	7	9	10
12.39822	1	3	8	10
12.22000	1	4	8	10
11.58959	3	4	8	10
11.22214	1	3	4	8
10.14982	1	2	4	8
10.13951	2	4	8	10
10.07950	1	2	3	9
10.69344	2	3	8	10
10.61533	2	3	4	9
10.37207	1	2	8	10
0.22681	1	2	3	4
0.22353	1	2	3	10
0.21490	2	3	4	10
0.20164	1	2	4	10
0.	1	3	4	10

Figure 15. CMFIL OUTPUT LISTING

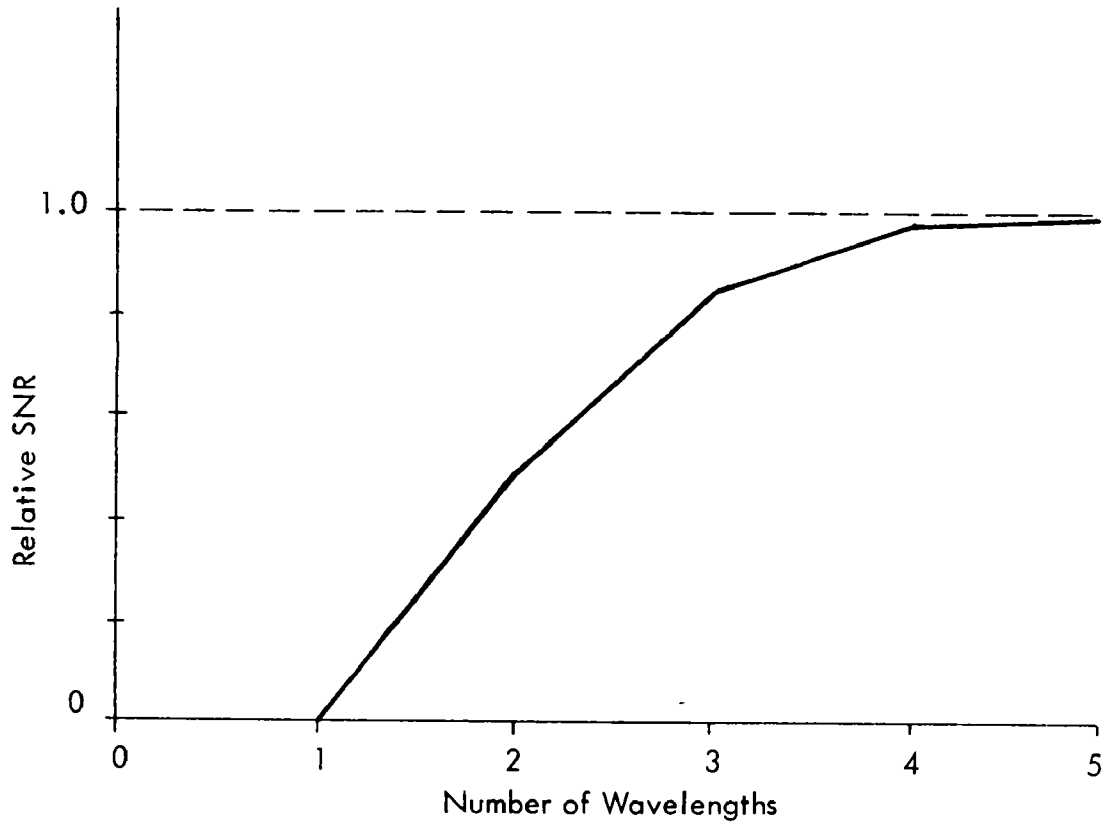

Figure 16. Signal-to-noise ratio as a function of the number of wavelengths used for the measurement of ozone.

4. LINEAR WEIGHT COMPUTATION (MFIL)

After the four wavelengths were selected, the optimum linear weights for measuring each species were computed using the MFIL program. The absorption coefficients for these lines (R14, P14, P24, P14) from Tables I and II are shown in Table V. For lack of any better data at that time, the same variances listed in Table C-1 in Appendix C were assumed and are also listed in Table V . As more field data is accumulated, these estimates can be revised and more accurate linear weights can be computed.

Table VI lists the linear weights and relative SNR's that were computed by MFIL using the input data listed in Table V. The relative SNR's shown in Table VI are computed for an optical thickness of CL = 0.1. Therefore, the noise equivalent concentration (NEC) is given by

$$NEC = (10\ L\ SNR_{rel})^{-1} \tag{4}$$

where L is the path length in cm. For example, the present system monitors over a 1.34 km folded path. The NEC for ozone is then

$$NEC_{O_3} = (10 \times 1.34 \times 10^5 \times 305.9)^{-1} \cong 2.5 \text{ ppb}$$

for the assumed noise variances.

The cross response of the linear weights in Table VI to 0.1 CL of each species is shown in Table VII. These responses have been scaled so that the background noise level is unity. Therefore, the diagonal terms are the same as the SNR's listed in Table VI.

Species	Absorption Coefficient - ATM^{-1} CM^{-1}				
	R14	P14	P24	P14	Variance (CL)
O_3	0.	1.265892E 01	6.918318E-01	0.	25×10^{-6}
CO_2	4.052363E-03	3.661722E-03	3.082101E-03	2.736121E-03	10.0
C_2H_4	9.032525E-02	1.500705E-01	4.607009E-01	3.197261E 01	25×10^{-6}
NH_3	3.698675E-01	3.416207E-01	4.698566E-01	8.535154E-04	25×10^{-6}
H_2O	1.379555E-04	1.407015E-04	1.417035E-04	1.737966E-04	10^6
Neutral	1.000000E 00	1.000000E 00	1.000000E 00	1.000000E 00	1.0

Table V. Absorption Coefficients and CL Variance of Atmospheric Species

Species	Linear Weights				
	R14	P14	P24	P14	Relative SNR
O_3	-0.4745	1.0000	-0.5286	0.0029	305.8907
CO_2	0.9302	0.0559	-1.0000	0.0145	0.0175
C_2H_4	0.6508	0.0520	-1.0000	0.2962	110.3722
NH_3	-0.9171	-0.0619	1.0000	-0.0212	1.7920
H_2O	-0.9469	-0.0519	1.0000	0.0000	0.0001

Table VI. Linear Weights and SNR's for Atmospheric Species

Linear Weight	Response to 0.1 CL					
	O_3	CO_2	C_2H_4	NH_3	H_2O	Neutral
O_3	305.8907	0.29339E-02	-0.10789E 01	-0.20457E 01	0.21225E-04	-0.29074E-02
CO_2	0.28537E 00	0.0175	0.17755E 01	-0.19995E 01	-0.56256E-04	0.99228E-02
C_2H_4	-0.40088E 00	0.67632E-02	110.3722	-0.25674E 01	0.83622E-04	-0.11857E-01
NH_3	-0.14985E 00	-0.15042E-01	-0.50682E 01	1.7920	0.45641E-04	-0.34612E-02
H_2O	0.60282E 00	-0.16402E-01	0.63966E 01	0.17689E 01	0.0001	0.21823E-01

Table VII. Cross Response of Linear Weights

5. FACTOR ANALYSIS OF DRIFT

An attempt was made to characterize the spectral nature of the drift/noise associated with the monitoring system. A teletype output chart was examined for the date of Saturday, 20 October 1973 between the hours of about 1535 PM to 1605 PM. During this period, the weather conditions were damp and overcast and the drift/noise of the system was similar to the erratic behavior experienced in the mornings of clear days. A total of 68 data points was selected out of this record and the effects of printout round off error were minimized by sampling only after the last digit of most of the channels changed simultaneously in the positive direction.

A sample covariance matrix was computed from the data and an eigenvector/eigenvalue analysis was performed using the FACD program (Reference 17). Eigenvectors and eigenvalues are listed in Table VIII. The eigenvectors, or factors, represent an optimal basis for representing the spectral data in the sense of minimizing the rms reconstruction error for the ensemble, and the associated eigenvalues are a measure of the importance of each factor in this representation. The rms reconstruction error for the ensemble depends on how many factors are used and is numerically equal to the square root of one minus the sum of the normalized (by 68 in this case) eigenvalues. This error, of course, diminishes to zero for four factors since that is the dimensionality of the space.

In order to remove the effects of neutral attenuation, the factors listed in Table VIII were projected onto the neutral hyperplane, (1, 1, 1, 1), by subtracting 1/4 of the sum of the components from each vector. These vectors were then normalized to unit length and are listed in Table IX. The absorption coefficients of known atmospheri species were also projected and normalized in the same manner and are listed in Table IX for comparison.

No.	Eigenvalue	RMS Error	Eigenvector			
			R14	P14	P24	P14
1	6.298509E 01	27.1%	-4.6076	1.3684	-0.2501	-0.1778
2	3.534071E 00	14.8%	-4.7461	-1.2651	-0.1220	-0.2743
3	1.051795E 00	7.9%	-4.3835	-0.0751	0.3697	0.4917
4	4.290484E-01	0	0.1213	-0.2355	-0.9153	0.2837

Table VIII. Eigenvector/Eigenvalue Analysis of Data Record

Factor/ Species	Wavelength			
	1 (R14)	2 (P14)	3 (P24)	4 (P14)
F1	-.295	-.329	-.240	.864
F2	.757	-.646	-.012	-.099
F3	-.023	.117	.653	-.748
F4	-.407	-.559	.647	.320
O_3	-.310	.865	-.245	-.310
CO_2	.659	.274	-.299	-.633
C_2H_4	-.296	-.291	-.279	.866
NH_3	.212	.127	.494	-.833
H_2O	-.368	-.266	-.232	.862

Table IX. Comparison of Factors and Atmospheric Species

Examination of Table IX reveals a similarity between the dominant factor and both ethylene and water vapor. Since the presence of ethylene on that particular day is unlikely, the finger of suspicion is pointed in the direction of water vapor as a possible atmospheric interferent. The uncertainties of the water vapor absorption coefficients have been previously mentioned in Section C.2. However, any conclusions at this point would be premature considering the limited amount of statistical data processed.

If repeatable factor analysis of data taken on other days was obtained, a linear weight could be computed to reject this source of spectral interference no matter what its underlying source is.

D. SPATIAL FILTER

Experiments performed under Contract EHSD 71-8 showed that substantial improvement in system performance could be expected from the introduction of a cleanup aperature or spatial filter in the output beam of the laser. These results led to incorporation of a spatial filter in the laser under this contract.

In terms of optical theory, the function of the clean up aperture (spatial filter) is to filter the higher spatial frequency variations in the transmitted laser output beam particularly in the far field pattern. We can visualize the far field as the Fourier transform of the near field and vice versa. A small aperture located in the far field provides an abrupt cutoff of the spatial frequency of the near field and at the same time edits any non-uniform clutter in the far field. An aperture with a two-dimensional gaussian amplitude distribution would be a better solution, but more difficult to fabricate.

For the purposes of this experimental program, it was decided to use a near-circular aperture like an iris in the far field. In the application of this device it must be kept in mind that the near field will be a classical Airy disk pattern $(J_x/x)^2$ which is the two-dimensional Fourier transform of the uniformly illuminated circular cleanup aperture. This Airy disk pattern is characterized by fringes in the shape of rings that do not carry a large percentage of the laser power but are important in shaping the far field pattern that is formed on the retroreflector. If a larger percentage of the power in the rings is collected then the far field pattern formed upon the retroreflector will be a disk with sharp edges (a true image of the clean up aperture). Because the beam expander will not collect all the power exiting from the clean up aperture then the illumination of the disk in the far field will be non-uniform especially near the edges. The more of the rings or fringes from the clean up aperture that are collected by the beam expanding optics the more uniform the disk pattern and the less the effect of incoherent illumination. The tradeoff between aperture configuration and beam expander size was a fundamental objective of the experiment.

The spatial filter was introduced to the CO_2 laser breadboard system at a point between the coupling mirror and the beam splitter. The layout is shown in Figure 17. The single mode beam diameters from the laser for this particular laser design configuration are indicated on the figure. Note that the beam diameter, w, at the spatial filter is 0.67 mm. This is the nominal beam diameter, w, which is the distance between the 60 percent power point or the half-width to the $1/e^2$ power point. Figure 18 describes the amplitude and power of a Gaussian beam. This optical configuration was designed with the assistance of a computer simulation of the optical elements and the diffraction limited Gaussian beam.

Ten optical apertures were made from 5 mil stainless steel sheet, ranging in size from 0.1 mm to 2.0 mm. The beam intensity at the exit of the 122 mm beam expander was observed for each of these apertures. Some improvement was obtained as the aperture diameter was decreased down to 1 mm. Smaller diameters than that showed no measurable improvement in the uniformity of the beam at the beam expander exit. Figure 19 shows the map of the beam intensity at the beam expander exit for the two extremes. There is some spreading as well as smoothing of the beam at the aperture.

The solid lines in the figure are a map of the beam expander output at a single wavelength without a spatial filter. The dashed lines are the same plot using the 1 mm aperture. The observed improvement in the beam pattern is responsible for the majority of the improvement in the signal-to-noise and drift of the system, over that during the previous study program.

The original intent of the spatial filter was to place the aperture at a focal point that represented the far field pattern of the laser, i.e., the pattern that would be formed at a plane located more than w^2/λ from the coupling mirror of the laser. If one places a short focal length lens at the exit of a laser with a near-collimated output beam, then the far field pattern will occur at the point where the beam diameter is minimum (the waist) which would also coincide with the focal point of the lens. In the more usual case as in the ILAMS, none of these points coincide. A waist is formed within the 762 mm long portion of the laser cavity between the coupling mirror and

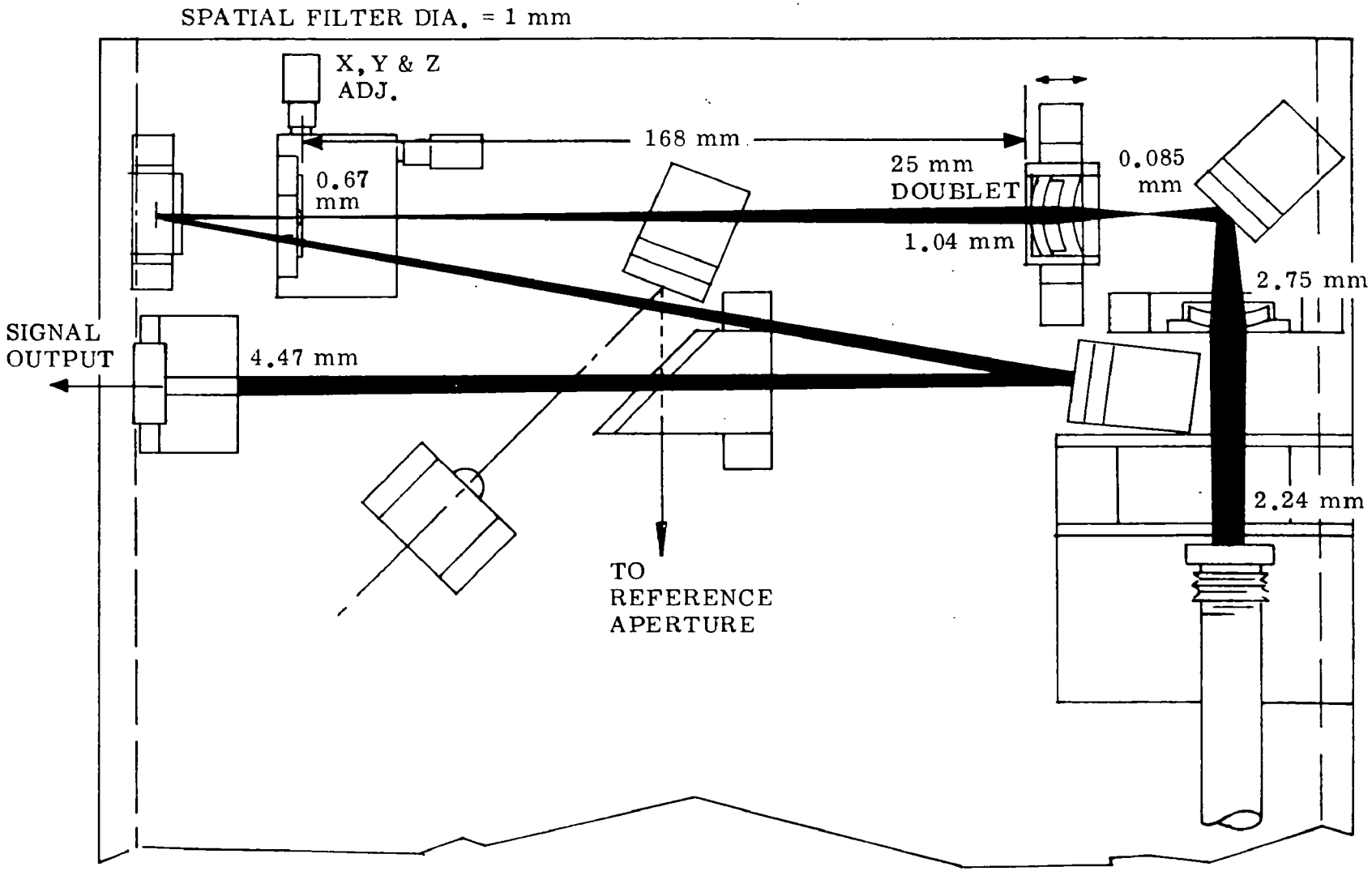

Figure 17. Spatial Filter Experiment Layout

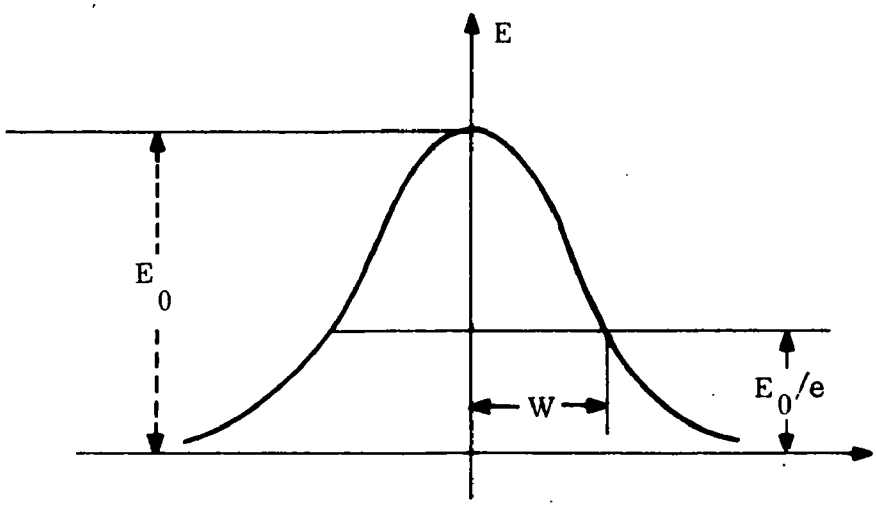

a. AMPLITUDE DISTRIBUTION OF THE FUNDAMENTAL BEAM

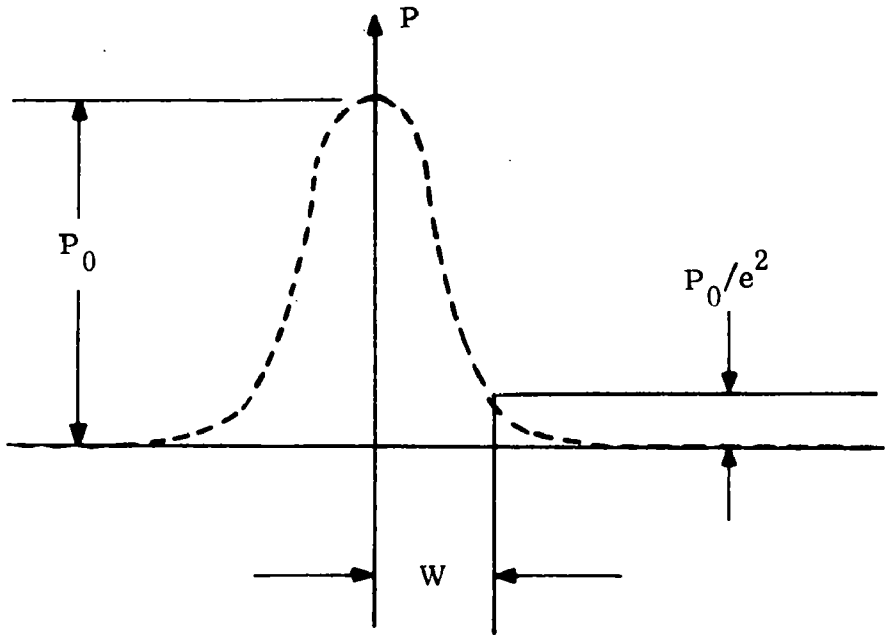

b. POWER DISTRIBUTION OF THE FUNDAMENTAL BEAM

Figure 18. AMPLITUDE & POWER DISTRIBUTION OF THE GAUSSIAN FUNDAMENTAL MODE

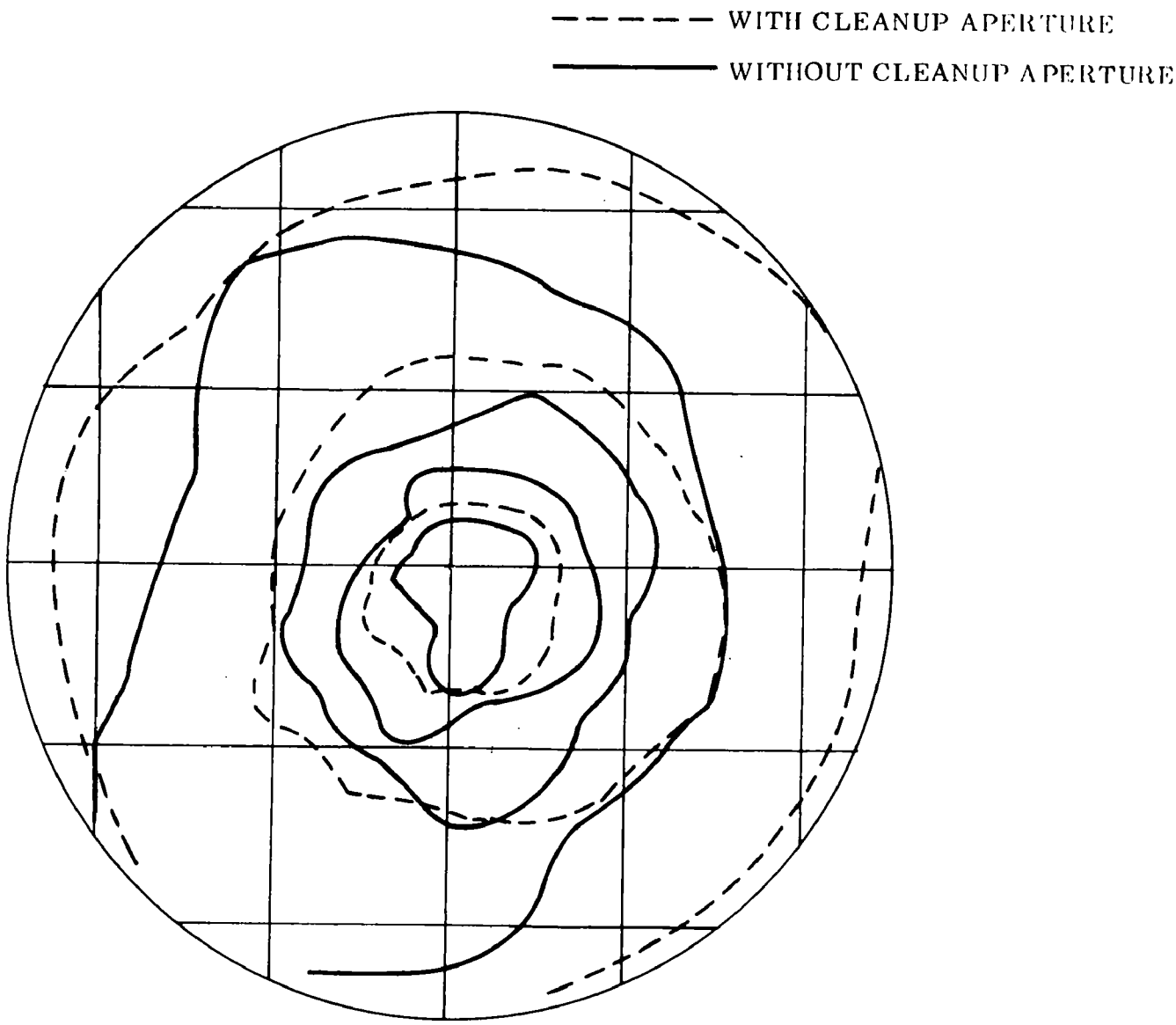

Figure 19. CONTOURS OF EQUAL DENSITY AT $\lambda = 9.504\ \mu m$ WITH AND WITHOUT A CLEANUP APERTURE

the concave mirror at the vertex of the "V". The design called for this waist to be positioned midway between the two mirrors, but it actually lies closer to the coupling mirror.

The true position of the waist (364 mm from the coupling mirror) was determined by computer simulation of the laser cavity and confirmed by measurement of the exit beam. A new waist is formed by the first lens following the coupling mirror and then again by the doublet as indicated in Figure 17. The position of these new waists does not coincide with the position of the real image of the waist of the beam within the laser cavity, but this fact does not reduce the effectivenss of a clean up aperture located at a particular waist. The aperture will strip off any undesirable side lobes in the diffraction pattern that represent high frequency clutter in the near field. The ideal optical configuration following the clean up aperture is a large transmitting telescope that would pick up the major side lobes of the diffraction pattern of the clean up aperture itself yielding good image of the clean up aperture on the retroreflector.

E. SEALED ISOTOPIC LASER DESIGN

1. Introduction

An isotopic CO_2 laser in ILAMS offers additional pollutant detection capability compared to the natural isotope, flowing CO_2 laser in current use. Figure 20 illustrates its greater spectral coverage. Use of $C^{13}O_2{}^{16}$ in the plasma tube adds, among others, HNO_3, PAN and PBzN to the system's list of potentially detectable pollutants. With $C^{12}O_2{}^{18}$ in the plasma tube a suitable absorption coefficient for long path monitoring of SO_2 has been reported. (Reference 18)

The CO_2 laser produces high CW power at high efficiency, i.e., more than 1 kw at up to 15% efficiency. Patel (Reference 19) demonstrated CO_2 lasing at approximately 10.6 and 9.6 microns and, subsequently, Moeller and Rigden (Reference 20) demonstrated CO_2 lasing at approximately 10.6 and 9.6 microns and, subsequently, Moeller and Rigden (Reference 19) demonstrated lasing in both the P and R branches of the rotational lines up to J values of over 50. Figure 20a shows the wavelengths at which lasing has been achieved by the investigators cited.

The use of the heavier, stable isotopes of carbon and oxygen shifts the energy levels of the CO_2 molecule. Figure 20c shows the predicted lasing wavelengths for the isotopic form of carbon dioxide, $C^{13}O_2{}^{16}$. These predictions were based on measurements of the molecular vibration levels of carbon dioxide by infrared

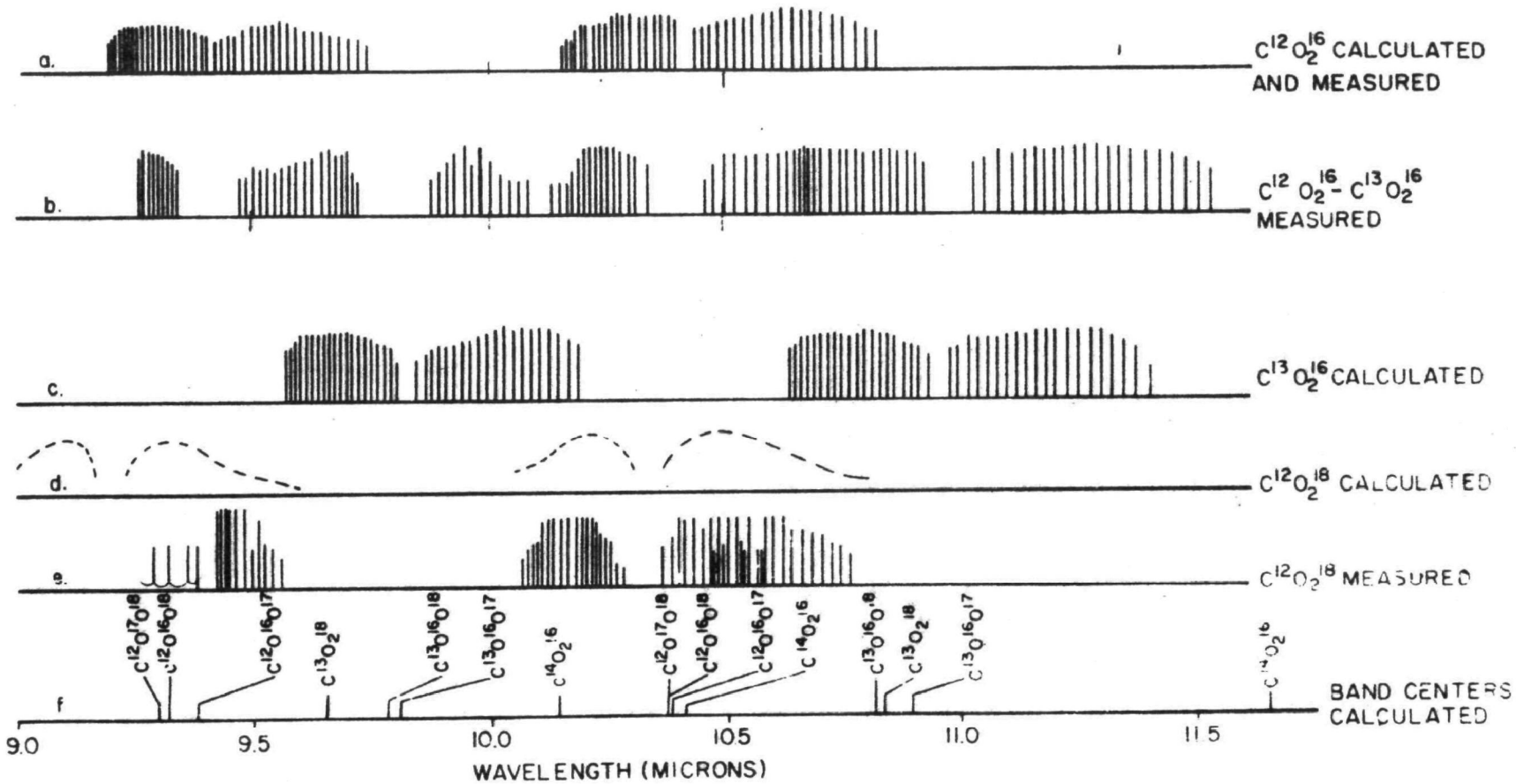

Figure 20. CO_2 LASING LINES

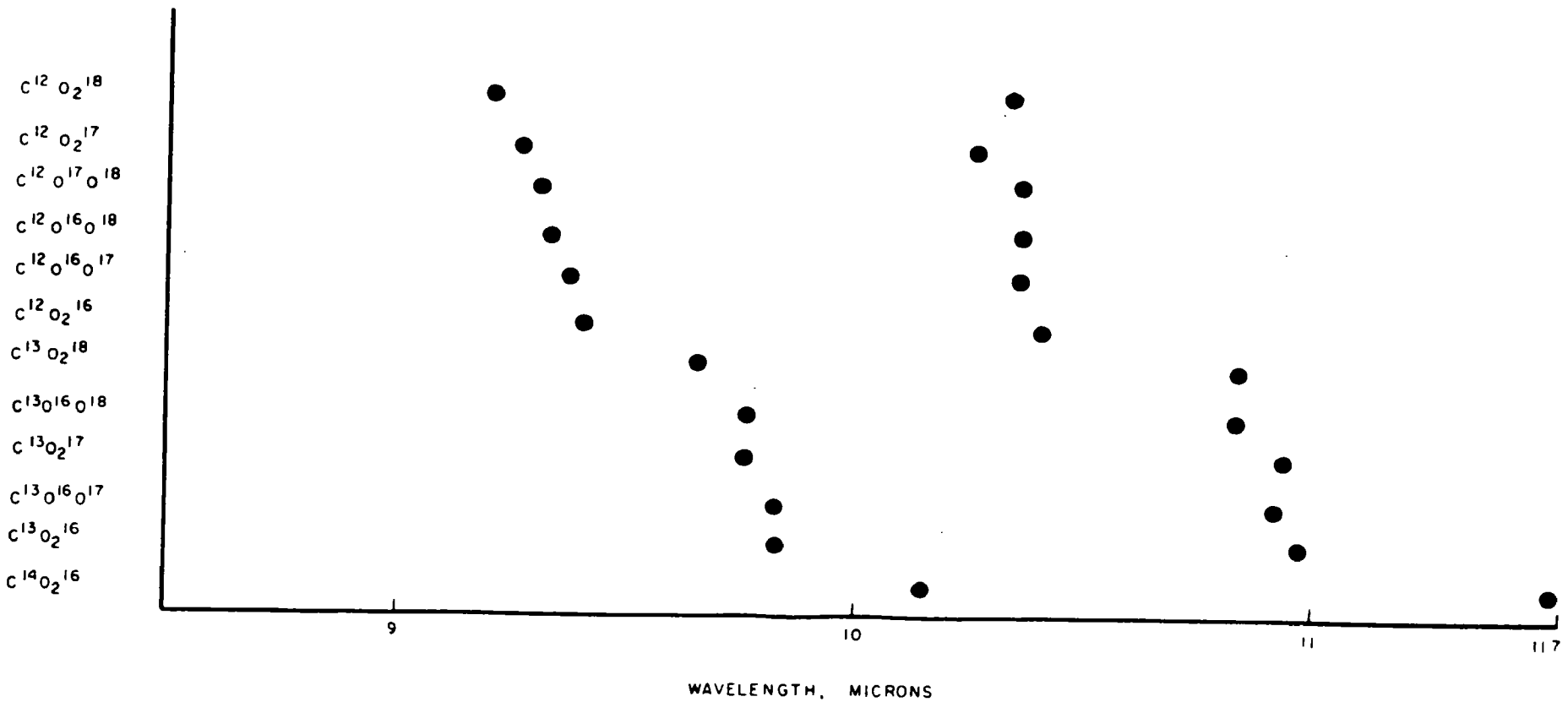

Figure 21. CALCULATED CO_2 ISOTOPE BAND CENTERS

spectroscopy. Verification of these predictions has been achieved using a mixture of 55 to 60% $C^{13}O_2^{16}$ and 40 to 45% $C^{12}O_2^{18}$. Spectral measurements of these lines with an infrared monochrometer were made at a resolution of +0.01 micron. Figure 20g indicates the spectral region spanned by the laser using the isotopic mixture $C^{12}O_2^{18}$ and $C^{13}O_2^{16}$. Note that lasing is occurring at the allowed transitions for both isotopes. Figures 20f and 21 show the band centers for several isotopic forms of carbon dioxide for both the $00^0 1 - 02^0 0$ and the $00^0 1 - 10^0 0$ transitions. Figure 20e shows measurements made of the lasing lines of $C^{12}O_2^{18}$ providing further verification of the validity of the analytical results, Figure 20d. These results indicate that the IR spectrum from 8.5 to 12 microns can be swept with a CO_2 laser filled with appropriate isotopes.

2. LASER PLASMA TUBE DESIGN CONSIDERATIONS

The primary objective in the design of the plasma tube is high gain. The requirement for spectral lines corresponding to remote "J" values of 50 or more using mixtures of isotopes in a sealed CO_2 laser demands high optical gain of the working plasma. In addition, the long path length (to maintain closely-spaced longitudinal modes) with multiple path folding plus a lossy spectral tuner within the optical cavity of the laser produces losses that must be compensated for with gain.

Since the gain of the plasma in a CO_2 laser is exceptionally high, laser designers are usually more concerned with output power and efficiency for a given working volume. Power output is usually obtained through the use of large fundamental mode diameters and correspondingly large tube diameters. Coupling coefficients are optimized for maximum power output at the P-20 line of the laser. For the sealed laser designed for this laser system, the power output of 1/4 watt is more than adequate.

The "V" laser concept is designed to take advantage of the fact that the gain of a laser is inversely proportional to the tube diameter. The stable mode diameter for the TEM_{00} traverse mode is proportional to the square root of the distance between curved mirrors for near confocal systems. The advantage of the zig-zag folding configurations of which the "V" laser is the simplest example, is that a curved mirror can be placed at each vertex and the beam diameter (and thus the tube diameter) can be kept to a minimum.

Once the smallest possible fundamental mode diameter is established, then the tube diameter can be chosen. In general, the gain increases for decreasing plasma tube diameter until diffraction losses are introduced which exceed the increase in gain. These diffraction losses are not introduced by the tube walls directly, but by the fact that the gain of the pumping plasma falls off near the walls. This effect is shown in Figure 22 to be a function of the exciting current. In order to establish the optimum size the laser on-axis gain was measured in an experimental setup as a function of nominal beam diameter and plasma tube diameter for the case of optimum plasma excitation (determined experimentally during each run). During each experimental run, gain was measured with a circular mode stop in place to confine lasing to a fundamental mode. A variable iris was used as a mode stop and was set at the largest aperture size that would constrain operation to the TEM_{00} mode.

The tube diameter for maximum gain was found to correspond to 1.532 times the stop size that would produce 0.1B diffraction loss. This stop size can be calculated using the curves of Kogelnik and Li (Reference 21). The advantage of a folded plasma tube configuration such as the "V" laser is illustrated in Figure 23. Note that a gain of 6.3dB may be obtained with two, 100 centimeter tubes, whereas a single, 200 centimeter tube produces about 4.5 dB of excess gain. The improvement in gain is 1.85 dB while incurring an additional loss of 0.1 dB because of the extra folding mirror. Aberration losses (coma) due to off-axis operation of the confocal mirror at the vertex are negligible because of the small beam diameter (low f number) within the plasma tube.

Because the glass envelope of the plasma tube is highly reflective at grazing incidence it is unfortunately easy for lasing to occur over paths not anticipated in the original design. To inhibit these "whisper" modes constrictions are introduced

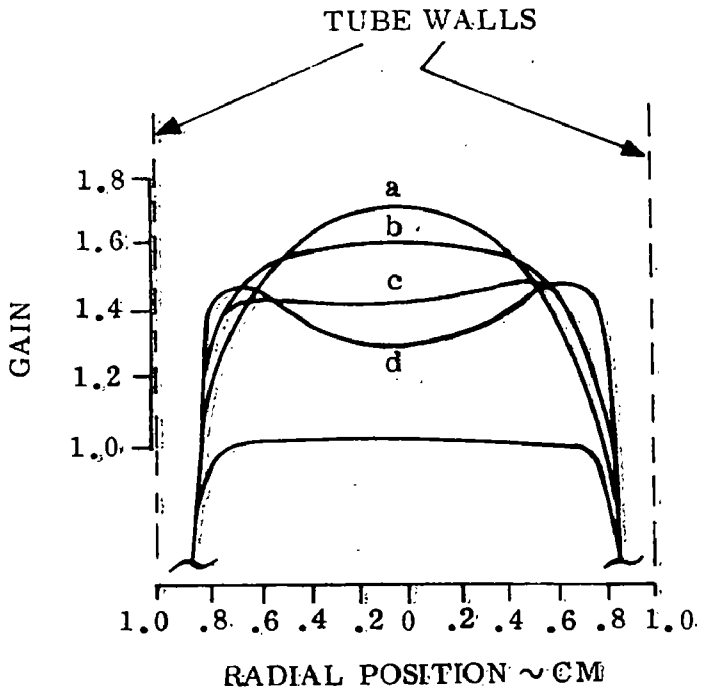

Figure 22. RADIAL GAIN PROFILE FOR A MIXTURE OF 1.8 TORR CO_2, 2.0 TORR N_2 AND 4.6 TORR He AT WALL TEMPERATURE OF 13° AND DISCHARGE CURRENTS OF : a.10 mA ; b.20 mA; c.30 mA; d.50 mA

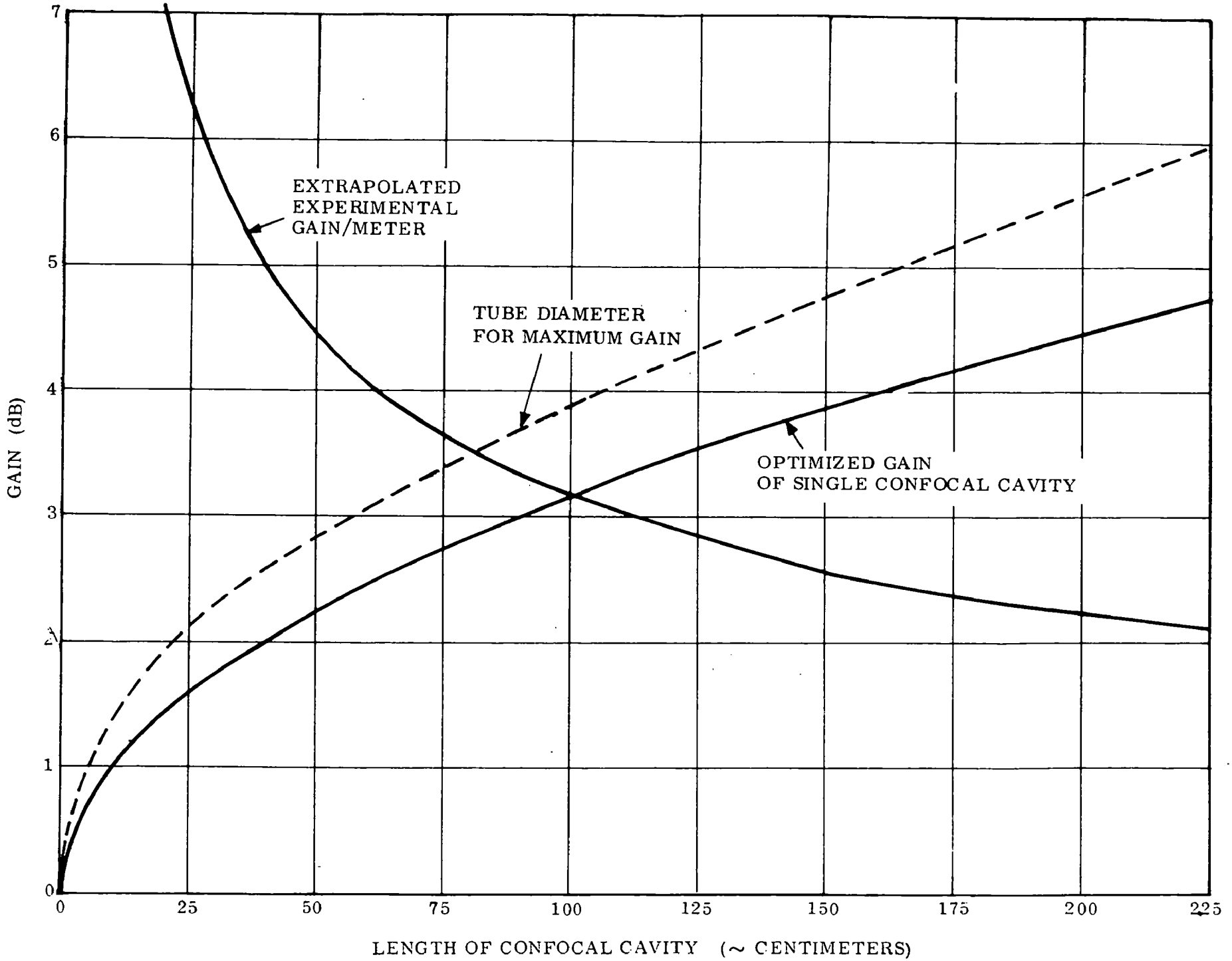

Figure 23. UNSATURATED GAIN OF A CO_2 LASER AT A J-40 TRANSITION CAVITY VS LENGTH ASSUMING THE TUBE DIAMETER IS OPTIMIZED FOR MAXIMUM GAIN

in the glass tubing every few inches. These rings in the glass have an internal diameter of one or two millimeters less than the I. D. of the bulk of the tubing; however they do not increase diffraction losses because they are spaced too far apart to shrink the diameter of the active plasma in the tube and are large compared to the mode stops deliberately introduced to inhibit higher order modes.

3. STABILITY CONSIDERATIONS

Laser stability places a limit on the system performance. Angular fluctuations and frequency fluctuations produced by changes in the plasma or in the optical alignment introduce spectral effects and measurement errors.

Dimensional changes in the laser cavity are introduced by temperature and mechanical vibration. These changes shift the laser's frequency, amplitude, and mode pattern. The percent change in laser frequency is proportional to the percent change in cavity length which is small (a few parts in 10^6) compared to the spectral bandwidth of the gases we are trying to detect. Amplitude fluctuations produced by changes in alignment, however, are of major concern when they lead to mode hopping that may occur at some spectral lines and not others. Table X gives some indication of the alignment tolerances that must be maintained to achieve satisfactory mode stability.

Mirror Tilt Milliradians	TEM_{00} % Losses	TEM_{01} % Losses	TEM_{01} Rejection Mode
-	2.3%	28%	12:1
0.16	2.5%	28%	11:1
0.33	4.0%	32%	8:1
0.66	6.8%	40%	6:1
1.64	35.0%	75%	2:1

Table X. Losses versus Mirror Tilt for a Confocal Resonator

Frequency and gain can also be influenced by the excitation; however, the effects on frequency stability as a result of changes in plasma current are considerably less than that contributed by other sources. The CO_2 laser will have a frequency drift in the range of 0.5 to 0.9 MHz per milliamp change in excitation current. A typical current for a cooled laser is about 30 ma; thus, for a frequency tolerance of 0.5 MHz the required regulation on the source current would only be about 3.7%. A typical setup for lasers uses large series ballast resistors. Prior to firing, the voltage at the electrode exceeds the maximum value needed for ignition; however, as current begins to flow, the voltage drop across the ballast resistor increases rapidly thereby lowering the voltage across the electrodes to the appropriate operating level. The ballast resistor is chosen to accommodate the desired voltage and is very much larger than the dynamic impedance of the laser (a factor which improves current regulation by causing the voltage source and the resistor to appear as a current source across the laser electrodes). If the use of ballast resistors is objectionable, because of power dissipation in the ballast or because of stability requirements, then an active current regulation system may be used.

4. INTRACAVITY WINDOWS

Practical design considerations make necessary at least one window within the laser optical cavity to seal off the plasma portion of the laser from the spectral tuner. Considerable effort in this design study was expended on the Brewster window problem. The requirement for wide spectral range tunability from the laser means that neither anti-reflection coated windows nor Fabry Perot etalons will suffice as a window. Metal halides having adequate transmission at 10.5 micrometers are unsatisfactory because they are hydroscopic, birefringent, and have been found to have poor surface quality. Germanium and gallium arsenide have been the choice as Brewster windows to date, but they have some disadvantages. The index of refraction of these materials is high (4.0 and 3.28 for Ge and GaAs respectively). They are opaque to visible light.

The absorption of laser radiation is sufficiently high that the change of index of refraction with temperature distorts the beam as the laser comes up to a stable operating temperature.

Until recently we felt that thin GaAs windows offered the best compromise. These windows can be polished to one (1) mm thickness maintaining a wedge angle of less than 40 arc seconds between the front and back surfaces. In practice they were cemented to a kovar flange which was then cemented to the borosilicate glass laser tubing cut at the Brewter angle. The kovar steel flange serves as a heat sink to minimize the thermal gradients across the window which produce defocussing of the beam. Kovar was chosen because its thermal coefficient of expansion lies midway between that of gallium arsenide and borosilicate glass. Thermal flexing is the major source of post sealing leaks in the laser system. The sealing material was Torseal high vacuum epoxy which was then overcoated with General Electric RTV-118. The RTV is used as insurance against hairline cracks that may develop in the seal with very large ambient temperature changes.

The recent introduction of vapor-deposition-fabricated zinc selenide windows has changed our philosophy somewhat with respect to sealed laser system design for spectrally tunable CO_2 lasers. The alignment procedure, which requires that all the mirrors be lined up within one-half milliradian before lasing can occur, is quite complicated when using an opaque Brewster window with even small wedge angles. However, in the proposed design, zinc selenide windows which transmit in the visible, and a coupling mirror external to the laser plasma tube will allow relatively easy alignment with a HeNe (6328Å) laser. The index of zinc selenide is 2.4 and its absorption coefficient is lower by more than 4:1 than either germanium or gallium arsenide. The smaller index yields a smaller Brewster angle and thereby somewhat lowers the tolerances on the optical surface flatness.

5. SPECTRAL TUNER DESIGN

Because of its high dispersion, relatively low losses, and easy maintainability, the reflectance diffraction grating has been the choice as a spectral tuning element for use within the laser cavity. Other possible approaches such as metal halide prisms, Fabry-Perot etalons and dielectric fibers have been evaluated under earlier study programs (Reference 22).

Used as an end mirror in the laser cavity, a blazed reflectance diffraction grating designed for 10 microns has a dispersion of approximately 100 milliradians/micron. The measured reflection efficiency of a Bausch and Lomb aluminized replica grating, to CO_2 laser radiation at ten microns, was 95 percent at the proper polarization. There is some change in properties with temperature at moderate power levels near 100 watts/cm^2, tending to increase losses.

The efficiency of a blazed, reflection, diffraction grating varies as a function of wavelength and angular orientation of the grating with respect to the incident radiation. Except for approximately 3% absorption and scattering losses (using a gold overcoat) all the losses from the first order reflection go into the zero order reflection. (The direction of the zero order reflection is such that the angles of incidence and reflection are equal about the normal to the grating surface). This zero order out-coupling can be adjusted by selection of blaze angle, grooves per mm, and angle of orientation, and varies strongly with wavelength.

The grating must be oriented with the grooves horizontal (with path folding in the horizontal plane) so as to minimize the zero order reflection losses for both ingoing and outgoing reflections. The first order reflections from the grating are dispersed in elevation with wavelength. The shorter wavelengths, for example, are directed slightly downward (the grating is facing slightly downward) and the longer

wavelengths reflect upward. The separate beams are collected in groups by the flat mirrors and redirected through the chopper wheel in a convenient orientation for sequential shuttering. The shorter wavelengths strike the lower mirrors and the longer wavelengths reflect off the upper mirrors. Because of the redirection of the beams by mirrors, the position of the beams at the chopper and the wavelength separation end mirrors is not proportional to wavelength. The number and location of the mirrors following the diffraction grating and the respective position of the holes in the chopper wheel both depend upon the wavelengths selected for the particular target detection problem.

The optical design of the laser cavity to include the grating element as a spectral tuner involves several, sometimes conflicting, requirements:

1. High spatial resolution between adjacent spectral lines at the end mirrors so that adjacent spectral lines may be used in the same laser system.

2. Large angular resolution between adjacent spectral lines so that unwanted spectral lines may be tuned out by angular alignment of the end mirror.

3. Low aberration losses from curved folding mirrors which must be operated off axis.

4. Small losses from the grating which must also be operated off axis.

5. Less than 100 watts/cm^2 power density on the grating surface.

The spatial resolution of the spectral tuner is dependent primarily upon the diameter of the laser beam incident upon the grating and the dispersion of the grating. Spatial resolution is measured by the spacing between adjacent spectral lines ($\Delta\lambda$ = 0.007 to 0.026 um) in spot diameters at the end mirrors. If the grating has a dispersion β then the resolution is given by:

$$R = \frac{\beta \pi w}{\lambda} \text{ diameters/micrometer} \quad (5)$$

where w is the nominal diameter of the beam at the diffraction grating. For example, if the spectral separation between two lines at 9.2 micrometers is 0.01 micrometers and $\beta = 0.1$ radians/micrometer, then in order to get a spectral separation of four diameters, the beam diameter on the grating must be:

$$w = \frac{4\lambda}{0.1\pi \times .01} = \frac{4 \times 0.0092 \text{ mm}}{.001\pi} = 11.7 \text{ mm} \quad (6)$$

In order for the grating to accommodate this beam without introducing appreciable diffraction losses within the laser cavity, it should be four diameters wide, which is 46.8 mm or 1.84 inches in diameter.

The use of a large beam on the grating poses another difficulty. Because the surface of the reflectance grating is inclined with respect to the vertical, beams with high numerical apertures (small f numbers) introduce large aberration losses. For example the "V" laser used in this program uses a spherical mirror of one meter focal length to focus the beam on the end mirrors via the grating. The beam diameter at the grating is 2.9 mm yielding a numerical aperture of NA = 1/2 x 2.1/1000 = .00145 for which the losses are negligibly small. However, in order to obtain the resolution indicated above, the numerical aperture for the same focal length mirror would be:

$$NA = 1/2 \times 46.8/1000 = .0234 \quad (7)$$

Measurements with the laser system using just this numerical aperture on the diffraction grating resulted in diffraction losses in excess of 3dB making the laser virtually inoperable for this configuration on any but the strongest transitions.

In addition to the requirement for spatial resolution, it is necessary for the spacing from the grating to the end mirrors to be large in order to preserve the angular resolution. The angular resolution is given by:

$$R = \beta \ (1 - a/F) \quad (8)$$

where

β is the dispersion of the diffraction grating

a is the spacing from the grating to the last concave mirror or focusing mirror, and

F is the focal length of the mirror.

The conflict between requirements is indicated in Figure 24. The angle, A, between mirrors M1 and M2 should be kept small to minimize zero order losses from the grating and the angles C and D at the mirrors must be minimized to reduce off axis aberration. The off axis image is degraded by coma, which is given by:

$$\alpha_T = \frac{3}{16} \quad \frac{\bar{u}}{(\text{f No.})^2} \tag{9}$$

where α_T is the third-order tangential coma expressed in the same units of angle as u, which is the semi-field angle. Note that for a given f number the coma increases with the square of the beam diameter and linearly with the off axis (semi-field) angle. The only way to reduce "C" and "D" is to reduce the beam diameter and make dimension "a" small. The beam diameter is set by the requirement for spatial resolution, and "a" is necessarily small because mirror M2 must intercept all the spectral lines dispersed by the grating. Alternate approaches are:

1. Forego the use of spectral lines that are closely spaced in wavelength and use small diameter beams of low numerical aperture at the diffraction grating. This approach is used in the General Electric ILAMS System.
2. Use off axis parabolas with long focal length (greater than 2.5 meters) in the configuration shown in Figure 24. This will permit the dimension "a" to become as large as 0.6 meters and keep angle "A" small. The axial image formed by a paraboloid is well known to be free of geometric aberrations. This method is recommended for the proposed sealed system design.

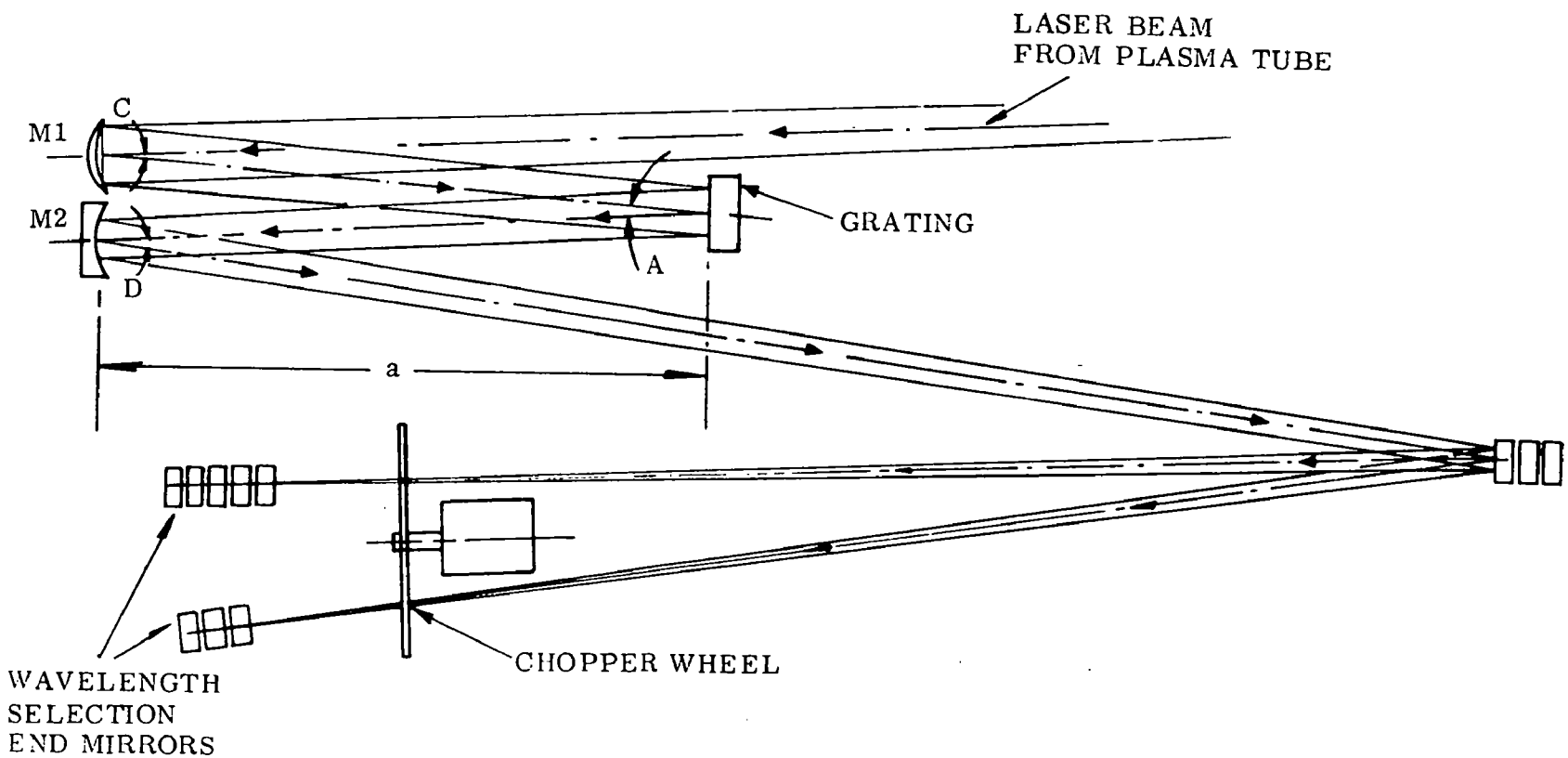

Figure 24. LAYOUT OF LASER OPTICAL SYSTEM

6. SEALED LASER DESIGN CONSIDERATIONS

The problem of building a CO_2 laser using the less common isotopes of carbon and oxygen is to construct a sealed plasma tube that will last from two to five thousand hours without serious degradation in gain. The techniques for accomplishing this require a marriage of the arts of vacuum technology and laser physics.

Because of the high cost of carbon-13 and oxygen-18, the CO_2 laser must be operated as a sealed (non-flowing) system. The gain, power output, and life time of a sealed CO_2 laser are a function of the gas mixture, the tube diameter, the proximity of the path taken by the laser beam to the walls, the means of excitation and the electrode structure and materials. The sealed CO_2 laser shows a gradual decay in gain and hence in power output with operating life. In order to have an operating laser detection system, the gain within the plasma envelope must be kept greater than the optical cavity's fixed losses and including those of the output coupling mirror, while maintaining an internal power density compatible with the desired output power. This minimum gain requirement must be met throughout the operating life of the plasma tube and at the weakest laser transitions that are to be used for gas detection.

This program included a detailed study and experimentation of the effects of gas fill mixtures, plasma tube configuration and excitation on laser performance and lifetime. A large background of work has already been accomplished by a variety of investigators in the areas of laser gain and lifetime using the most common isotopic form of carbon dioxide, i.e., $C^{12}O_2^{16}$ (References 23, 24, 25, 26, 27 and 28). Witteman (Reference 23) achieved 10,000 hours of continuous operation with a forty watt CO_2 laser operating at 10.6 micron wavelength. The results of this work have been extremely valuable to us, but there are significant differences between the 10.6 micron laser and the laser designs being considered. The isotopic

CO_2 laser must maintain high gain over a large number of wavelengths at high J values. The purchased $C^{12}O_2{}^{18}$ isotopes will necessarily be contaminated with more than ten percent $C^{12}O_2{}^{16}$. At each wavelength corresponding to energy transitions in both of the CO_2 gases, the gain-saturation characteristic is different. The gain-saturation characteristic at a wavelength corresponding to an energy transition in one of the isotopic forms is influenced by the presence of other species because of the competition effects. The optimum ratios of carbon dioxide to the other gases in the system are not the same for all isotopes of mixtures as for ordinary CO_2.

The lifetime of the CO_2 laser is directly related to the gas mixture, the cleanliness of the internal surfaces of the plasma tube and the flow rate from outgassing and leaks. A gas filling station must be used to bake out the plasma tube under high vacuum, to fill the plasma tube with the desired mixture of the isotopic forms of CO_2, N_2, He, Xe, and H_2O, and to monitor the partial pressure of each gas. (See Figure 25).

When direct current excitation of the plasma is used the electrode material and the configuration of the electrodes are extremely important to the laser lifetime. The electrode material may act as a sponge to some of the gases in the laser, it may act as a catalyst for the production of undesirable compounds and it may sputter away material from the cathode which may in turn react with the gases in the laser or batter them against the glass walls of the tube. Platinum is one of the better choices as an anode material because it does not encourage the production of compounds (carbonyls, etc.) that interfere with lifetime, nor does it oxidize to use up the oxygen in the CO_2. However, platinum is a notorious sputterer and therefore not suitable as a cathode material. Cathodes made from high purity nickel and designed to operate at from 300 to 500 degrees Centigrade have been tested and found to be acceptable.

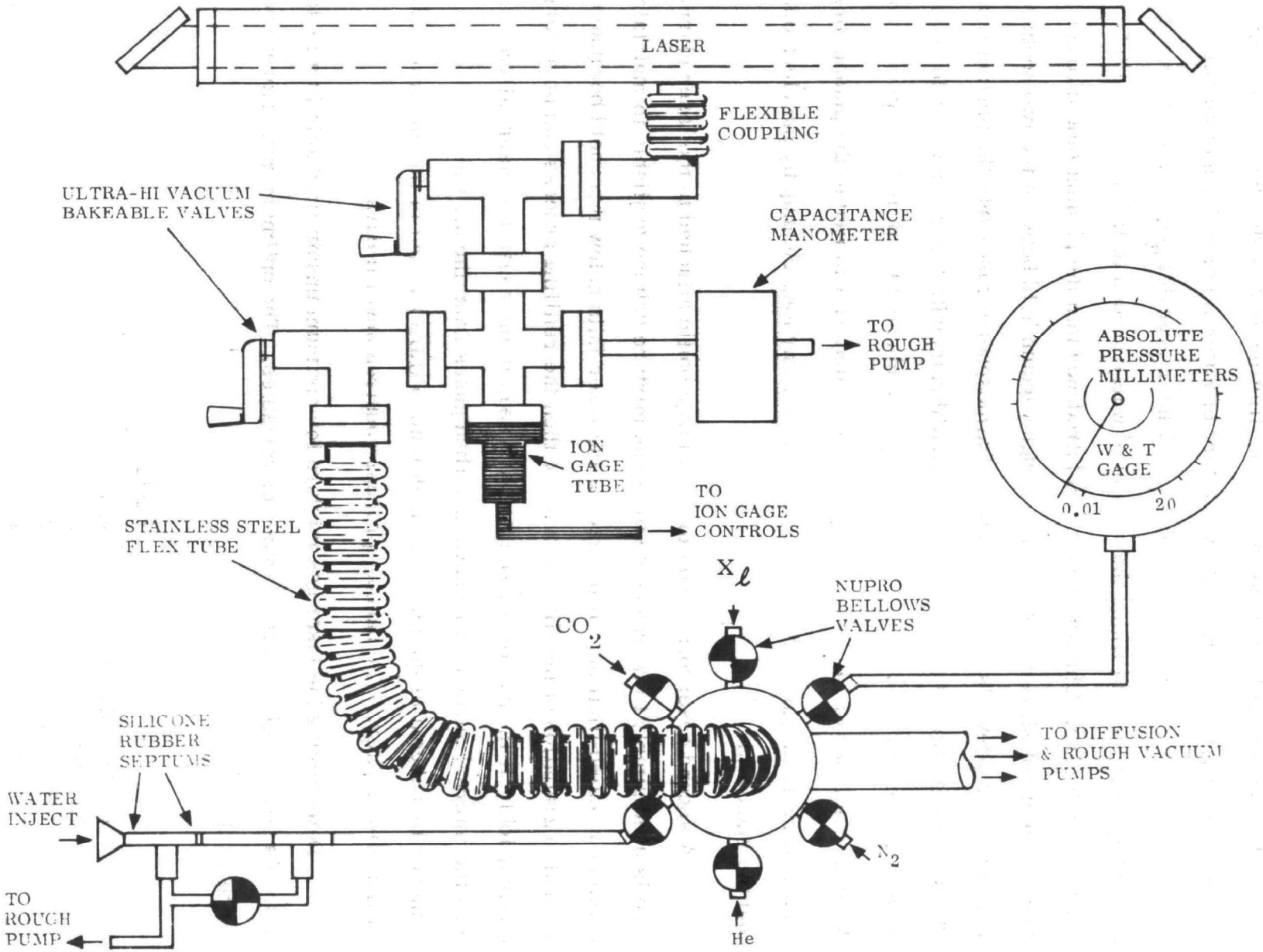

Figure 25. MANIFOLD FOR HIGH VACUUM FILL STATION

Another essential ingredient for long lifetime in a sealed laser is to maintain a partial pressure of approximately 1.5 torr of water vapor in the gas mixture. Because the electrodes and the glass walls tend to absorb H_2O, it is necessary to add to the laser several times the amount of water needed to fill the plasma tube volume to 1.5 torr. The water vapor is introduced into the plasma tube through a double septum of silicon rubber with a rough vacuum held between the two septums. This approach prevents the introduction of atmospheric gases into the plasma tube. The system is allowed to come to stable equilibrium with the water vapor following each injection and the amount of injected H_2O is adjusted for peak laser power output. A small container of Linde 4-a Molecular Sieve material is tied to the plasma tube as a reservoir of water vapor to compensate for any long cleanup by the electrodes and the glass walls.

A second reservoir consisting of a large bottle attached to the laser plasma tube is used simply to increase the total gas mixture volume available to maintain maximum sealed lifetime. If the gain of the laser falls below threshold because of normal degradation of the fill gas mixture then the refilling process can be accomplished fairly quickly at the gas filling station. If a leak is the cause for laser failure, however, then the internal surfaces will have absorbed gases from the air which will have to be removed by bakeout of the glass and high temperature bakeout of the electrodes with an induction heater. The bakeout process requires several days.

Determining the laser gas mixture for optimum unsaturated gain is a tedious business because of the large number of variables. The optimum mix determined for use with $C^{12}O_2^{18}$ is:

	Torr
Carbon Dioxide	4.5
Helium	9
Nitrogen	2
Xenon	1
Water Vapor	1.5

Given this mix as a starting point, the optimum mix using ninety percent $C^{12}O_2{}^{18}$, ten percent $C^{12}O_2{}^{16}$ can be determined by trial and error monitoring output power.

7. PROPOSED SEALED LASER DESIGN

The critical elements in this sytem are the seals, reservoirs, and the gas fill mixture. Bakeout with a good, high-vacuum filling station is essential. The proposed sealed system design is illustrated in Figure 26. It is a water-cooled "V" shaped plasma tube with two Brewster windows. The coupling mirror will not be connected directly to the plasma tube as in the present ILAMS system laser. This avoids the problems associated with a flexible seal between the coupling mirror and the plasma tube, which was necessary in order to obtain adequate alignment of the optics. Such a seal presents a high vacuum problem and must be insulated against the high voltage between the plasma tube and the support frame. The tube is necked down by two millimeters at regular intervals to inhibit whisper modes from developing.

The Brewster windows are of zinc selenide and are cemented directly to the laser tube with high vacuum epoxy Torseal. The epoxy is then over-coated with RTV-118 as a seal against hairline cracks that may appear in the epoxy as a result of age or large temperature changes. The laser tube and associated glass plumbing is made of pyrex type borosilicate glass (Glass Code Number 7740). At the two ends where the Brewster windows are sealed this glass is graded to a soda lead glass (Number 0120) which is a better match for the thermal coefficient of expansion of zinc selenide. The glass is cut to the approximate Brewster angle and then hand ground to meet the Brewster angle and to provide a smooth, flat mating surface for the window.

The length of the tube is approximately 1.1 meters with a convex one-meter radius-of-curvature gold mirror at the vertex. The glass tubing at the vertex is cut and hand ground to prealign the mirror which is cemented directly to the glass. This

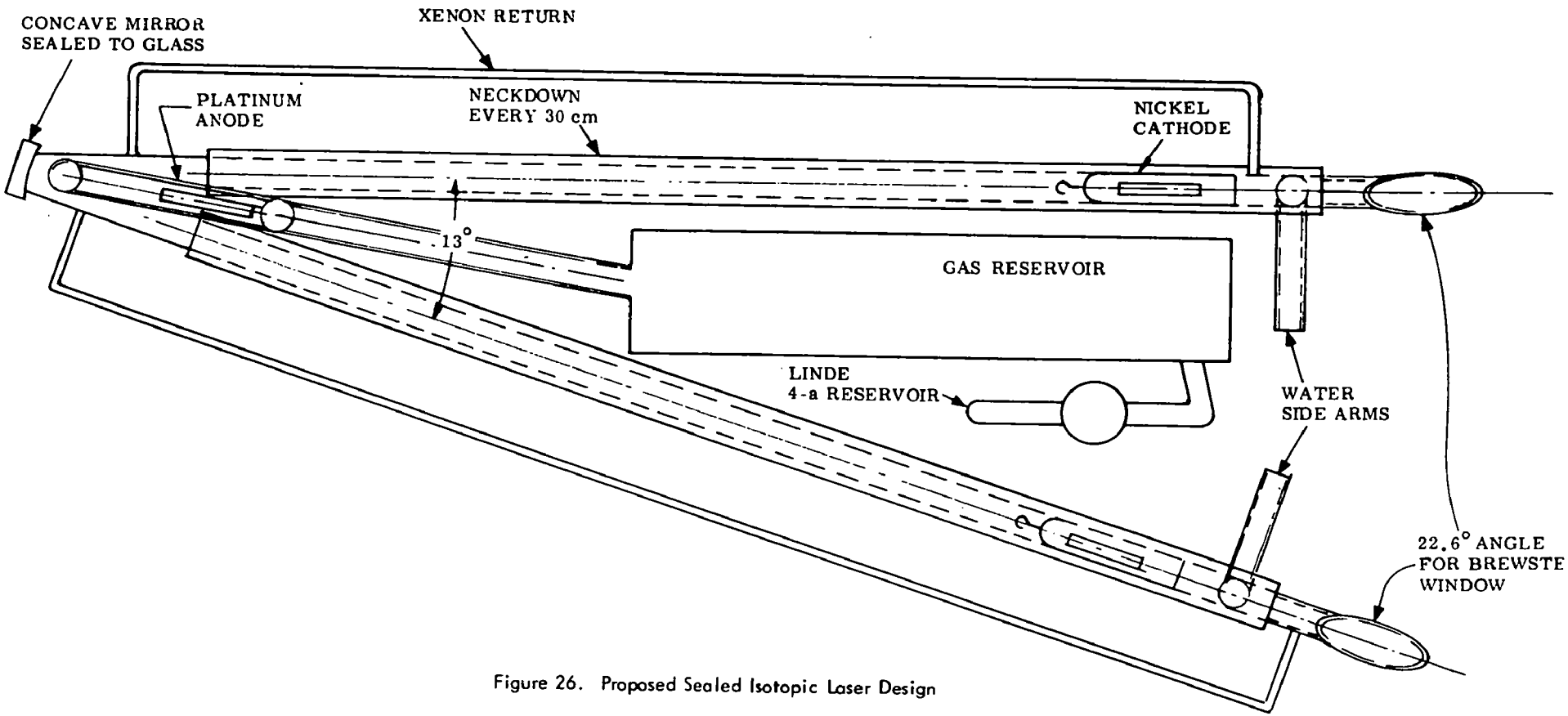

Figure 26. Proposed Sealed Isotopic Laser Design

again, is to avoid sealing and high voltage problems. Water cooling of the tubes out beyond the electrodes provides sufficient temperature stability so that alignment is maintained. A circular metal aperture is cemented to the center of this mirror as a stop for higher order modes.

Xenon being a heavy molecule tends to drift in the plasma toward the cathode so a return or bypass is provided for each leg of the "V". This bypass must have smaller diameter and/or longer length than its associated plasma tube in order to prevent the discharge from firing along the bypass.

A gas reservoir is attached to one of the legs of the "V" and the inlet valve is in turn connected to the reservoir. This is a high vacuum bellows type valve with sufficiently high conductance to allow bakeout of the system in less than a week at temperatures of 250 degrees Centigrade. A second reservoir of molecular sieve material is used to keep the water vapor concentration fixed in spite of the clean up effects of the internal surfaces of the system. The capacity of the molecular sieve material is large compared to that of the inner surfaces at the same vapor pressure.

The anode is platinum and the cathodes are made from Number 270 Nickel. They are 6 mm cylinders with a 2.6 mm hole drilled in one end. The other end is welded to a kovar wire for the glass seal.

REFERENCES

1. L.R. Snowman and D.R. Morgan, "Studies on An Isotopic CO_2 Laser LOPAIR System," Department of the Army Edgewood Arsenal DDEL, First Quarterly Report, Contract DAAA15-72-C-0359, February 1973.

2. L.R. Snowman, D.A. Ware, and D.R. Morgan, "Gas Laser Detector", Air Force Armament Lab., Eglin AFB, Florida, Final Report, Contract F08635-68-0116, September 1969; also, General Electric Company, Electronics Laboratory, Syracuse, New York, Report No. R69ELS-1, September 1969.

3. D.R. Morgan and D.A. Roberts, "Computer Signal Processing Study", Dept. of the Army, Edgewood Arsenal DDEL, Final Report, Vol. 1: Analytical Results, DAAA15-71-C-0186, September 1972.

4. J.H. McCoy, D.B. Rensch and R.K. Long, "Water Vapor Continuum Absorption of Carbon Dioxide Laser Radiation Near 10μ" Applied Optics Vol. 8, No. 7, pp 1471-1478, July 1969.

5. W.A. McClenny, EPA, Private Communication, August 1973.

6. E.H. Christy, Tulane University, Private Communication, June 1973.

7. P.L. Hanst, EPA Research Triangle Park, North Carolina, Private Communication, 1972

8. L. Gasiorek, Stanford Research Institute, Private Communication, August 1973.

9. R.A. McClatchey, et al., "AFCRL Atmospheric Absorption Line Parameters Compilation", Air Force Research Laboratories, Bedford, Massachusetts, AFCRL-TR-73-0096, January 1973.

10. R.K. Long, Ohio State University, Electroscience Laboratory, Private Communication, September 1973.

11. G.L. Trusty, "Absorption Measurements of the 10.4 Micron Region Using a CO_2 Laser and a Spectrophone" Air Force Avionics Laboratory, Wright-Patterson AFB, Ohio, AFAL-TR-72-413, January 1973.

12. W.A. McClenny, EPA Research Triangle Park, North Carolina, Private Communication, September 1973.

13. D.E. Burch, "Semi-annual Technical Report; Investigation of the Absorption of Infrared Radiation by Atmospheric Gases" Philco-Ford Corporation, Aeronautic Division, Contract No. F19628-69-C-0263, U-4784, January 1970.

14. D.E. Burch, "Radiative Properties of the Atmospheric Windows" Conference on Atmospheric Radiation, pp 61-68, August 7-9, 1972, Fort Collins, Colorado; published by AMS, Boston, Massachusetts.

15. H.R. Carlon, "Model for Infrared Emission of Water/Aerosol Mixtures" Applied Optics, Vol. 10, No. 10, October 1971.

16. P.L. Hanst, NASA Electronics Research Center, Cambridge, Massachusetts, Private Communication, 1970.

17. D.R. Morgan and D.A. Roberts, "Computer Signal Processing Study" Final Report, Vol. 2: Computer Programs, Dept. of the Army, Edgewood Arsenal, Contract No. DAAA-71-C-0186, September 1972.

18. R.T. Menzies, "Remote Detection of SO_2 and CO_2 with a Heterodyne Radiometer" Appl. Phys. Letters, Vol. 22, No. 11, p592, 1973.

19. Patel, Phy. Rev. 136, 5A, November 1964, pA1187.

20. G. Moeller and J. Ridgen, Appl. Phys. Letters Vol. 8, No. 3, p 68, 1966.

21. H. Kogelnik and T. Li, "Laser Beams and Resonators" Proceedings of the IEEE, Vol. 54, No. 10, October 1966.

22. L.R. Snowman, "Laser Coincidence Absorption Measurements", General Electric Co., Electronics Laboratory Report No. R72ELS-15, March 1972.

23. W.J. Witteman, "Sealed-off High-Power CO_2 Lasers" Phillips Technical Review, Vol. 28, Nov. 10, 1967.

24. R.J. Carbone, "Characteristics of a Single-Frequency Sealed-off CO_2 Amplifier" IEEE Journal of Quantum Electronics, January 1969.

25. V. Hoffman and P. Toschek, "One-year Operation of Sealed-off CO_2 Laser" IEEE Journal of Quantum Electronics, November 1970.

26. R.J. Carbone, "Continuous Operation of a Long-lived CO_2 Laser Tube" IEEE Journal of Quantum Electronics, March 1968.

27. H.W. Mocker and H.A. Gustafson, "New Contender for Space Communication" Laser Focus, October 1970.

28. W.J. Witteman and H.W. Werner, "The Effect of Water Vapor and Hydrogen on the Gas Composition of a Sealed-off CO_2 Laser" Physics Letters, Vol. 26A, No. April 10, 1968.

29. M.M. Whatley and D.A. Smity "Atmospheric Effects on Digitally Modulated Laser Transmission" U.S. Army Electronics Command, Fort Monmouth, New Jersey, Tech. Rep. ECOM-3005, July 1968.

30. R. Paulson, E. Ellis and N. Ginsburg, "Atmospheric Noise Measurements" Air Force Cambridge Research Laboratories, Tech. Rep. AFCRL-62-869, AD 287 517, August 1962.

31. W.L. Wolfe, Handbook of Military Infrared Technology, Office of Naval Research, Dept. of the Navy, Washington, D.C., 1965.

APPENDIX A

INTERFERENCES

Anything that frustrates the detection of the IR absorption pattern associated with a particular gas is considered as a source of interference.

System Noise

System noise is composed of detector, optical, and other noise sources that arise in the measuring apparatus. This type of noise usually consists of fairly rapid zero-mean fluctuations of the received energy.

An actual instrument will time-average the demodulated signal. Therefore, if response time is not a consideration, then the effect of system noise may be reduced to an arbitrarily small level by choosing a large enough integration time. Of course, any real-time measurement problem does necessitate a finite response time and so there are limitations on how much noise reduction may be attained in this manner.

Detector noise is additive and usually uncorrelated between wavelengths for a scanning-type system. The amplitude distribution of detector noise is Gaussian and its variance depends on the particular type of detector that is used. The spectrum of the noise usually consists of a uniform thermal noise components and a 1/f "flicker noise" component that dominates at lower frequencies. Detector noise will be negligible if the source strength is large enough.

Optical noise or "scintillation" is a modulating type of noise that results from inhomogeneities of the index of refraction in the atmosphere. This type of noise is strongly correlated between wavelengths over a large range because the refractive index does not vary much with wavelength. The amplitude distribution of optical noise is log-normal (Reference 29) and its variance is a function of aperture, range, and meteorological factors (Reference 30). Its spectrum shape is of a $1/f^2$ nature (Reference 28) although the exact value of the exponent varies, depending on conditions. Unlike detector noise, the relative magnitude of scintillation noise does not depend on the source strength, since it is a multiplicative type of noise.

Laser systems may be either optical or detector-noise-limited. Past experience indicates that, in most cases where a cooperative reflector is used, enough laser energy is available so that detector noise can be neglected. Under these circumstances, the laser system is optical noise limited. Typical detector and scintillation noise densities as a function of frequency are plotted in Figures A-1, and A-2, respectively.

For a system corrupted by additive detector noise and multiplicative optical noise, the measured absorption at wavelength i is given by:

$$A_i = -\log(MP_i e^{-\alpha_i CL} + N) + \log P_i \qquad \text{(A-1)}$$

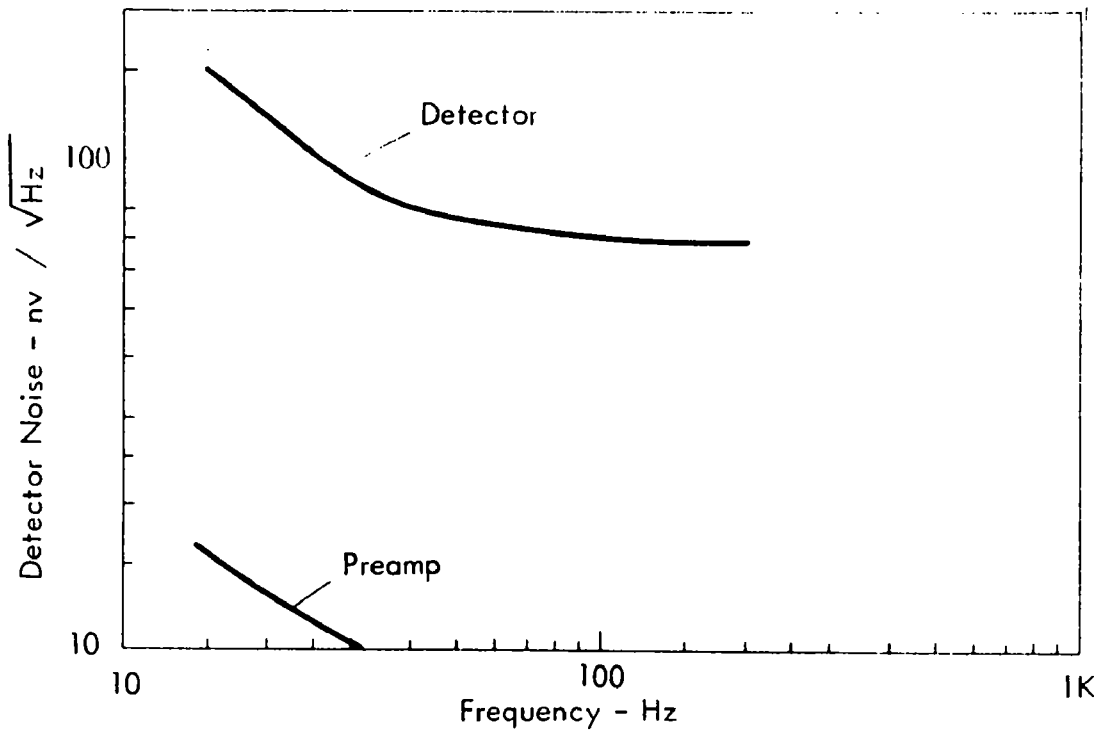

Figure A-1. DETECTOR NOISE VERSUS FREQUENCY

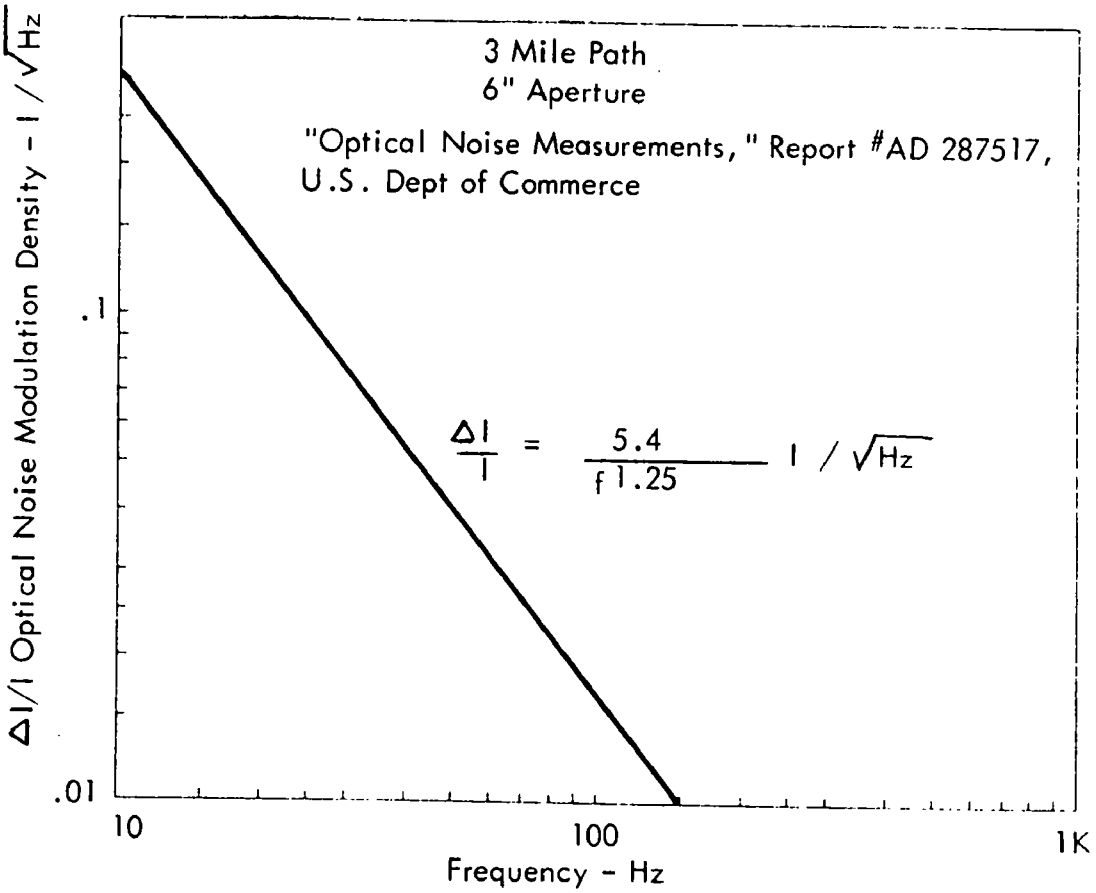

Figure A-2. OPTICAL SCINTILLATION NOISE VERSUS FREQUENCY

where P_i is received power, α_i the absorption coefficient at wavelength i and CL is the optical thickness or mass per unit area of target gas. The optical modulation noise M is assumed to be distributed log-normal with unit mean and variance σ_M^2 cycle of bandwidth. The detector noise N is assumed to be Gaussian distributed and is specified by the noise equivalent power NEP of the detector which is defined as the amount of optical power necessary to produce a signal-to-noise-ratio of one at the detector output in a bandwidth of one Hz. Here, the svstem is assumed to have been initially balanced by adding the quantity log P_i corresponding to CL = 0.

If detector noise is small, then for small absorptions, (A-1) reduced to:

$$A_i \tilde{=} \alpha_i CL - \log M - N/MP_i, \quad (1 - \sigma_M) P_i \gg \text{NEP} \qquad \text{(A-2)}$$

Each noise component in (4) is now additive and linear mean-square estimation theory can be applied.

If detector noise is not negligible, then some pre-log integration (filtering) is necessary in order to reduce the noise level so that the approximation in (A-2) can be made.

The first noise component in (A-2), log M, is now zero-mean Gaussian-distributed with variance log $(1+\sigma_M^2)$. The second noise term is somewhat more unwieldy in distribution. However, if $\sigma_M < 1$, then this term is also approximately Gaussian-distributed. For an optical-noise-limited system, $P_i \ggg$ NEP and the second noise term can be neglected.

Specific Interferents

An interferent is defined as any spectral absorber that may be present in sufficient quantity as to interfere with the detection of the target gas absorption pattern. Unlike system noise, this type of interference does not necessarily consist of rapid fluctuations and therefore is not appreciably reduced by increasing the integration time of the measurement.

Neutral Attenuation

One of the most dominent interferents in any system is neutral attenuation. This effect is caused by:

1) Unfavorable atmospheric conditions such as rain or fog,
2) Changes in the transmission or reflectivity of optical components (e.g., dust accumulation on mirrors), and
3) Gain variations of electronic components (e.g., responsivity variations of a thermistor bolometer due to ambient temperature changes).

An automatic gain control (AGC) amplifier is used in the system to control large average variations of signal level and thereby reduce the dynamic range requirements of the signal processor. However, neutral attenuation must still be considered as an interferent since it perturbs the absorption pattern. Specifically, the effect of the AGC amplifier is to adjust the system gain so that the average signal level is constant. For example if there is a 4% absorption at λ_1, then the AGC will boost the average signal which will result in a 3% absorption at λ_1 and a -1% absorption at λ_2, λ_3, and λ_4. This effect is equivalent to the combination of the 4% absorption at λ_1 and a -1% neutral attenuation.

Other Specific Interferents

The amount of an interferent that is present may be regarded as a random quantity. The absorption pattern of a particular interferent is of the form:

$$S_i = I_i \bar{C}L, \quad i = 1, 2, \ldots, n \tag{A-3}$$

where I_i is the absorption coefficient of the interferent at the i^{th} wavelength and $\bar{C}$ is the average concentration of the interferent over the path length L. This interferent constitutes a noise source whose covariance between wavelengths is given by:

$$\text{cov}(S_i S_j) = I_i I_j \text{ var } (\bar{C}L) \tag{A-4}$$

In the absence of detailed statistical information, the variance of the $\bar{C}L$ factor may be bounded by the square of the largest $\bar{C}L$ factor that has been observed in the field. The danger in using such coarse statistical measures is that the actual probability distribution is obscured. This leads to difficulties if the system is optimized by treating system noise and interferent noise on an equivalent rms statistical basis, that is, by summing their covariances. A more detailed discussion is given in Appendix B.

Random Interferents

Besides the known interferents, there may be certain other interferents of an unknown absorption pattern. One model that is both intuitively appealing and mathematically tractable assumes a Poisson distribution of Lorentz-broadened lines (Reference 31).

It is shown in Appendix A of Reference 2 that the spectral autocovariance of such a model is given by

$$C(\Delta\nu) = \frac{C(0)}{(\Delta\nu/2a)^2 + 1} \qquad (A-5)$$

where C(0) is the variance of the noise, and a is the half width of the lines. At atmospheric pressures, a is on the order of 0.1 cm^{-1}, although the value depends to some extent on the absorbing gas.

Thus, the random interference model is equivalent to a correlated noise source and can be lumped together with the other sources of noise.

Other Interferents

If a particular interferent is not well-defined or is of an unstable nature, for example, dependent upon meterological and/or environmental conditions, then a factor analysis of this behavior pattern must be performed. This implies that any particular variation of the interferent ensemble can be suitably approximated by a linear combination of a set of factors. Each factor is in turn considered as in interferent in its own right and is used in the design of the linear spectral weights. To the extent that the subspace spanned by the factors represents the interferent ensemble, a design based upon such an approach will be successful in rejecting this interferent.

Such an approach was taken in a previous study (Reference 2) in which dust particulates were a serious source of interference. For the present program it appears that water vapor may be of such a nature as to require a similar treatment. This will depend a great deal on the results of the SRI simulation study which are expected shortly.

APPENDIX B

OPTIMUM LINEAR WEIGHTS

Introduction and Notation

In this Appendix, techniques for the design and evaluation of optimum linear weights for detecting and estimating quantities of spectral absorbers and discussed. They are a summary of the results derived in Reference 2. The purpose of determining optimum systems is to establish a theoretical limit on the performance that may be obtained. This limit can then be used as a goal in the design of actual systems, that is, a frame of reference by which tradeoffs between complexity and performance may be reasonably conducted. In addition, optimum solutions often serve as a guide in designing an actual system. If a solution is arrived at by this or any other means and it is close to optimum, then there is no need to search further.

Spectral information will be contained in the transmission values $T_1, T_2, \ldots, T_n$ where n is the total number of wavelengths used. If a single absorber is placed in the sample region, the transmission at each wavelength will be of the form

$$T_i = \exp(-A_i \bar{C}_A L) \quad , \; i = 1, 2, \ldots, n \tag{B-1}$$

where A_i is the absorption coefficient of absorber A at wavelength i, $\bar{C}_A$ is the average concentration of absorber A over the total optical path, and L is the total optical path through the sample region. Typically, C has units of grams/liter or atmospheres of partial pressure, and L is in centimeters. A_i is in units to make $A_i \bar{C}_A L$ dimensionless.

In vector notation, eq. (B-1) becomes

$$\underline{T} = \exp(-\underline{A}\, \bar{C}_A L) \tag{B-2}$$

where $\underline{A} = (A_1, A_2, \ldots, A_n)'$ and $\underline{T} = (T_1, T_2, \ldots, T_n)'$ are n-dimensional column vectors representing the absorption coefficients of absorber A and the transmission values of the sample region, respectively, and the prime (') denotes transpose. If a second absorber B with absorption coefficients $\underline{B}$ is introduced into the region, the net transmission will be the product of the transmission due to each absorber; thus:

$$\underline{T} = \exp\left(-\underline{A}\,\bar{C}_A L - \underline{B}\,\bar{C}_B L\right). \tag{B-3}$$

First, some discussion of possible patterns is necessary. Figure B-1 shows possible transmission patterns for an absorber A characterized by absorption coefficients, $A_1 = 1$ liter/gm-cm and $A_2 = 5$ liter/gm-cm, and a second absorber B characterized by absorption coefficients, $B_1 = B_2 = 1$ liter/gm-cm. Transmission patterns are plotted for various amounts of each single absorber. Some mixtures of the two absorbers are shown in Figure B-2. All possible mixtures of A and B will be a smooth distribution lying between the contours for each pure absorber. For small absorptions, i.e., $1 - T_i \ll 1$, eq. (B-3) becomes

$$\underline{T} = \underline{1} - \underline{A}\,\bar{C}_A L - \underline{B}\,\bar{C}_B L, \tag{B-4}$$

where $\underline{1} = (1, 1, \ldots, 1)'$.

If the measured transmission is subtracted from a reference level at each wavelength, the signal is

$$\underline{S} = \underline{1} - \underline{T} \cong \underline{A}\,\bar{C}_A L + \underline{B}\,\bar{C}_B L. \tag{B-5}$$

Under these circumstances, the absorption coefficients add vectorially and a linear space is defined.

Another method of displaying transmission patterns is to plot the natural logs of the transmissions. Let $\underline{S} = -\ln \underline{T}$. If $\underline{T}$ is due to several absorbers, then

$$\underline{S} = \underline{A}\,\bar{C}_A L + \underline{B}\,\bar{C}_B L + \ldots \tag{B-6}$$

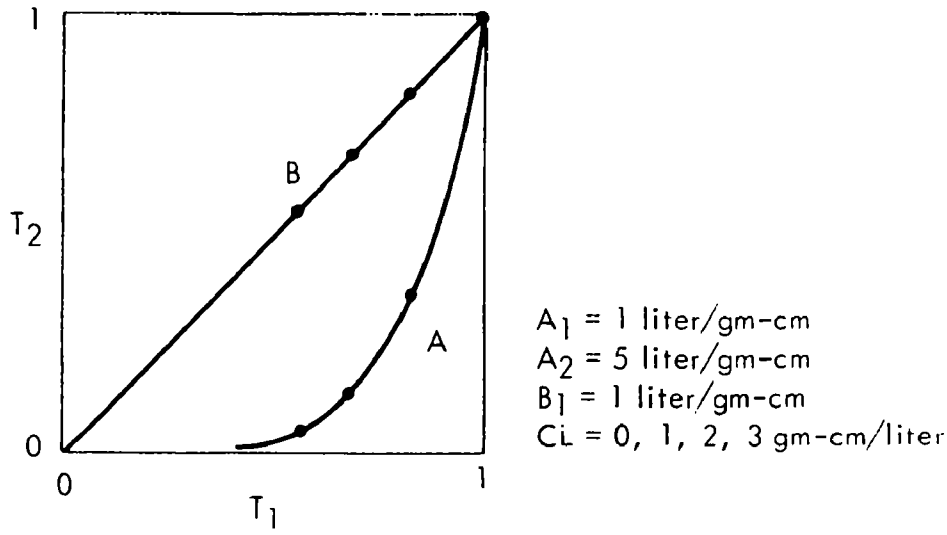

Figure B-1. POSSIBLE TRANSMISSION PATTERNS FOR SINGLE ABSORBERS

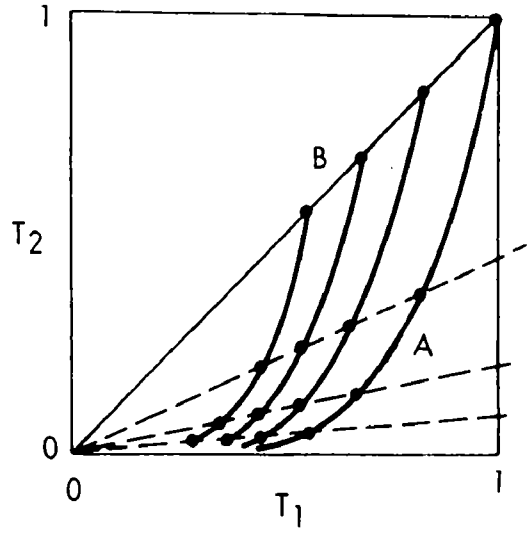

Figure B-2. POSSIBLE TRANSMISSION PATTERNS FOR MIXTURES OF ABSORBERS

which is the exact version of eq. (B-5). Figure B-3 is the equivalent of the patterns of Figure B-2. For this method of display, a linear space is defined for all absorption levels, and so the vector for each absorber is constant in direction, has a magnitude proportional to CL, and obeys vector addition. Visualization of possible transmission patterns is also easier in this manner.

The linear model adequately represents the actual process and hereafter, it is assumed for this discussion that the linear vector space model adequately represents the actual process over the range of interest either by virtue of small absorptions or by a log transformation. The system can therefore be considered as a black box with an output column vector $\underline{X}$ that is composed of the sum of a signal vector $\underline{A}$ and a noise component $\underline{N}$ that represents all sources of interference. The signal vector represents the absorption coefficients of the target gas over a selected set of wavelengths.

A detailed mathematical derivation of optimum linear weights is given in (Reference 32) and the major results are summarized in this section. The optimum linear weights maximize the signal-to-noise-ratio

$$\phi = \underline{W}'\underline{A}/(\text{Var } \underline{W}'\underline{X})^{1/2} \qquad \text{(B-7)}$$

for various constraints.

Unconstrained Weights

The direction of the optimum unconstrained weight for a single target in a field of correlated noise is derived as

$$W = \Sigma^{-1}\underline{A} \qquad \text{(B-8)}$$

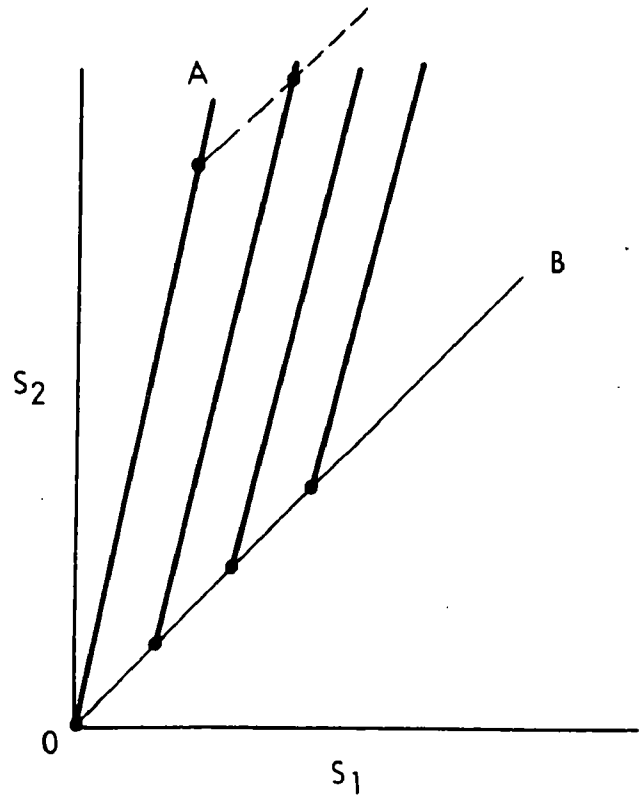

$S_i = -\ln(T_i)$

Figure B-3. POSSIBLE PATTERNS FOR THE NATURAL LOG OF THE TRANSMISSION

where Σ is the covariance matrix of the noise vector and $\underline{A}$ is the signal vector which represents the absorption coefficients of the target gas. The optimum signal-to-noise ratio is given by

$$\phi_{max} = (\underline{A}' \Sigma^{-1} \underline{A})^{1/2} \tag{B-9}$$

If the noise is uniform and uncorrelated, then $\Sigma = \sigma^2 1$ and $\underline{W}$ is the "matched filter" for the signal vector.

The composition of Σ takes into account the interferents as well as other sources of correlated or uncorrleated noise. If an interferent is of the form $\rho \underline{I}$ where ρ is a random variable and $\underline{I}' = (I_1, I_2, \ldots, I_n)$ is a fixed pattern vector, then its contribution to the total covariance matrix is

$$\sigma_{ij} = I_i I_j \text{ var } (\rho) \tag{B-10}$$

For a spectrally absorbing interferent gas, the quantity ρ represents the CL factor or mass per unit area. In addition, the covariance matrix provides a convenient means of handling random interferents since this is just another correlated noise source. A detailed description of interference was covered in the Appendix A.

The disadvantage of a signal-to-noise optimization is that all interferences are characterized only by second-order statistics. This leads to difficulties if system noise and interferent noise are treated on an equivalent rms statistical basis, that is, by summing their covariances. The reason for this is that while the system noise probability distribution is fairly well-defined, an interferent distribution may be of a very non-stationary and erratic nature; e.g., a passing truck stirring up a dust cloud. For these reasons, it is often desirable to design a system in which certain "well-behaved" interferents are described by the covariance matrix and a null response is required for the more irregular distrubances.

Orthogonal Weights

Orthogonality constraints of the type

$$\underline{W} \cdot \underline{I}_j = 0, \; j = 1, 2, \ldots, \; m < n \tag{B-11}$$

are now considered. That is, a zero response is required for certain interferents of a perverse nature. It is shown that the direction of the optimum weight is given by

$$\underline{W} = P\underline{A} \tag{B-12}$$

where

$$P = \Sigma^{-1} \left[I - Q(Q' \Sigma^{-1} Q)^{-1} Q' \Sigma^{-1} \right] \tag{B-13}$$

and

$$Q = (\underline{I}_1, \underline{I}_2, \ldots, \underline{I}_m) \tag{B-14}$$

is an n x m partitioned matrix whose columns consist of selected interferent vectors. The optimum SNR in this case is given by

$$\phi_{max} = (\underline{A}' P \underline{A})^{1/2} \tag{B-15}$$

If the noise is uniform and uncorrelated, eq. (B-13) reduces to

$$P = I - Q(Q'Q)^{-1} Q' . \tag{B-16}$$

This form has the simple geometric interpretation of dropping a perpendicular from the signal vector down to the subspace spanned by the m interferents.

On the other hand, if there are no orthogonality constraints, Q = 0, and eqs. (B-12) and (B-13) reduce to eq. (B-8) as expected.

An alternative method of imposing orthogonality constraints is to assign an equal amplitude variance μ to the m interferents and to include them in the covariance matrix using eq. (B-10) it can be shown that as μ becomes large, the optimum weight calculated by eq. (B-8) will converge to a vector that is orthogonal to the m selected interferents. An alternative method of computation is therefore available. The choice of methods will depend on the particular problem at hand. For example, if the noise is uniform and uncorrelated, then eq. (B-16) applies which only involves the inversion of an m x m matrix as opposed to the n x n inversion required in eq. (B-8). On the other hand, for correlated noise, the alternative method may be preferable.

Multiple Weights

In some applications, several linearly independent targets can be present simultaneously. If it is desired to measure or detect each target independently, then the linear weight for each target is required to be orthogonal to the other targets, i.e.,

$$\underline{W}_i' \underline{A}_j = \begin{cases} 1, & i = j \\ 0, & i \neq j \end{cases} \tag{B-17}$$

In matrix notation, eq. (B-17) becomes

$$W'A = I \tag{B-18}$$

where $W = (\underline{W}_1, \underline{W}_2, \ldots, \underline{W}_m)$ and $\underline{A} = (\underline{A}_1, \underline{A}_2, \ldots, \underline{A}_m)$ are n x m matrices whose whose columns are the W_i and A_i vectors respectively.

The optimum constrained weight matrix is given by

$$W = \Sigma^{-1} A(A' \Sigma^{-1} A)^{-1} \tag{B-19}$$

and the SNR for each target is given by

$$\phi_i = r_{ii}^{-1/2} \tag{B-20}$$

where the r_{ii}'s are diagonal elements of the matrix

$$R = A' \Sigma^{-1} A \tag{B-21}$$

It is noted that R is the cross response matrix in the absence of orthogonality constraints.

For m = 1, eq.(B-19) reduces to the usual form $\underline{W}_1 = \alpha \sum^{-1} \underline{A}_1$, where α is a scalar constant. On the other hand, if the number of targets is equal to the dimensionality of the space, i.e., m = n, then

$$W' = A^{-1} \tag{B-22}$$

For the special case when the noise is uniform and uncorrelated, i.e., $\Sigma = \sigma^2 I$, eq. (B-19) reduces to

$$W = A(A'A)^{-1} \tag{B-23}$$

This expression is the well-known "generalized inverse" of the matrix A and $W'\underline{Y}$ is the "least squares" solution to the overdetermined system of equations $A\underline{X}=\underline{Y}$.

Application

For the present problem, the number of targets is m = 3. Since neutral attenuation is a dominant interference and is not very statistically well-behaved or modeled, the weights will be orthorgonally constrained to reject this interferent, i.e.,

$$W_1 + W_2 + W_3 + W_4 = 0 \tag{B-24}$$

for each target. This will be indirectly accomplished by considering neutral attenuation as a 4th "target" in the formulation of equations (B-17) through (B-21). All other interferents will (by necessity in this case, since we only have 4 wavelengths) be considered to be "well behaved" and will be described by the noise covariance matrix. At least one such interferent, H_2O vapor will be included in this set.

APPENDIX C

WAVELENGTH SELECTION

Introduction

A large number of spectral lines are typically available using the CO_2 laser. However, practical considerations limit the number of lines used to about 4 to 8. A selection of the best subset of available lines is based on maximizing the signal to-noise-ratio (SNR) for a specified set of targets and interferents.

For the present 4 wavelength $C^{12}O_2^{16}$ laser system, there are about 74 possible lines from which to select. A direct combinatorial approach to selecting the best 4 wavelengths out of the available 74 would require $\binom{74}{4} = 1,150,626$ combinations; an exceedingly large number of computations. Each SNR computation involves an expression of the form of (B-21). This equation involves the construction and inversion of a 4 X 4 matrix, 20 multiplications, and 20 adds to determine the SNR for ozone alone - the target we are optimizing. Consequently, even if each computation were on the order of one cent, the required total cost would be prohibitive.

Fortunately, a viable and expedient alternative exists that can at least narrow down the number of wavelengths to be considered to a manageable number. As a bonus, the method can also determine the increase in performance that could be attained if

more than 4 wavelengths were used. This technique was developed (Reference 1) as an outgrowth of Reference 3 and is referred to as the "squeeze method" of wavelength selection.

Squeeze Method

For a scanning system, the noise σ_i associated with a measurement at each wavelength λ_i is indirectly proportional to the time T_i spent at that wavelength:

$$\sigma_i^2 = K_i^{2/} T_i \tag{C-1}$$

where K_i is a constant determined by the system noise sources. For a fixed scan rate, the sum of the time intervals is fixed, i.e.,

$$T_1 + T_2 + \ldots + T_n = T. \tag{C-2}$$

Assuming uncorrelated noise, the variance of a weighted sum of measurements is given by

$$\sigma^2 = \sum_{i=1}^{n} \sigma_i^2 |W_i|^2 \tag{C-3}$$

where W_i is the weight attached to the measurement at λ_i.
By using a variational argument, (Reference 3, Appendix E) it can be shown that the time intervals that minimize (C-3) subject to the constraint (C-2) are given by

$$T_i = TK_i |W_i| \left(\sum_{j=1}^{n} K_j |W_j| \right)^{-1}, \tag{C-4}$$

i.e., the optimum time intervals are proportional to the product of the noise constant and the absolute value of the weight. Substituting (C-4) into (C-1)

gives $$\sigma_i^2 = \frac{K_i}{T|W_i|}\sum_{j=1}^{n} K_j |W_j| , \qquad (C-5)$$

and determines the system noise component of the noise covariance matrix used in computing the optimum linear weights.

In Appendix B, procedures were developed for selecting optimum weights. These procedures were dependent on the noise covariance matrix. If the optimum time intervals are selected according to Eq. (35), then the covariance matrix is of the form

$$\sum = \Lambda + D(\underline{W}) \qquad (C-6)$$

where D is a diagonal matrix, representing system noise, whose elements are given by (C-5) and is a function of $\underline{W}$, and Λ represents the noise due to other interferents. Since D and hence $\sum$ are themselves functions of $\underline{W}$, the solution of $\underline{W}$ is in implicit form. An iteration procedure is therefore indicated. An initial guess of the solution, say $\underline{W}_0' = (1, 1, \ldots, 1)$, is substituted into Eq. (C-6) and the optimum weighting vector $\underline{W}_1$ is calculated by one of the techniques given in Appendix B. For the next iteration, $\underline{W}_1$ is substituted into eq. (C-6) and $\underline{W}_2$ is calculated. In this manner, a sequence of weights will be determined which will converge to the desired optimum weight.

A consequence of this procedure is that weights corresponding to wavelengths of low information will converge to zero and the required wavelength selection process is thereby attained. In general, m + p wavelengths will be retained in the limit, where p is the number of independent agents to be detected and m is the number of interferents (assuming $n \geq m + p$).

If several targets are to be simultaneously optimized, a suitable averaged weight can be used in the feedback loop.

A computer program (LWSP) was developed for implementing the above procedure (Reference 1) and is described in Appendix D. It assumes a detector-noise-limited system so that $K_i = NEP/P_i$ where NEP is the noise-equivalent-power of the detector and P_i is the received power at λ_i. The program is restricted to computing weights by (B-11) and (B-12) with a diagonal covariance matrix, i.e., it assumes that enough wavelengths are available so that all interferents can be completely rejected and that all system noise is uncorrelated.

Application

In order to use the LWSP program for the present application, ozone was considered as a single target and all other gases were considered as interferents. In addition, the present application was expected to be optical-noise-limited rather than detector-noise-limited and so, the P_i's were all set equal except for those that are so low as to preclude reliable operation. In this manner, the 74 available lines were reduced to a set of 10 from which a final selection was based.

The final selection uses another program (CMFIL) in order to compute the performance of all $\binom{10}{4} = 210$ combinations of wavelengths using equations (B-20) and (B-21). This program was adapted from another existing program (MFIL).

LWSP

A description of the LWSP program which implements the "Squeeze Method" as previously noted is given in Appendix D. This program essentially eliminates wavelengths of low information by an iteration process of adjusting the power allocation according to an optimization algorithm. In this manner, the power allocated to unimportant wavelength coverages to zero thus accomplishing the selection process.

The present configuration of the LWSP program operates in the orthogonal mode, i.e., the linear weights are constrained to completely reject all of the gasses in the prescribed interferent set. In this mode of operation, the number of significant wavelengths will converge to the sum of the number of linearly independent targets and the number of linearly independent interferents.

For the present application, the detection of one target, O_3, was considered in the presence of 5 interferents: CO_2, H_2O, C_2H_4, NH_3, and neutral attenuation. With this target and interferent set, the number of significant wavelengths will then converge to 6.

A 25 iteration LWSP run with the above target and interferent set resulted in the line selection illustrated in Figure 14. The solid lines in this figure represent the linear weights applied to each wavelength and their length is indicative of the relative importance of each line. The X's designate normalized ozone absorption coefficients and the +'s designate the average interferent noise level. As can be seen, the number of significant wavelengths converged to 6 as advertised.

CMFIL

A four-wavelength system was selected on the basis of compromising performance and complexity. This choice is later justified as explained in the introduction and illustrated by Figure 16. In this case, the number of wavelengths used is not

sufficient to null out all of the interferents. Therefore, the strength (variance) of each interferent must be estimated and a linear weight is computed that gives the best performance on the average. The details of this method are described in Appendix B. A program (MFIL) that computes the linear weights and SNR's for a given set of wavelengths using this algorithm is described in Reference 17. This program was modified (CMFIL) in order to evaluate all combinations of N wavelengths taken M at a time and to order the combination according to SNR.

Table V shows the input data that was used for the CMFIL program. The wavelength set was obtained from the top 9 wavelengths of the LWSP output combined with the ethylene line. The interferent CL variances listed in Table I were estimated from the best guesses available of the environment. The CMFIL output listing that was obtained with the input data of Table V and the spectral data in Tables I and II is shown in Figure 15. As expected, the P12 and P14 (5 and 6) which correspond to the peak ozone absorption, appear in all of the highest rankings. The R16, R14, and P24 (3, 4, 8) lines also predominately appear in all of the highest rankings and are therefore indicated as good reference lines. The combination 4, 6, 8, 10 (R14, P14, P24, P14) was selected as the combination that gave the highest SNR while retaining the ethylene line.

By examining the linear weights associated with the output listing, the performance of 2 and 3 wavelength systems was estimated and is shown in Figure 16. As can be seen, a three-wavelength system (which we essentially have at the present due to the retention of the 10.5321 micron ethylene line) provides near optimum performance with a minimum of complexity. A two-wavelength ozone system results in about 1/2 the sensitivity.

WAVELENGTH SET

001-020	R30	9.219690 microns
	R18	9.282444
	R16	9.293786
	R14	9.305386
	P12	9.488354
	P14	9.503937
	P20	9.552428
	P24	9.586227
	P30	9.639166
001-100	P14	10.532080

TARGETS (RECORD NO.)

Ozone 0_3 (244)

INTERFERENTS (RECORD NO.)	VARIANCE (CL)	COMMENTS
Neutral (201)	1.0	If T log-normal, 4:1 variation 50% of time
Carbon Dioxide CO_2 (243)	10.0	10% x 320 ppm x 1 km
Ethylene C_2H_4 (245)	25×10^{-6}	50 ppb x 1 km
Ammonia NH_3 (246)	25×10^{-6}	50 ppb x 1 km
Water Vapor H_20 (244)	10^6	~58 - 100% RH at 73 degrees F x 1 km

DETECTOR NOISE VARIANCE

10^{-5}

Table C-1. CMFIL Input Data

APPENDIX D

LWSP - LASER WAVELENGTH SELECTION PROGRAM

PURPOSE

To select those laser lines from the CO_2 laser bands which are best for etection of agents in the presence of noise.

GIVEN

a. Spectra of $C^{12}O_2^{16}$ laser, including relative power at each wavelength

b. Spectra of agents and interferents.

c. Relative importance of each agent.

COMPUTE

The weight which should be applied to each line for optimum S/N and the time fraction (power) to be allocated to each line.

DATA FORMAT

Same as MFIL (Reference 17). Laser data can be input by either cards or tape. Individual and combined spectra are in the library.

PROGRAM OPERATION

Deck setup and operation are almost identical to that for MFIL. Fewer cards are required and a laser must be specified, along with the usual target and interferent list.

There are two modes of operation. One uses independent wavelengths for each target and optimizes the weights for each individually. The second method uses a common set of wavelengths and involves the use of an average weight in the iteration loop which causes the weights for each target to move more nearly together. If this option is chosen, the relative importance of each target is specified by use of the "AVG" card.

Five iterations will be made unless otherwise specified on the "G" card. If cards are used for laser data, they must contain wavelength and power, in that order, in (7X2F8.4) format. A blank card (wavelength = 0) terminates reading of the laser data. These cards must immediately follow the "LASER/CARD" command.

COMMAND LIST FOR LWSP

COMMAND	TYPE	X1	X2	X3	X4	X5
LASER		Lib. Scan No				
LASER	CARD	(Follow by λ, pin (7X2F8.4) format, term, with blank card)				
TRGTS		Same as MFIL (Reference 17)				
IFNTS						
NEVT						
AVG		W_1	W_2	W_3	W_4	W_5
RESET						
GØ						
END	(ZERØ)	K-plot	K-λ/N	K-iter	NDP	

MATHEMATICAL METHOD

1. Construct Interferent Matrix

$$Q = (I_1, I_2, \ldots, I_m) \qquad (n \times m) \qquad (D\text{-}1)$$

where the columns are n-dimensional interferent absorption coefficient vectors, n is the number of wavelengths available, and $m < n$ is the number of interferents.

2. Initialize Average Weight and Weight for Each Target

$$W^{(O)} = W_i^{(O)} = (P_1, P_2, \ldots, P_n)', \; i = 1, 2, \ldots, p \qquad (D\text{-}2)$$

where p is the number of targets and P_j is the relative power at wavelength j.

3. Compute the Diagonal Matrix, Scale Factors, and Time Intervals

for each iteration $k = 0, 1, 2, \ldots, K$ as follows:

a. Independent Wavelengths

Compute the diagonal matrix

$$D_i^{(k)} = \underset{j}{\text{diag}} \; (P_j \mid W_{ij}^{(k)}. \qquad (n \times m) \qquad (D\text{-}3)$$

and scale factor

$$F_i^{(k)} = \sum_{J=1}^{n} |W_{ij}^{(k)}| / P_j \qquad (D-4)$$

for each target i = 1, 2,..., p where $\underline{W}_i^{(k)} = (W_{i1}^{(k)}, W_{i2}^{(k)}, \ldots, W_{in}^{(k)})'$ is the k^{th} iteration weight vector for target i. Also, compute the time fraction (power) allocated to wavelength j

$$T_{ij}^{(k)} = |W_{ij}^{(k)}| / P_j F_i^{(k)} \qquad (D-5)$$

for each target i = 1, 2, ..., p.

b. Common Wavelengths

Compute the diagonal matrix

$$D^{(k)} = \underset{j}{diag} \ (P_j \bar{W}_j^{(k)}) \qquad (D-6)$$

and scale factor

$$F^{(k)} = \sum_{j=1}^{n} \bar{W}_j^{(k)} / P_j \qquad (D-7)$$

where $\underline{\bar{W}}^{(k)} = (W_1, W_2, \ldots, W_n)'$ is the k^{th} iteration average weight.

In this case, it is only necessary to perform the computation once for each iteration. The common time fraction allocated to wavelength j is computed as

$$T_j^{(k)} = \bar{W}_j^{(k)} / P_j F_j . \tag{D-8}$$

4. Compute Next Weight Vector

$$\underline{W}_i^{(k+1)} = D_i^{(k)} \left[I - Q(Q' D_i^{(k)} Q)^{-1} Q' D_i^{(k)} \right] \underline{A}_i \tag{D-9}$$

for each target absorption coefficient vector $\underline{A}_i$, i = 1, 2, ..., p. (In the common mode, D_i is replaced by D in the above).

5. Compute Relative Signal-To-Noise Ratios

$$SNR_i = (\underline{W}_i'^{(k+1)} \underline{A}_i / F_i)^{1/2} \tag{D-10}$$

for each target i. (Again, in the common mode, F_i is replaced by F in the above).

6. Normalize Each Weight to an Absolute Peak of 1.

7. Print Weights, SNR's, and Time Fractions for each Target

8. Compute Average Weight

$$\underline{\bar{W}}^{(k+1)} \qquad \sum_{i=1}^{p} \qquad K_i \left| \underline{W}_i^{(k+1)} \right| \tag{D-11}$$

where the K_i's are weighting factors corresponding to the relative importance of each target.

9. Print Summary and Compute Next Iteration

Go to Step 3 and repeat until $k = K$.

10. Compute Target Cross-Response Matrix R (p x p)

with elements

$$R_{ij} = G_i \underline{W}_i^{(K)} \underline{A}_j, \quad i,j = 1, 2, \ldots, p \tag{D-12}$$

where

$$G_i = SNR_i^{(K)} / \underline{W}_i'^{(K)} \underline{A}_i, \quad i = 1, 2, \ldots, p \tag{D-13}$$

11. Compute Interferent Cross-Response Matrix U (p x m)

with elements

$$U_{ij} = G_i \underline{W}_i'^{(K)} \underline{I}_j, \qquad \begin{matrix} i = 1, 2, \ldots, p \\ j = 1, 2, \ldots, m \end{matrix} \tag{D-14}$$

12. Compute Next Iteration (Go to Step 3).

A flow chart describing these operations is shown in Figure D-1.

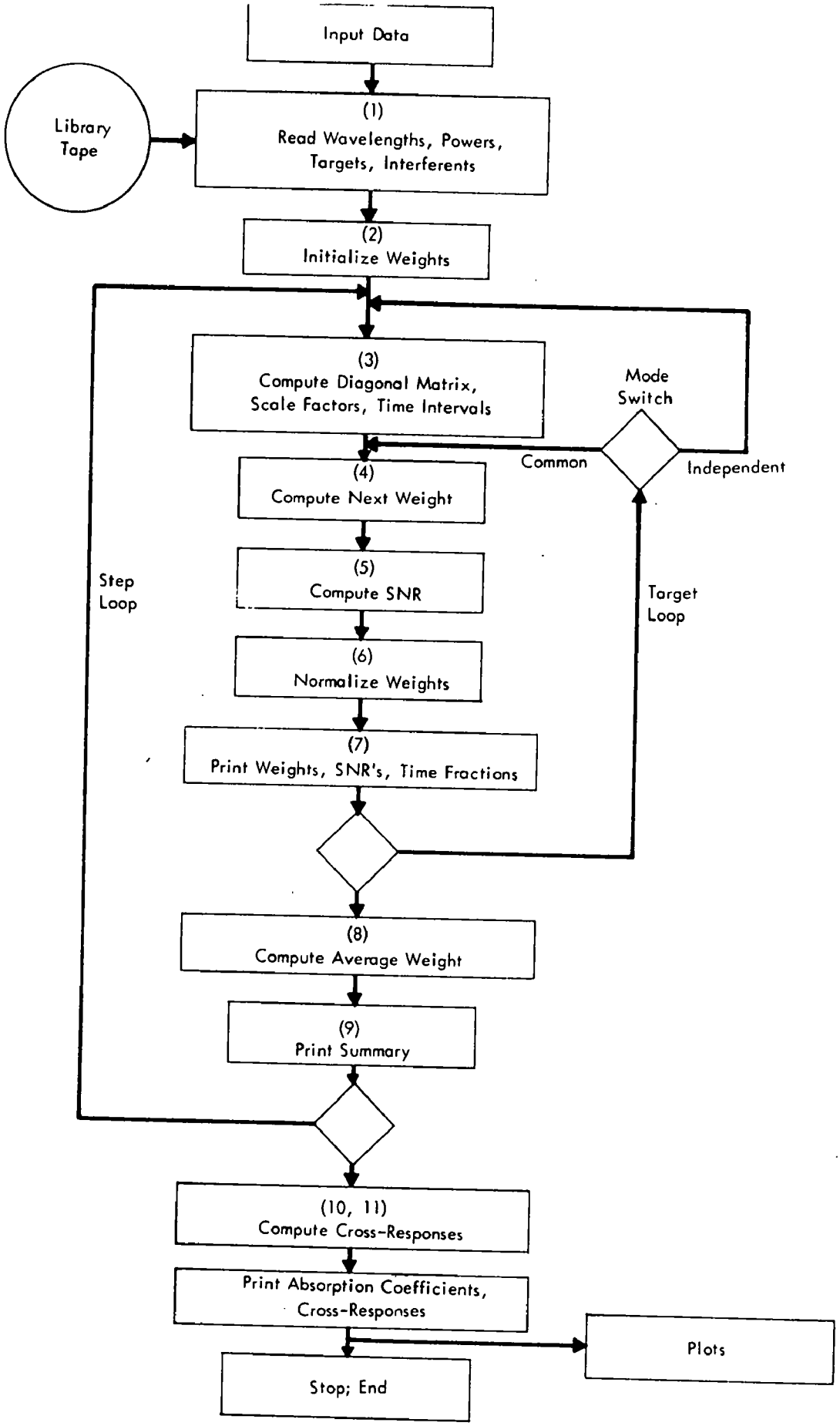

Figure D-1. FLOW CHART OF LWSP PROGRAM

TECHNICAL REPORT DATA
(Please read Instructions on the reverse before completing)

1. REPORT NO.	2.	3. RECIPIENT'S ACCESSION NO.
EPA-650/2-74-046-a		

4. TITLE AND SUBTITLE
Development of a Gas Laser System to Measure Trace Gases by Long Path Absorption Techniques, Vol. I: Gas Laser System Modifications for Ozone Monitoring

5. REPORT DATE
June 1974

6. PERFORMING ORGANIZATION CODE

7. AUTHOR(S)
S.E. Craig, D.R. Morgan, D. L. Roberts, L.R. Snowman

8. PERFORMING ORGANIZATION REPORT NO.
OS 74-13

9. PERFORMING ORGANIZATION NAME AND ADDRESS
General Electric Company, Ordnance Systems, Electronic Systems Division, 100 Plastics Avenue, Pittsfield, Mass., 01201

10. PROGRAM ELEMENT NO.
1A1010 (26 ACX)

11. CONTRACT/GRANT NO.
68-02-0757

12. SPONSORING AGENCY NAME AND ADDRESS
U.S. Environmental Protection Agency
National Environmental Research Center
Research Triangle Park, North Carolina, 27711

13. TYPE OF REPORT AND PERIOD COVERED
Final

14. SPONSORING AGENCY CODE

15. SUPPLEMENTARY NOTES
Volume II of the set is being published as EPA-650/2-74-046-b

16. ABSTRACT

Modifications of a gas laser system for long path monitoring of trace atmospheric constituents by infrared absorption are described. Modifications were made in preparation for an ozone field measurement program reported in Volume II wherein path monitor data were compared with those from a point monitor moved along the optical path. System modifications included incorporating a digital signal processor in the system and a spatial filter in the laser beam. Spectral studies of ozone, carbon dioxide, water vapor, ethylene and ammonia are presented in connection with the selection of laser wavelengths used in the system to discriminate ozone effects from interferences. Design considerations and a proposed configuration for an isotopic CO_2 laser are presented.

17. KEY WORDS AND DOCUMENT ANALYSIS

a. DESCRIPTORS	b. IDENTIFIERS/OPEN ENDED TERMS	c. COSATI Field/Group
Lasers Atmospheric Absorption Ozone Air Pollution Monitoring	ILAMS Methodology for Point Monitor, Path Monitor Comparisons	1705

18. DISTRIBUTION STATEMENT	19. SECURITY CLASS *(This Report)*	21. NO. OF PAGES
Release Unlimited - Copies Available from NTIS; APTIC (EPA)	Unclassified	123
	20. SECURITY CLASS *(This page)*	22. PRICE
	Unclassified	

EPA Form 2220-1 (9-73)